The Synthesis of High Strength Titanium Alloy and Titanium Alloy Matrix Composite by Powder Compact Extrusion from Blended Elemental Powders

A thesis

submitted in fulfilment

of the requirements for the degree of

Doctor of Philosophy

in the School of Science and Engineering,

University of Waikato

by

Huiyang Lu

THE UNIVERSITY OF
WAIKATO
Te Whare Wānanga o Waikato

2016

Abstract

Powder compact extrusion (PCE) from blended elemental powders is an effective way to produce titanium alloys and titanium matrix composites with high performance. Its main advantage is cost effectiveness, where high cost pre-alloyed powders are replaced by lower cost elemental powders and a need for lengthy sintering times to achieve sufficiently high enough density is removed. However a blended elemental approach has some disadvantages, for example the ductility and strength of PCE materials are normally lower than those obtained in cast alloys. This thesis is a study of the feasibility of producing a high strength titanium alloy and titanium matrix composite using PCE from blended elemental powders. It investigates and seeks to address the effects of inhomogeneous elemental distribution on structure and properties. In this study two very different ways of producing a high strength titanium alloy using PCE through a blended elemental approach are investigated. The first approach is through the synthesis of the high strength alloy Ti-4%Al-4%Mo-4%Sn-0.5%Si and the second approach investigates the feasibility of achieving high strength by producing a titanium alloy composite and for this TiB/Ti6Al4V was chosen for this study.

For synthesising the alloy Ti-4%Al-4%Mo-4%Sn-0.5%Si, the effect of extrusion temperature, different starting powders and heat treatment on the microstructure and mechanical properties were studied. The extrusion temperature has a significant effect on the degree of elemental dissolution. An increase in the extrusion temperature significantly improves the dissolution of Si and Mo. However, an extrusion temperature of 1350^{o}C is still not enough to achieve complete dissolution of the elemental particles, especially Si and Mo particles. The results showed that by using an extrusion temperature 1350^{o}C with a holding time of 5 min prior to extrusion, elemental dissolution was much improved and a relatively homogenous microstructure was achieved. As-extruded bars with undissolved elemental particles showed low tensile strength without any ductility, while those samples without any inhomogeneities in the microstructure caused by undissolved particles and defects showed an ultimate tensile strength and elongation to fracture of 1423MPa and 5.1%, respectively.

After achieving dissolution of the elemental particles, some localized areas with an inhomogeneous elemental distribution still existed. The diffusion interactions between different elements during high temperature processing were also discussed in this thesis. The study also showed that some dendrites such as Ti_5Si_3 and β Ti grew during cooling due to the local elemental inhomogeneities. These dendrites are detrimental to the mechanical properties of the alloy, being the main reason for premature failure during tensile testing, leading to a large variation in tensile properties. The precipitation of dendrites was monitored.

When the starting powders were dominated by gas atomized (GA) titanium powders, a good combination of tensile strength and ductility was achieved which showed a UTS of 1220-1250 MPa with an elongation to fracture of 7-11%. GA titanium powders have a beneficial effect on elemental diffusion and the achievement of more uniformity in mechanical properties.

A beta transus temperature of 1075^{o}C has been confirmed. The solutioning temperature and the concentration of beta stabilizer, especially Mo, in the beta matrix has a significant effect on martensite phase transformation. After heat treatment the microstructural homogeneity and tensile properties were significantly improved. The cooling rate after solutioning plays a key role in determining the morphology of the α lamellar structure and the α colony and beta grain size. A faster cooling rate causes a decrease in the width of the α lamellae, the size of the α colonies and the beta grain size. After heat treatment an ultimate tensile strength of 1584MPa, a yield strength of 1505MPa and an elongation to fracture of 2.5% were obtained.

The method of synthesis of this alloy by powder compact extrusion from a pre-consolidated compact was also introduced. The effect of extrusion temperature on microstructure and mechanical properties was investigated. When the extrusion temperature is increased to 1200^{o}C a fine lamellae microstructure with good tensile properties giving a yield strength, UTS and elongation to fracture of 1278MPa, 1421MPa and 7.2%, respectively, were achieved. Good tensile properties were obtained at elevated temperature, and for testing between 300^{o}C and 500^{o}C the tensile strength decreased from 907MPa to 720MPa, but the elongation to fracture increased from 10% to 13%.

For synthesis of TiB/Ti6Al4V composite, a Ti-6wt%Al-4wt%V alloy (Ti6Al4V) matrix composite, reinforced by in-situ synthesized TiB whiskers (TiBw) was successfully fabricated by powder compact extrusion, using a blended powder mixture. The microstructural characterization of the various extruded samples showed that the different starting powders, pre-alloyed powder plus boron powder or titanium plus Al-40V master alloy powder plus boron powder, had a significant effect on the morphology of the in-situ synthesized TiB whiskers. It is also evident that the TiB whiskers affected the microstructural evolution of the Ti6Al4V matrix. The tensile test results indicated that a composite with a dispersion of fine TiB whiskers with high aspect ratios exhibited a high ultimate tensile stress (UTS) and yield stress (YS) of 1436MPa and 1361MPa, respectively, a reasonably good tensile ductility reflected by an elongation to fracture of 5.6% was also achieved. This is a significant improvement compared with as-extruded monolithic Ti6Al4V alloy produced in this study.

List of Publications

Publications:

Huiyang Lu, Deliang Zhang, Brian Gabbitas, et al. "Synthesis of a TiBw/Ti6Al4V composite by powder compact extrusion using a blended powder mixture." *Journal of Alloys and Compounds* 606 (2014): 262-268.

Yang, Fei, De Liang Zhang, **Hui Yang Lu**, and Brian Gabbitas. "Preparation, microstructure and properties of Ti-6Al-4V rods by powder compact extrusion of powder mixture." In *Key Engineering Materials*, vol. 520, pp. 70-75. 2012.

Conference presentations:

“Synthesis of Ti-4%Al-4%Mo-4%Sn-0.5%Si alloy by powder compact extrusion from blended elemental powders”, 1st International Conference on Powder Processing, Consolidation and Metallurgy of Titanium, Brisbane, Australia, 4-7 December, 2012.

Acknowledgements

First and foremost, I would like to acknowledge and express my grateful thanks to my chief supervisor Professor Brian Gabbitas, for his patient instructions, thoughtful help and vital encouragement, all of which have been played a crucial role for the completion of my study and thesis, and also much meaningful for my future.

I would like to extend my appreciation to my former chief supervisor Professor Deliang Zhang, Shanghai Jiao Tong University, Shanghai, China, for leading me to the powder metallurgy research, his patient guidance and generous help. Also many thanks to my co-supervisor Dr Rob Torrens from Waikato University and Dr Steven Matthews from Massey University, for their intensive academic help.

I also would like to extend my thanks go to everyone who gave me generous help and advice for my study and daily life during the past few years in the University of Waikato. I have benefited a lot from their advice and suggestions:

-Dr Fei Yang, Stella Raynova, Chris Wang, Yuanji Zhang, Helen Turner for their technical support and academic support, especially Dr Fei Yang, thanks a lot for his patient help and always helpful advices.

-Jia Lou, Qian Xu, Mingtu Jia, Denshan Zhou, Paul Ewart, Navaneeth and other group members for their full cooperation.

Last but not least, many thanks to my families, my parents, my wife Haixia and my two lovely children Jinwen and Jinyu, for their patience and love during my PhD study.

Table of Contents

List of Figures

List of Tables

Abbreviations

PM	Powder Metallurgy
TMCs	Titanium matrix composites
BEPM	Blended elemental powder metallurgy
PCE	Powder compact extrusion
HE	Hot extrusion
BSE	BackScattered Electron
CP	Commercial pure
DTA	Differential Thermal Analysis
EDX	Energy Dispersive X-ray analysis
GA	Gas atomised
HDH	Hydrogenation–dehydrogenation
MM	Mechanical milling
HEMM	High energy mechanical milling
OM	Optical Microscopy
SPD	Severe Plastic deformation
PREP	Plasma rotating electrode process
SEM	Scanning electron microscopy
TGA	Thermogravimetic analysis
XRD	X-Ray Diffractometry

Chapter 1 Introduction

1.1 Titanium and titanium alloys

Nowadays titanium and titanium alloys are becoming increasingly attractive for a wide range of applications in many fields such as military and civil transportation as shown in Fig.1.1, due to their unique merits of low density, high specific strength (strength to weight ratio), heat resistance, corrosion resistance, low temperature resistance, and excellent biocompatibility. Table 1.1 shows the general characteristics of titanium and its alloys as compared to other important structural metallic materials, such as Fe, Al and Ni, which are already widely used [1]. The advantages of titanium are notable: it combines the high melting point of iron and nickel and the superior corrosion resistance (room temperature) and density of aluminium. Furthermore, its strength is modest, and like iron it is capable of strengthening by allotropic transformation.

Fig.1.1 Use of titanium and titanium alloys in military and civil applications. For the F-22 aircraft about 41% of the structure is made from titanium.

However, this table also indicates the disadvantages of titanium and its alloys. The most critical problem is its chemical reactivity with impurities (O, H, N, Cl), especially oxygen. A protective TiO_2 film provides excellent resistance to

corrosion and contamination below 535°C. Above 535°C, the film breaks down and interstitial elements easily diffuse into the bulk and embrittle titanium alloy [2]. As a result, the reduction, casting and even wrought processing of titanium needs to be conducted under a strictly protective atmosphere. Furthermore, the energy consumption in the production of titanium alloys are much higher than that for steel and aluminum alloys [3]. Lastly, for wrought material the ratio of final cost of a product to the initial price of titanium is very high. Also, recycling of titanium alloys is very difficult [4]. These factors contribute to the extremely high cost of titanium alloys.

Table 1.1 Some general characteristics of titanium as compared to other structural metallic materials based on Fe, Al and Ni [1].

	Ti	Fe	Ni	Al
Melting Temperature (°C)	1670	1538	1455	660
Allotropic Transformation (°C)	$\beta \xrightarrow{882} \alpha$	$\gamma \xrightarrow{912} \alpha$	-	-
Crystal Structure	bcc → hex	fcc → bcc	fcc	fcc
Room Temperature E (GPa)	115	215	200	72
Yield Stress Level (MPa)	1000	1000	1000	500
Density (g/cm^3)	4.5	7.9	8.9	2.7
Comparative Corrosion Resistance	Very High	Low	Medium	High
Comparative Reactivity with Oxygen	Very High	Low	Low	High
Comparative Price of Metal	Very High	Low	High	Medium

The processing and behaviour of titanium and its alloys is strongly dependent on two allotropic forms of titanium: the α phase, with a hexagonal close-packed structure, exists from room temperature to 882°C for pure titanium. Some elements dissolve preferentially in the α phase and are α stabilisers. The α phase field is therefore expanded with an increase in the α/ β transus temperature. Typical α stabilisers are Al, O, N etc. [5]. The β phase, which is a body-centred cubic structure, exists from 882°C to the melting point for pure titanium. Some elements depress the α/ β transus promoting β phase retention when cooling from the single β phase. Elements which are β stabilisers are Mo, V, Nb, Fe, H_2, etc. [5]. These transformations enable titanium to have alloys designated as α, β or α/β with various microstructures and specific properties. Strengthening by heat treatment is also possible.

However, applications of titanium and titanium alloys are limited by many of the shortcomings in titanium itself, such as a low elastic modulus compared with ferrous alloys, low heat conductivity, more difficult to plastically deform compared with other engineering alloys, poor oxidation resistance at high temperature, low wear resistance and a high friction coefficient. So to overcome these drawbacks, the development of titanium matrix composites and titanium based alloys with high performance have become more and more important research topics.

When alloying titanium there are some difficulties to be confronted. Some elements are hard to dissolve into titanium. For example, rare earth elements have only a limited solid solubility in β-Ti (for La < 8wt%), whereas they are undissolved in α Ti [6]. On the other hand, some elements have acceptable solubility but have a low diffusivity in titanium at certain processing temperatures. An example of this is Mo, where at 1020ºC and 1250ºC it's diffusivity in titanium is only $0.33 \pm 0.15 \times 10^{-13}$ m^2 s^{-1} and $3.25 \pm 1.25 \times 10^{-13}$ m^2 s^{-1}, respectively. This is much lower when compared with other elements as shown in Table 1.2. Difficult diffusion of such elements directly leads to an inhomogeneous distribution in the titanium alloy microstructure and this significantly affects the mechanical properties. The mechanical properties of titanium alloys are shown in Table 1.3 [7]. It is known that processing parameters, such as temperature are key to improving the microstructure of alloys. So exploring new processing techniques and optimizing processing parameters, to achieve an optimised microstructure with good mechanical properties, has become important for improving material quality and reducing the cost of titanium alloys.

Table 1.2 Average diffusivity of alloying elements in β-Ti at sintering temperatures [8-10].

	Al	V	Mo	Cr	Fe
Temperature	($\times 10^{-13}$ m^2 s^{-1})	($\times 10^{-13}$ m^2 s^{-1})	($\times 10^{-13}$ m^2 s^{-1})	($\times 10^{-13}$ m^2 s^{-1})	($\times 10^{-13}$ m^2 s^{-1})
1250 °C	~12.5 ± 7.5	14 ± 01	3.25 ± 1.25	~40	~300
1020 °C	1 ± 0.2	1.25 ± 0.25	0.33 ± 0.15	~4	~30

Table 1.3 Influence of microstructure on selected properties of titanium alloys [7].

fine	*coarse*	*properties*	*lamellar*	*equiaxed*
O	O	Elastic modulus	O	+/- (texture)
+	-	Strength	-	+
+	-	Ductility	-	+
-	+	Fracture toughness	+	-
+	-	Fatigue crack initiation	-	+
-	+	Fatigue crack propagation	+	-
-	+	Creep strength	+	-
+	-	Superplasticity	-	+
+	-	Oxidation behaviour	+	-

1.2 Powder metallurgy (PM) technology and powder compact extrusion from blended elemental powders

Among the different production technologies, the powder metallurgy of titanium alloys and titanium matrix composites is receiving attention because it possesses a series of advantages such as near net shape processing, an easily controllable elemental composition, finer grain size and a homogenous microstructure [11-13]. The general process of powder metallurgy is shown in Fig.1.2. Compared with other technologies, powder metallurgy has a potential to reduce product costs by 20-50% [14]. There has been significant research effort directed towards improving the properties of titanium alloys or titanium matrix composites using powder metallurgy. For titanium alloy and TMCs, changing elemental components to make non-standard alloys, or in the case of MMC's, changing the reinforcing phase and the reinforcement volume fraction, is easily achieved during the mixing stage as we can see in Fig.1.2). Improving the processing technology and refining the microstructure become the main methods to enhance the mechanical properties.

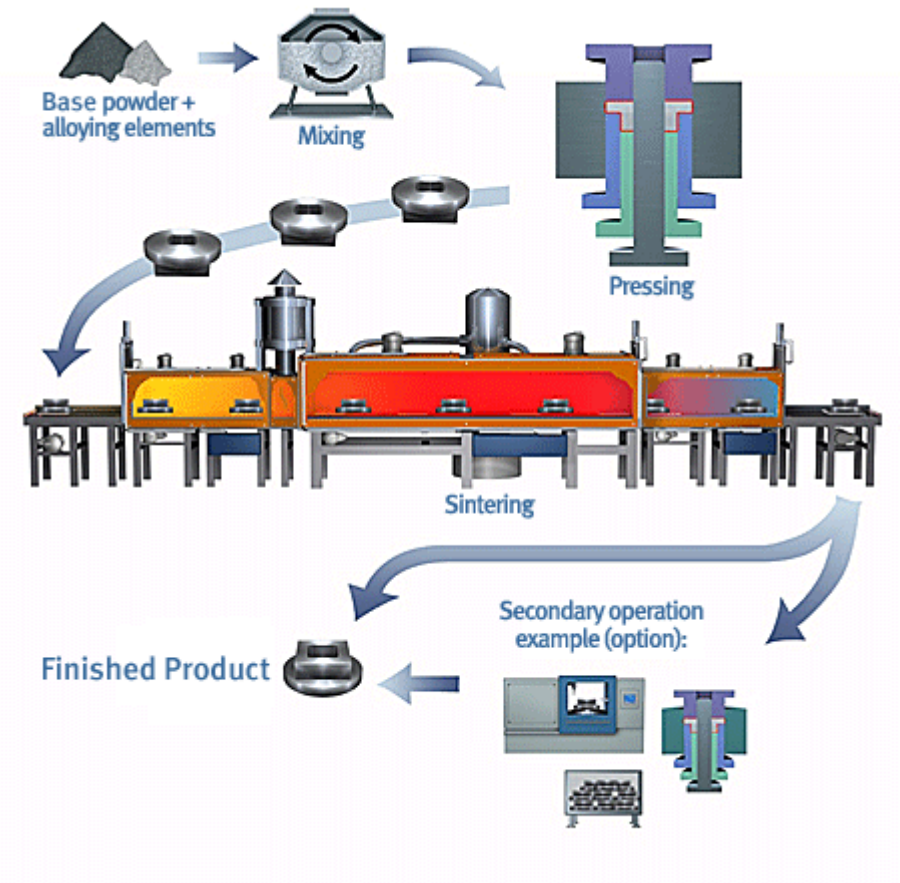

Fig.1.2 General process of powder metallurgy [15].

PM titanium alloys can achieve high strength and more uniform mechanical properties despite their low ductility. Furthermore, there is no anisotropy of grain shape. If a powder compact or sintered compact is not hot worked it is difficult to achieve full density and a component will have a degree of porosity. Sometimes PM processes are used to produce a porous part. Due to porosity, the grain size of a PM alloy is smaller than that found in a cast alloy. Residual pores create stress concentrations which facilitate cracking, thus the material has poor ductility. Hot working (powder compact extrusion, powder compact forging and powder rolling etc.) eliminates the porosity. A PM approach is attractive for economical manufacture of near net shape complex parts where the cost is minimised by reducing the amount of machining and recycling required.

Powder compact extrusion from blended elemental powders (BEPM) is a common way to prepare titanium alloys. Another way is by using pre-alloyed powder. In

BEPM Ti powder is blended with alloying element powders in appropriate proportions to obtain an alloy with a desired composition. The powder mixture is then pressed to produce a powder compact followed by consolidation using extrusion, for example, to give a prismatic bar. A main advantage of this method is added flexibility in the choice of alloying additions and the amounts added, which therefore overcomes the limited alloy chemistry from using pre-alloyed powder. Thermo-mechanical processing also increases the density of final parts and gives a refined grain size which increases yield stress and provides ductility. Various titanium alloys, with good tensile properties, have been successfully produced in this research group using powder compact extrusion or forging from blended elemental powder [16, 17].

Although the microstructural uniformity and tensile strength of PM Ti alloys can be superior to those found in cast Ti alloys, however the ductility and toughness of PM material are generally lower than these properties in cast alloys. This situation is more pronounced in the BEPM process since the alloying process easily introduces impurities to titanium. Furthermore, the compositional heterogeneity in Ti alloys made using BEPM is not as good as that found in pre-alloyed Ti alloys. An even mixing of several types of powder is hard to achieve and the diffusion rate of some elements is very low. As a result, final products can exhibit variable properties.

1.3 Microstructure and corresponding mechanical properties of a two phase titanium alloy

Generally, titanium alloys are classified into three main groups: α (near α), α/β and β alloys. The most common titanium alloy is a two phase alloy such as Ti-6Al-4V which may contain 10-50% β phase at room temperature [18]. The microstructure of two phase alloys can be easily changed by heat treatment to control the amounts and types of β phase. There are four main kinds of microstructure found in a two phase titanium alloy: A Widmanstatten structure (fully lamellar), a basket-weave like structure (fully lamellar), an equiaxed structure and a duplex microstructure as shown in Fig.1.3.

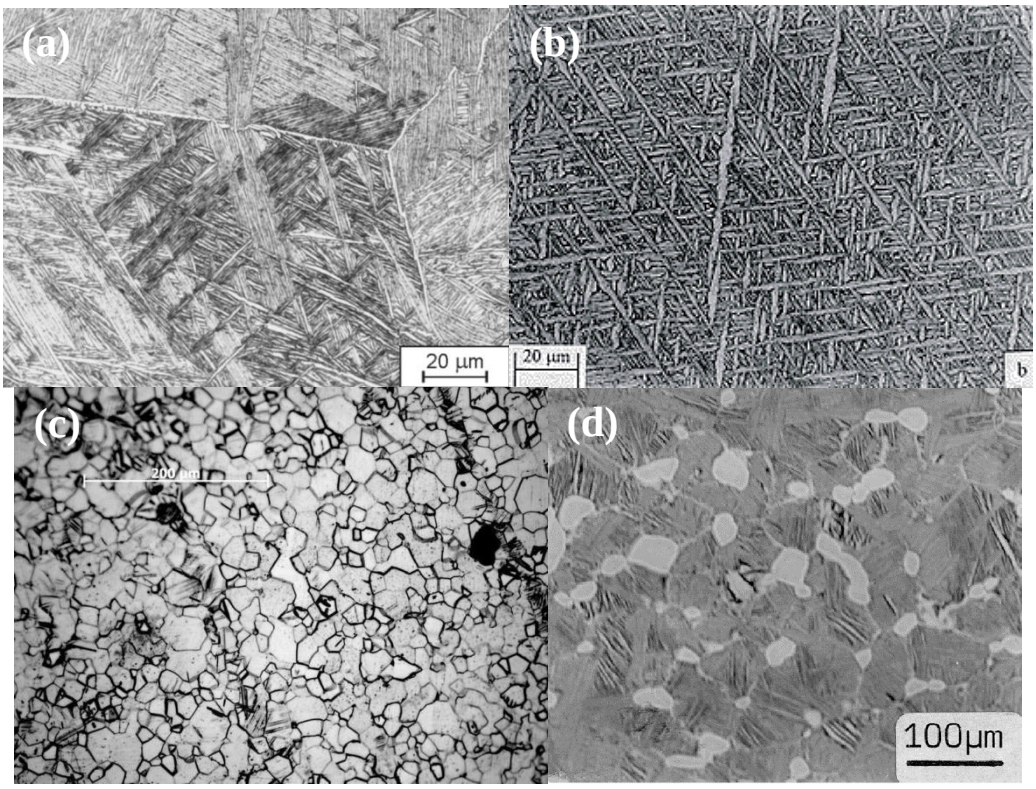

Fig.1.3 Main microstructural types found in a two phase titanium alloy: (a) Widmanstatten structure (fully lamellar) [19], (b) Basket weave like structure (fully lamellar)[20], (c) equiaxed structure and (d) duplex [21].

The main characteristics of a Widmanstatten structure are coarse primary β grains, a continuous α phase along the grain boundaries, a lamellar α phase within the prior β grains and β phase between the α lamellae. The Widmanstatten microstructure is always formed when both the starting and finishing temperatures during deformation remain within a single phase region. The cooling rate determines the final morphology of the α phase: fine lamellae are always obtained at faster cooling rates while coarser lamellae are obtained at lower cooling rates. A two phase alloy with a Widmanstatten structure always exhibits a relatively high tensile strength at room temperature but with low ductility [22]. The ductility and fatigue properties given by an alloy with a basket-weave type of microstructure are always better than those found in material with a Widmanstatten microstructure. However, the fracture toughness is always lower than that found in material with a Widmanstatten structure. An equiaxed microstructure always gives better ductility but lower strength and fracture toughness compared with the other three type of microstructure.

So different processing methods produce different kinds of microstructure which directly affect the mechanical properties of a two phase titanium alloy. A clear understanding of microstructure development and the relationship between microstructure and mechanical properties is very important for designing the processing parameters for titanium alloys.

1.4 Ti-4Al-4Mo-4Sn-0.5Si alloy

Ti-4Al-4Mo-4Sn-0.5Si alloy (Timetal551) is a two phase alloy with similarities to IMI550 which has a composition Ti-4Al-4Mo-2Sn-0.5Si. The reason for increasing the amount of Sn is to enhance room temperature strength while maintaining good forging characteristics [18]. IMI 551 is one of the strongest commercial titanium alloys and is already used for undercarriage components, mounting brackets, pump casings and also for gas-turbine engine components. It can be also used for manufacturing steam-turbine blades, axial and radial compressor parts, connecting rods and other high speed rotating and reciprocating components[18]. Its room temperature strength ranges from 1250-1400 MPa and this alloy has useful creep properties up to 400^{o}C. The traditional processing technology for Timetal551 is by forging and subsequent heat treatments. But because the beta transus temperature of Timetal551 is higher than that for other common titanium alloys, it is more difficult to forge than other titanium alloys such as Ti64. There is very little reported work on the PM processing of Timetal551.

1.5 Titanium and titanium alloy matrix composites

Titanium matrix composites (TMCs) possess a combination of excellent mechanical properties and high temperature durability that make them attractive materials for commercial automotive, aerospace and advanced military applications. Two main kinds of reinforcement, such as continuous fibres and discontinuous whiskers or particles, are used. Continuous fibres, e.g., SCS-6, have been used to reinforce Ti and Ti alloys and applied successfully in many fields

[23-25]. However, there are several disadvantages from using continuous fibre reinforced composites such as expensive fibres, a costly complex fabricating process, residual thermal stresses induced by large differences in the coefficients of thermal expansion between fibre and matrix, chemical reactions between titanium and fibres, highly anisotropic mechanical and physical properties. These disadvantages have urged researchers to turn their attention to particulate reinforced titanium composites [26]. Particulate reinforced TMCs have attracted much attention because of their more isotropic properties, easy secondary operation, improved mechanical properties, low reaction tendency between particles and matrix, and other significant technical and economic benefits. Many kinds of ceramics have been introduced as reinforcements for titanium matrices with satisfactory results: TiC, TiN, TiO_2, Si_3N_4, SiC, TiB_2, TiB, etc. [27-33]. The application of TiB as a reinforcement is of interest because of its attractive properties, such as a high melting point (The melting point of TiB is 2473^{o}C), high compatibility with and a similar Poisson's ratio to titanium, little interfacial reaction and a high elastic modulus etc.. In this study, the structure and properties of titanium composites with TiB reinforcement were investigated.

1.6 Objectives of this thesis

This thesis aims to produce a high strength titanium alloy and titanium matrix composite using PCE from blended elemental powders. In this study two very different ways of producing a high strength titanium alloy using PCE through a blended elemental approach are investigated. The first approach is through the synthesis of the high strength alloy Ti-4%Al-4%Mo-4%Sn-0.5%Si and the second approach investigates the feasibility of achieving high strength by producing a titanium alloy composite and for this TiB/Ti6Al4V was chosen for this study.

It is well known that an inhomogeneous elemental distribution is easily formed when BEPM is used for preparing titanium alloys or titanium alloy matrix composites. A non-uniform elemental distribution affects the performance of the alloy, and also contributes to a variation in the alloy properties after repetitive manufacturing steps. There is no reported information in the literature on

Timetal551 produced by PM and especially using BEPM technology. There are many reports on TMCs reinforced by TiB, but the overall mechanical properties especially ductility are not satisfactory. Therefore this study investigates the feasibility of using BEPM to produce the alloy Timetal551 and TiB/Ti6Al4V with the following targets in mind:

Firstly, an optimisation of the processing parameters by studying their effect on elemental diffusion and resulting microstructure. This is followed by a study of the relationship between microstructure and mechanical properties for Timetal551.

Secondly, a study of the effect of starting powder characteristics on microstructure and tensile properties for Timetal551.

Thirdly, a successful route for processing Timetal551 with good properties using BEPM. The aim of this study is to provide constructive ideas and guidance for BEPM processing of other titanium alloys with complex elemental components.

Lastly, an optimisation of the processing parameters for producing a TiB/Ti6Al4V composite by studying their effect on the morphology of the reinforcement and the mechanical properties of the composite. This includes a study of the effect of starting powder characteristics on the morphology of the reinforcement and the tensile properties of a TiB/Ti6Al4V composite.

References

[1] G. Lütjering, J.C. Williams, Titanium, Springer, 2003.
[2] D. Askeland, W. Wright, Essentials of Materials Science & Engineering, Cengage Learning, 2013.
[3] I.J. Polmear, London and New York, Edward Arnold, 1989, 288, (1989).
[4] M. Qian, International journal of powder metallurgy, 46 (2010) 29-44.
[5] C. Leyens, M. Peters, Titanium and titanium alloys, Wiley Online Library, 2003.
[6] SML Sastry, P.J.Meschter, J.E.O'Neal. Metall. Trans. A, 15 (1984) 1451-1463.
[7] C. Layens, M. Peters, Wiley-VCH, 2003, pp. 12-13.
[8] A. Carman, L. Zhang, O. Ivasishin, D. Savvakin, M. Matviychuk, E. Pereloma, Materials Science and Engineering: A, 528 (2011) 1686-1693.
[9] G. Neumann, C. Tuijn, Self-diffusion and impurity diffusion in pure metals: handbook of experimental data, Elsevier, 2011.
[10] C.H. Y. Mishin, Acta Mater., 48 (2000) 589-623.
[11] F. Froes, D. Eylon, International Materials Reviews, 35 (1990) 162-184.
[12] T. Fujita, A. Ogawa, C. Ouchi, H. Tajima, Materials Science and Engineering: A, 213 (1996) 148-153.
[13] Y. Liu, L. Chen, H. Tang, C.T. Liu, B. Liu, B. Huang, Materials Science and Engineering: A, 418 (2006) 25-35.
[14] F.H. F, Titanium Net shape Technologies. The metallurgy society of AIME press, 1984, pp. 1-20.
[15] http://www.gkn.com/sintermetals/capabilities/conventional-pm/process/Pages/default.aspx.
[16] M.T. Jia, D.L. Zhang, B. Gabbitas, Key Engineering Materials, 520 (2012) 82-88.
[17] F. Yang, D.L. Zhang, H.Y. Lu, B. Gabbitas, Key Engineering Materials, 520 (2012) 70-75.
[18] G. Welsch, R. Boyer, E. Collings, Materials properties handbook: titanium alloys, ASM international, 1993.
[19] J. Sieniawski, W. Ziaja, K. Kubiak, M. Motyka, Titanium Alloys-Advances in Properties Control, (2013) 69-80.
[20] V. Oliveira, R. Chaves, R. Bertazzoli, R. Caram, Brazilian Journal of Chemical Engineering, 15 (1998) 326-333.
[21] G. Lütjering, Materials Science and Engineering: A, 243 (1998) 32-45.
[22] W. Jinyou, Shanghai Science and Technology Press, Shanghai, 1985.
[23] McCullough C. Continuous fiber reinforcements for metal–matrix composites. ASM handbook online, Vol. 21. Composites, Materials Park: ASM International; 2002.
[24] Larsen JM, Russ SM, Jones JW. An evaluation of fiber reinforced titanium matrix composites for advanced high temperature aerospace applications. Metall Mater Trans A 1995;26:3211–23.
[25] Mall S, Fecke T, Foringer MA. Introduction. In: Mall T, Nicholas T, editors. Titanium matrix composites. Lancaster [PA]: Technomic Co.; 1998. p. 1–21.
[26] Gorsse S, Petitcorps Y Le. A new approach in the understanding of the SiC/Ti reaction zone composition and morphology. Composites A 1998;29:122–1228.
[27] Kim YJ, Chung H, Kang SJL. Mater Sci Eng A 2002;333(1–2):343–50.

[28] Cui ZD, Zhu SL, Man HC, Yang XJ. Surf Coatings Technol 2005;190:309 13.
[29] Joshi PB, Marathe GR, Murti NSS, Kaushik VK, Ramakrishnan P. Mater Lett 2002;56:322.
[30] Alman DE, Hawk JA. Wear 1999;225–229:629.
[31] Selamat MS, Watson LM, Baker TN. J Mater Proc Technol 2003;142:725 37.
[32] Furuta T, Yamaguchi T, Shibata Y, Saito T. Titanium'99. In: Proceedings of the ninth world conference of titanium, 1999. p. 1917–24.
[33] Godfrey TMT, Goodwin PS, Ward-Close CM. Titanium'99. In: Proceedings of the ninth world conference of titanium, 1999. p. 1868–77.

Chapter 2 Literature Review

2.1 Introduction

This thesis focuses on the preparation of the titanium alloy Ti-4Al-4Mo-4Sn-0.5Si and a titanium alloy matrix composite TiB/Ti6Al4V by powder compact extrusion using Blended Elemental Powder Metallurgy (BEPM). The scope of this thesis also includes work on an optimisation of processing parameters through a study of the effects of different processing conditions and parameters on microstructure, phase morphologies and mechanical properties. This literature review mainly focuses on the current knowledge and technologies related to blended elemental powder metallurgy which includes powders, powder compaction and extrusion, and their relationship to the microstructure and mechanical properties of two phase titanium alloys. Then the current situation and achievements for TMCs reinforced by TiB will be reviewed. Furthermore this review also considers some of the obstacles, such as the different diffusivity rates of different elements in a titanium matrix, to getting a homogenous microstructure using BEPM for preparing titanium alloys. This literature review presents guidance and recommendations for experimental design, results analysis and optimization of processing parameters.

2.2 Powders

The purity and cost of powders directly determine the mechanical properties and cost of PM titanium and titanium alloys. Although many approaches for producing titanium or titanium alloy powders with satisfactory purity and cost have been developed or are under development, high purity carries a cost premium [2]. Different types of titanium powders are illustrated in Table 2.1. Among the different types of titanium powders, except for powders under development, three kinds of powder are widely used, namely HDH (Hydride–dehydride) (Kroll), atomized and PREP (Plasma rotating electrode process) powders. From Table 2.1 we can see that HDH titanium powder has many advantages such as low cost, good compactability at room temperature and low chloride content. Although it is much cheaper than atomized and PREP powders,

it has in general a higher oxygen content and lower purity than the other two kinds of powder. Atomized and PREP powders have high purity but their cost is too high, especially for PREP powder. So HDH titanium powder and atomized titanium powder, especially Gas Atomized (GA) powders are widely used to reduce cost and improve the mechanical properties. The morphologies of HDH Ti and GA Ti powder are shown in Fig.2.1. Another reason for the wide application of HDH titanium is that the oxygen and chloride level can be kept at acceptable levels, for example oxygen levels below 0.4wt% are common, but significantly lower oxygen content in the region of 0.15wt% incurs much higher production costs [3, 4]. Researchers [5, 6] already have shown that powder morphology impacts its area of application. For example, spherically shaped GA titanium powder has good flowability and low oxygen content makes it suitable for producing injection molded parts. Furthermore regular and irregular shape of the powder demonstrates different distribution type of oxygen outlayer, and may impact the diffusion of oxygen and other alloying elements in titanium matrix [6, 7].

Table 2.1 Characteristics of different types of titanium powders [2, 8-10].

Type/process	Powder type	Advantages	Status/disadvantages
Hunter process (pure sodium)	Elemental	Low cost; excellent for cold press and sinter	Limited availability and high chloride
HDH (Hydride-dehydride) Kroll process (pure magnesium)	Elemental	Low cost, good compactability, readily available and low chloride	
HDH powder produced from alloys	Prealloyed	Readily available	High cost and fair compactability
Gas Atomized	Prealloyed	High purity and available	High cost and not cold compactable
REP/PREP (rotating electrode powder/plasma rotating electrode powder)	Prealloyed	High purity	High cost and not cold compactable
Titanox (Titanox development Ltd. New Zealand)	Prealloyed	Low cost and available	Quality and production scale up
ITP (international Titanium Powder)/Armstrong	Elemental and prealloyed	Compactable, moderate cost and potential for low cost	Processibility/quality, production scale up
Fray	Elemental and prealloyed	TBD	developmental
MER (MER corp.,Tucson, Ariz)	Elemental and prealloyed	TBD	developmental
CSIRO TiRO (Melbourne, Australia)	Elemental and prealloyed	TBD	developmental

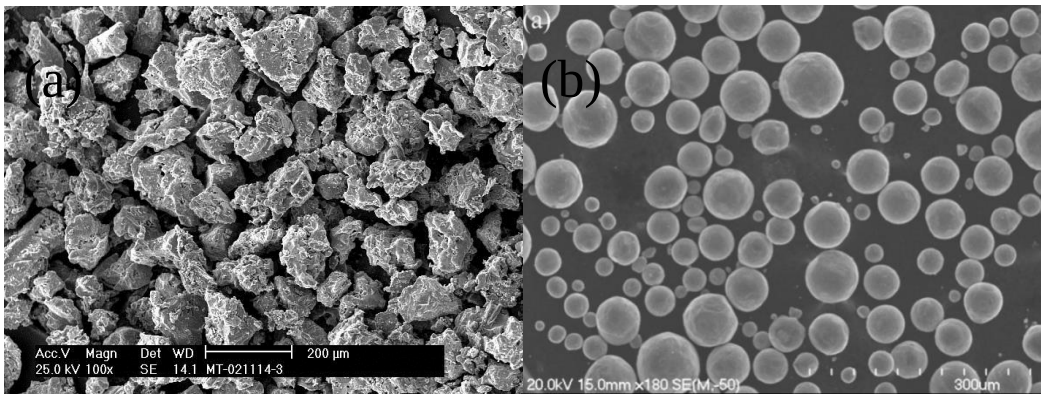

Fig.2.1 SEM photomicrograph of (a) HDH titanium powder (Courtesy of Metal Titanium Co., Ltd, China) and (b) GA titanium powder.

When selecting elemental powders for alloying, high purity and proper particle size are the highest priority. Impurities introduced through the powders can directly impact on the mechanical properties of titanium alloys since titanium is sensitive to most impurities such H and O. Particle size mainly impacts on the degree of elemental diffusion, especially for some alloying elements such as Mo and rare earth elements, which have low diffusivity in titanium [1, 11].

2.3 Powder consolidation

Powder consolidation is usually categorised into two principle groups: conventional PM which is known as press-and-sinter, and those methods which achieve densities close to full density. For all consolidation processes good powder compaction is important for achieving satisfactory density. Powder compact extrusion using an elemental powder mixture belongs to the second group in which the extrusion process consolidates the powder to nearly full density and refines the microstructure. This section of the thesis mainly focuses on powder compaction and powder compact extrusion.

2.3.1 Powder compaction

Under high pressure powders are compacted by various methods such as die compaction, cold isostatic compaction, cold forging and warm compaction, where the application of pressure packs the powders and reduces porosity (some compaction options are illustrated in Table 2.2 [12]).

Table 2.2 Some compaction options [12].

Process	Cold Isostatic Compaction	Cold Forging	Die Compaction	Warm Compaction
Pressure	Moderate 400MPa	Very high >800MPa	High 700MPa	High 700MPa
Temperature	Ambient	Ambient	Ambient	Warm
Deformation Rate	Low	High	High	High
Pressing Direction	3	1	1	1
Use	Moderate	Low	Extensive	Low

Although many compaction methods are used, as shown in Table 2.2, the most prevalent method for PM production is die compaction, which is cost effective and can be done with relatively straightforward tooling. During die compaction, pressure is applied to the powder with punches that move in the vertical direction and green density increases with increasing compaction pressure. The general die compaction process is illustrated in Fig.2.2. For die compaction a lubricant such as graphite should always be applied between the die wall and the powder. This is because the friction between the powder and die wall during die compaction leads to an inhomogeneous density distribution which causes residual stresses in the green body. This may cause unwanted defects, such as pores and cracks in PM parts during subsequent high temperature consolidation [13].

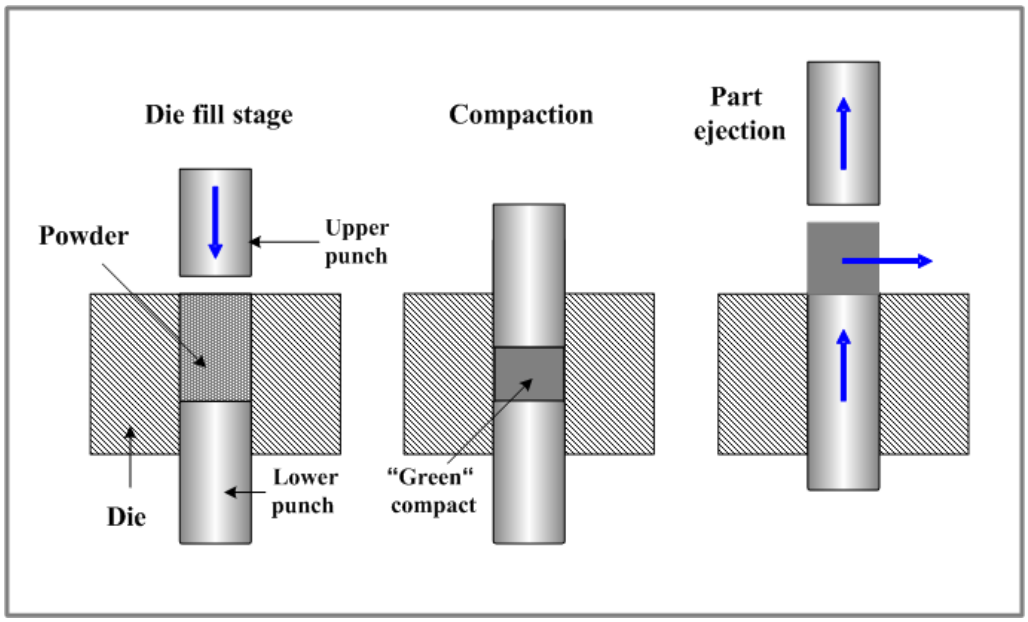

Fig.2.2 General die compaction process of general metal powders (Cold die compaction) (Courtesy of SubsTech)

Previous research has shown that there are certain advantages to heating the powders above room temperature before powder compaction. From this, warm compaction emerged. A practical application of warm compaction of powders was applied in 1994 with the introduction of Hoegamaes Inc Ancordense and Densemix Powders [14]. It was found that when the powder and die were heated, with every 100^{o}C rise in compaction temperature there was an 0.08g/cm^{3} increase in green density [15, 16]. Experimental work at Hogamas AB showed that there was a 30% decrease in the compressive yield strength of iron powder when the powder was heated to 150^{o}C [17]. It should be noted that warm compaction cannot be applied when a powder mixture contains low melting point elements, such as Sn, since these elements may melt if the temperature is increased too much. When under pressure from other un-melted elemental particles, the melted elements may be squeezed out leading to their loss leading to an inhomogeneous distribution of such elemental powders. So in this thesis, due to the presence of Sn in the alloy compositions investigated, warm compaction is not recommended.

2.3.2 Hot pressing and Forging

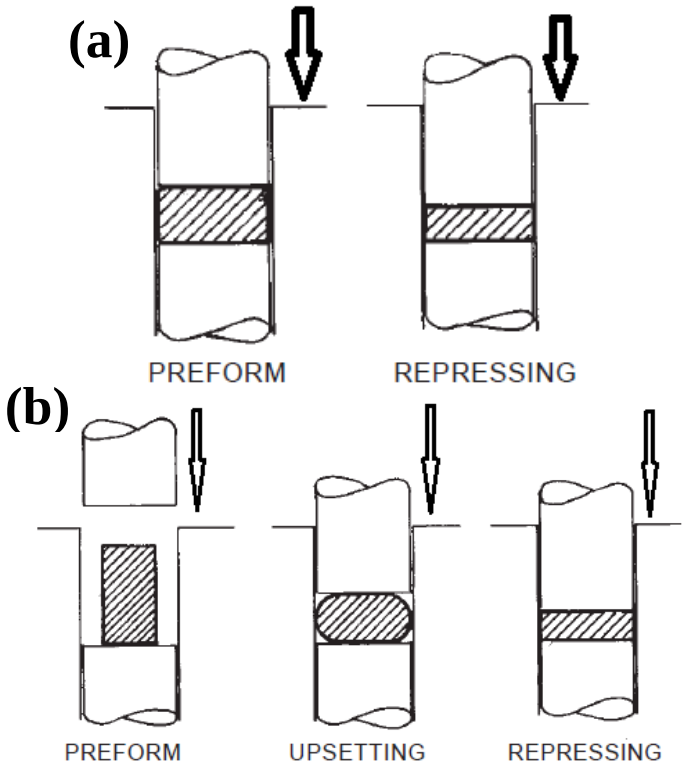

Fig.2.3 Deformation mode for (a) hot pressing and (b) forging

Hot pressing and forging are similar but have different deformation modes (as shown Fig.2.3). Forging deformation involves considerable lateral flow and shearing of the powder particles [18]. This action causes any oxide films on the powder particles to be broken up, then the clean metal is exposed and this enables a strong metallurgical bond to form across the collapsed pore interfaces. This enhances the material properties. Die forging at higher temperatures has been investigated and proved to be a possible economical method for the production of Ti-6Al-4V alloy and near net-shape intermetallic blade forms [19]. In a study to investigate turbine blade forging, a preform was furnace heated to 920^{o}C, but it cooled to a temperature of about 850^{o}C during transfer from the furnace to the die. A finished blade forging is shown in Fig.2.4.

Fig.2.4 Forging of a blade [19].

Hot pressing is another common way to consolidate powder at high temperature using axial pressure. The production of large billets can be accomplished by compacting powder in heated dies. The use of elevated temperature and long dwell times allows densities of nearly full density to be achieved at compaction pressures that are one third to one half those needed for cold pressing to lower levels [18]. But after hot pressing there is always 3-5% porosity remaining and the parameters used during hot pressing can directly influence the quality of the pressed part. So another hot processing method, such as extrusion can be applied after hot pressing, to reduce the porosity level.

Hot pressing has been explored as a method for producing large-scale amorphous and nanomaterial by PM processing due to the limited size bulk materials based on the present technology. Although consolidation by hot pressing destroys the original microstructure of amorphous and nanomaterial [20-24], by adjusting the consolidation conditions such as temperature, pressure and time, used for the powder, large bulk material can be produced. However serious problems occur because of the reactions between these alloys and the tool materials. Such problems can be overcome by using hot isostatic pressing (HIP), where these interactions are more easily controlled [18]. Currently hot pressing is also a very important process in the development of new ceramics and metal matrix or ceramic matrix composites for a wide variety of applications. For example a material consisting of 40% silicon carbide fibres in a ceramic matrix that has been processed by hot pressing [25]. Bulk metal matrix composites have also been produced by hot pressing a blend of prealloyed Al 6061 powder with 15vol.% silicon carbide powder [26, 27]. A yield strength of 400MPa and an elongation to

fracture of 2.5% were obtained. Also the sliding wear resistance of metal matrix composites was better than that obtained for monolithic Al 6061 alloy [27].

2.3.3 Extrusion

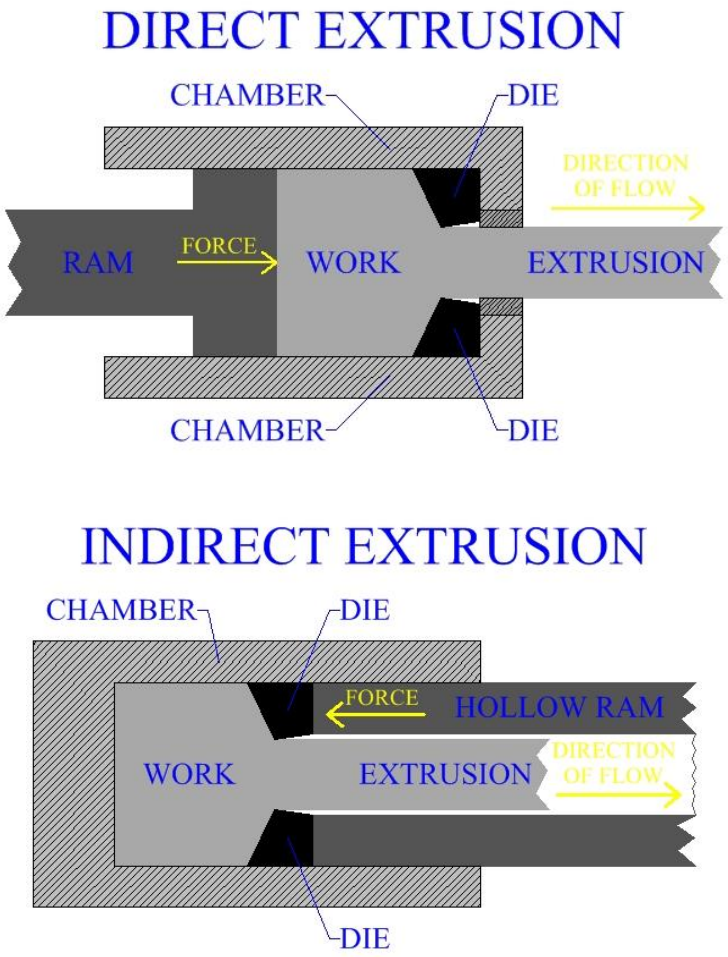

Fig.2.5 General illustration of the direct extrusion and indirect extrusion (Courtesy of The Library of Manufacturing.)

There are two main types of extrusion mechanisms, direct and indirect. A general illustration of direct and indirect extrusion is shown in Fig.2.5. In direct extrusion, which is more widely practiced since it is more cost effective, the ram pushes a workpiece forward through a die, causing a reduction in cross-sectional area of the workpiece (as show in Fig.2.5). Hot extrusion possesses the merits of improving the deformability of metals and enhancing the overall quality of the product, so it is widely used for producing large scale or high quality required titanium tubes, rods and so on [28-30]. The extrusion parameters for some titanium and titanium alloys are shown in Table2.3.

Table 2.3 Extrusion parameters for bar products of titanium and titanium alloy[31]

Alloy	Extrusion temperature(°C)	Extrusion ratio	Lubricant	Extrusion speed/(mm/s)
CP-Ti	700-800	4-30	Copper can	25-150
Ti-6Al-4V	900-1000	5-15	Glass	90-120
Ti-5Al-2.5Sn	950-1200	5-15	Glass	90-120

Parameters such as extrusion ratio and extrusion speed have a direct impact on the quality of final products. The extrusion ratio expresses the deformation extent of the material, so in order to improve the microstructure and properties a high extrusion ratio is usually preferred. A study [32] has shown that for some titanium alloys a high extrusion ratio causes an additional increase in temperature to beyond that for some phase transformations. This can lead to a coarsening of the microstructure and a deterioration in mechanical properties. However, if the temperature can be controlled to be within a certain range, an increase in extrusion ratio can reduce the grain size with an improvement in mechanical properties [32-35]. It has been shown that for an aluminium-magnesium alloy AZ31, a further increase in the extrusion ratio beyond a certain value has little effect on the microstructure and changes in mechanical properties will not be so obvious [32, 33], as shown in Fig.2.6 and Fig.2.7 and Table 2.4. Overall the choice of suitable extrusion parameters mainly depends on the properties of the material to be extruded.

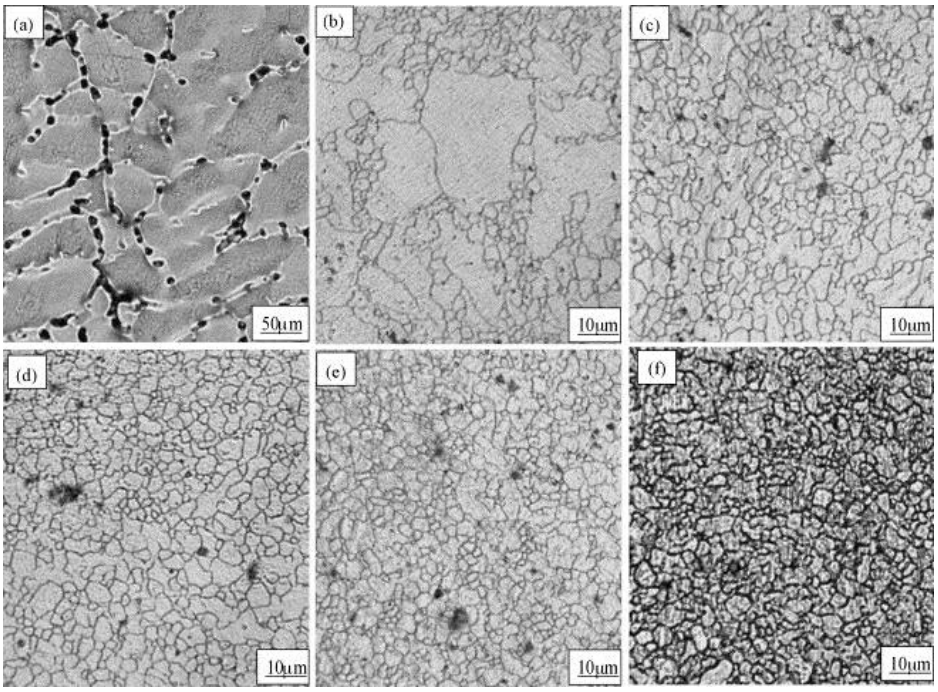

Fig.2.6 Microstructure of AZ31 Mg alloy extruded at 250 C with different extrusion ratio: (a) 0, (b) 7 (c) 24, (d) 39, (e) 70, and (f) 100 [32].

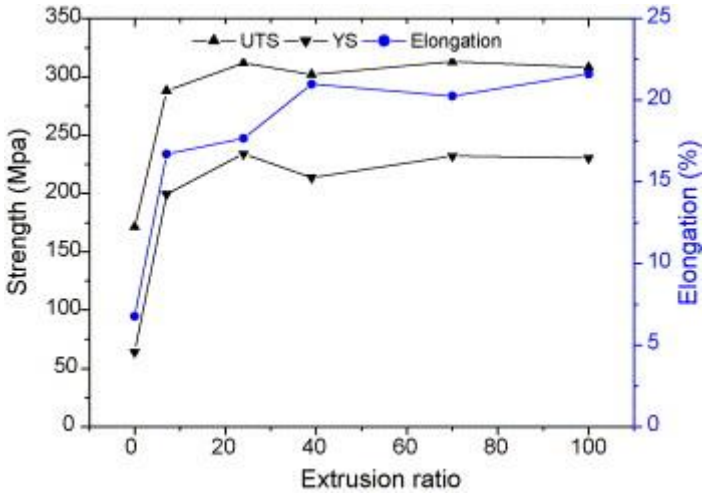

Fig.2.7 Influence of extrusion ratio on tensile properties of AZ31 alloy [32].

Table 2.4 Grain size and extrusion ratio for extruded AZ31 Mg alloy at 250°C[32].

Extrusion ratio	Mean grain size (μm)
7	25
24	10
39	8
70	5
100	4

A moderate extrusion speed for titanium is normally in the range 80-130mm/s. The effect of extrusion speed on the degree of additional heating can help towards maintaining the temperature of titanium during extrusion. The amount of process heating as a function of extrusion speed and extrusion ratio could be determined through computer simulation which would allow for better processing control [31, 36-38].

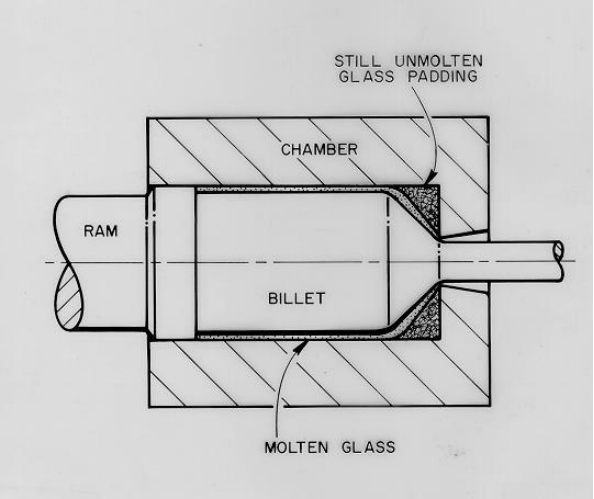

Fig.2.8 Glass lubricated hot extrusion process (Courtesy of Metalforming-Inc.).

Lubrication plays an important role in extrusion. Efficient lubricants prevent direct metallic contact, reduce extrusion loads and wear and improve product quality and tool life. Glass lubricated hot extrusion is widely used for many different kinds of products (as shown Fig.2.8). In glass lubricated hot extrusion, the behaviour of the glass lubricant is quite sensitive to process conditions and die design. The use of improper conditions can lead to surface defects. A typical thickness of the glass film is very small, making measurement difficult and numerical analysis of lubricant behaviour impractical. A mathematical model has been explored by Dinesh Damodaran [39] which can be used in the selection of processing conditions that result in improved surface quality. For extruding titanium and titanium alloys and even titanium matrix composites a graphite lubricant can be successfully and cost effectively applied [6, 7].

2.3.4 Powder Compaction Extrusion

Powder compact extrusion (PCE) is a typical powder metallurgy process for Ti and titanium alloys. In recent years it has been investigated as a low-cost titanium

and titanium alloy powder consolidation technique and successfully applied to a variety of titanium alloys and titanium matrix composites [6, 7, 40-43]. The general process of PCE is illustrated in Fig.2.9. There are two different approaches for PCE as shown in Fig.2.10. The difference between Approach I and Approach II is between using hot pressing and vacuum sintering. The cost of Approach II is higher than of Approach I and used for those titanium alloys where the amount of oxygen pick-up during processing has to be minimised. In practice most titanium alloys and composites can be prepared using approach I with a satisfactory oxygen content, normally between 0.3-0.4wt%, in the final parts [6, 7, 41, 42].

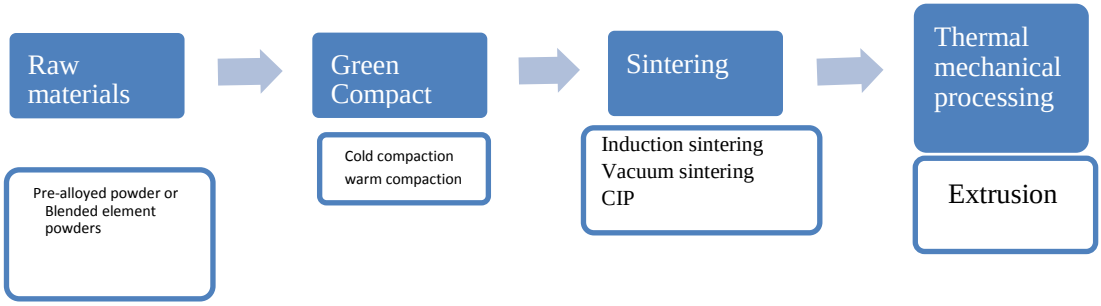

Fig.2.9 General Process of powder compact extrusion

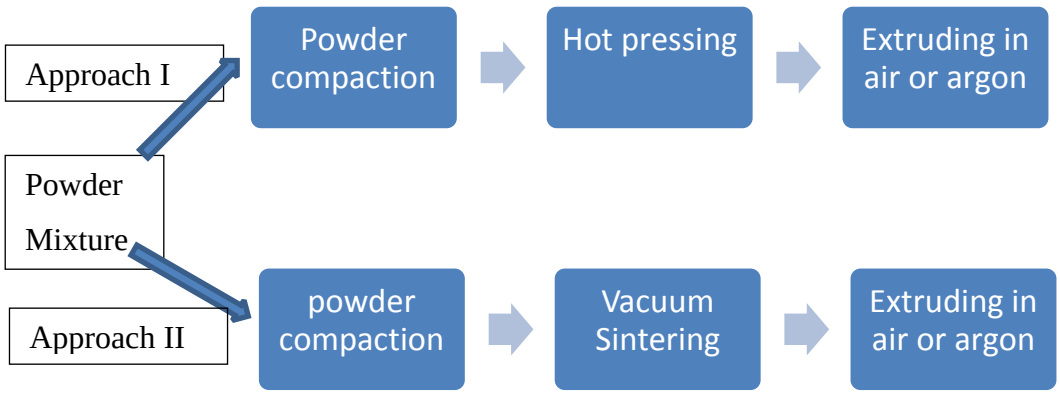

Fig.2.40 Two approaches for powder compaction extrusion of titanium and titanium alloys.

For each Approach (I or II) there are four stages, namely powder mixing, powder compaction, sintering and extrusion, which can effect the quality of final parts. Costs can be reduced when blended elemental powders are used. At the powder

mixing stage it is imperative that proper equipment is used to achieve a homogenous elemental distribution in a powder mixture, otherwise an inhomogenous microstructure will be formed which will directly impact on the mechanical properties of the final extruded parts. The approach used for powder compaction depends on the type of powder to be compacted. Normally cold compaction is used when the main powder constituent is HDH titanium due to relative good compaction behavior, but if the main constituent is GA or PREP titanium powder, warm compaction can be always used due to their relative bad compaction behavior[44]. When carrying out warm compaction the temperature should be below 350^{o}C, because at temperatures above 350^{o}C, there is increased risk of oxygen pick-up. If it is necessary to carry out warm compaction above 350^{o}C, a protective argon atomosphere is used. Compact sintering must be carried under argon protection and to avoid large amounts of oxygen pick-up, the oxygen content should be $\leq$ 200ppm. But the role of argon protection for extrusion is not required as long as the sintered density before extrusion is >93%. This is because the time for an extrusion is short and only a thin oxide layer is formed on the surface of a workpiece.

The main advantages of using PCE for titanium alloy processing are lower cost, especially when blended elemental powders are used, flexibility in selecting the alloy chemical composition and in microstructural design. Last but not least there is a potential for minimising oxygen pick-up during processing. Previous work, using a blended elemental approach, has shown that inhomogenous microstructures can result after PCE [7, 41, 42] if the elemental distribution in the starting powder mixture is not homogenous, and if the processing parameters, such as the sintering temperature and holding time at the sintering temperature are not the optimum. The importance of an appropriate sintering temperature and sintering time to achieve complete dissolution and diffusion of alloying elements was introduced in chapter 1. The effect of extrusion temperature and holding time on the mechanical properties of Ti-64 extruded rods is shown in Fig.2.11 and Fig.2.12, respectively. So in the design of processing parameters for a titanium alloy prior to PCE, achievement of a homogenous elemental distribution in a powder mixture, a high enough sintering temperature with a long enough holding time during sintering to achieve a homogeneous elemental distribution, >93% full

density and an appropriate extrusion temperature and extrusion speed, are considered to be high priorities.

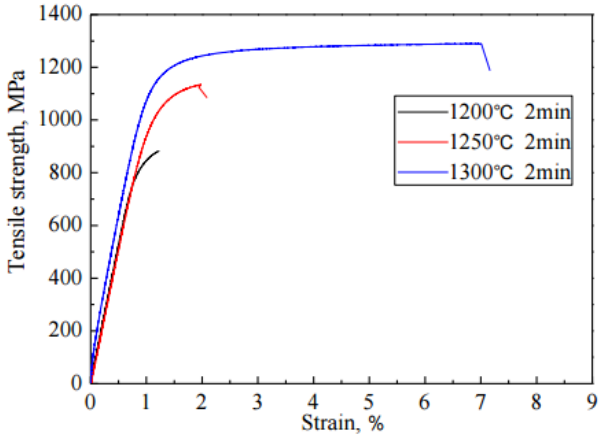

	1200 ℃ 2min	1250℃ 2min	1300 ℃ 2min
Yield strength(MPa)	-	1061	1255
Tensile strength(MPa)	886	1135	1300
Ductility (% elongation to fracture)	1.2	2.0	7.0%

Fig.2.11 The effect of extrusion temperature on the mechanical properties of Ti-64 extruded alloy [41, 42].

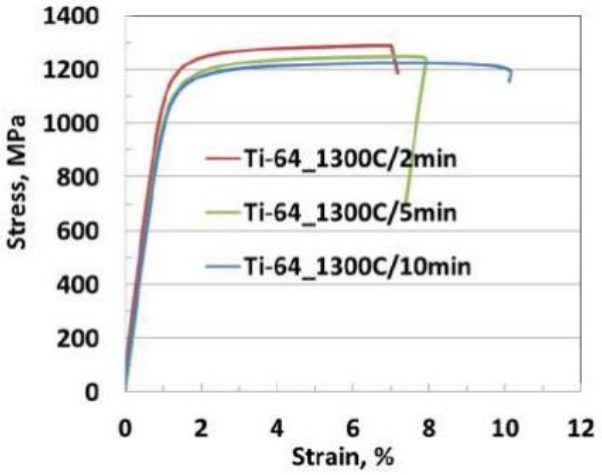

	1300 ℃ 2min	1300℃ 5min	1300 ℃ 10min
Yield strength(MPa)	1255	1216	1180
Tensile strength(MPa)	1300	1254	1215
Ductility (% elongation to fracture)	7.0%	8.0%	10.0%

Fig.2.15 The effect of holding time on the mechanical properties of Ti-64 extruded alloy [6].

2.4 The effect of alloying elements on the mechanical properties of titanium alloys

The chemical composition of titanium alloys directly determines the mechanical properties, because as indicated in chapter 1, the chemical composition primarily determines the volume fraction and morphology of the α and β phases. The number of slip systems in the hcp crystal structure α is limited [45], therefore the ductility of α is much lower of the bcc β structure. So the morphology and volume fracture of the α and β phases influences the mechanical properties of titanium alloys, especially their ductility. The most important consideration in designing new titanium alloys is the influence of alloying elements on microstructure and mechanical properties.

The stability of α and β phases [46, 47] is influenced by particular alloying additions and this depends on the number of electrons per atom of alloying element. Alloying elements with an electron/atom ratio less than 4 (Al, Ga, O, N, C) stabilize the α phase and elements with an electron/atom ratio greater than 4 (V, Mo, Nb, Fe, Cr, Ni, etc.) stabilize the β phase, while elements with an electron/atom ratio equal to 4 (Sn and Zr) are neutral [46]. Depending on the interaction of elements with titanium, Kornilov classified the elements into four groups [48] as shown in Table 2.5. This table indicates the mechanisms of phase stabilisation and clarifies the role of particular elements in stabilsing the α or β phase. For example, Mo is a β phase stabiliser because Mo is isomorphic with the β phase and normally forms a continuous solid solution with the β allotrope of titanium. Al stabilises the α phase because it forms a peritectoid reaction with titianium and raises the β transus temperature.

Table 2.5 Four groups elements classified depending on the interaction of elements with titanium [48].

Group	Main characteristics	Example
Continuous Solid-solution-forming elements with α or β titanium	Outer-shell electronic configuration identical to that of titanium so the structure is also isomorphic to titanium.	V, Mo and Ni are isomorphic to β titanium and form a continuous solid solution with the β allotrope of titanium.
Limited solid-solution-forming elements with α and β titanium	Elements undergo eutectoid transformation and lower the β transus or peritectoid reaction and raise the β phase.	Cr, Ni, Fe lower the β transus while Al shows a peritectoid reaction and raise the β transus.
Ionic and Covalent compounding-forming	Form ionic and covalent compounds with titanium and do not go into solid solution in α or β titanium.	Fluorine, chlorine, bromine, iodine, sulphur, etc.
Elements not interacting with titanium	No interaction with titanium	Alkali or alkaline earth metal except beryllium.

The amount of alloying additions to titanium is also critical for determining mechanical properties. Al being an α stabilizer is of commercial importance and is a constituent of most key commercially available titanium alloys. But if the amount of Al exceeds a certain level the embrittling intermetallic compound, Ti_3Al, will be precipitated [45]. So as the Al content increases the ductility and the deformation capability deteriorates. Based on accumulated practical knowledge a so-called aluminium-equivalent [45, 46], represented by the following equation, was deduced by researchers.

Al eq. = wt.% Al + 1/3 wt.% Sn + 1/6 wt.% Zr + 10 wt.% O < 9 wt.%

For this reason the Al content is normally restricted to a maximum of 7% in commercial titanium alloys to avoid precipitation of Ti_3Al. In addition to the upper limit there is also a lower limit of 2% of Al [49]. This is because if the Al content is extremely low, the effect of Al on the microstructure will not be obvious. The content ranges and effects of some popular alloying elements are given in Table 2.6.

Table 2.6 Ranges and effects of some popular alloying elements[49].

Alloying elements	Range (approx.) wt.%	Effect on microstructure and properties of titanium alloy
Aluminium	2-7	α stabilizer,
Tin	2-6	α stabilizer
Vanadium	2-20	β stabilizer, improve high temperature and properties corrosion resistance
Molybdenum	2-20	β stabilizer, improve high temperature properties and corrosion resistance
Chromium	2-12	β stabilizer, significant strengthening effort, normally used for high strength β alloy
Copper	2-6	β stabilizer
Zirconium	2-8	α and β strengthener
Silicon	0.2-1	Improve creep resistance, improve the heat resistance and thermos-stability of alloy

But the alloying element content is not rigidly fixed in a particular titanium alloy, it can vary within a certain range without there being any obvious impact on

mechanical properties, Table 2.7 shows the typical chemical composition of Timetal551 [50].

Table 2.7 Typical chemical composition of Timetal551

Element	Minimum wt.%	Maximum wt.%	Normal wt.%
Al	3	5	4
Sn	3	5	4
Mo	3	5	4
Si	0.3	0.7	0.5
Fe	…	0.2	…
C	0.05	0.2	…
O	…	0.25	…
N	…	0.05	…
H	…	0.125	…

2.5 Alloying element diffusivity in titanium

An understanding of the diffusion rates of alloying elements in α and β phases of titanium is critical to the design or evaluation of appropriate processing parameters for producing a titanium alloy with a complex chemical composition. Much of alloy processing technology depends on diffusion for structural change [51]. Examples of this are solutioning and aging heat treatments, hot working and the recrystallization temperature. A lot of diffusivity data for different alloying elements, such as Mo, Cr, Al has been measured recently or in the past few years [1, 52-60]. But the mechanism of diffusivity is complicated and still not completely understood. With progress in our understanding of diffusivities, new diffusivity data has been determined in recent years. A selection of diffusivity data is shown in Fig.2.13. Typical solubility of alloying elements in Ti at typical processing temperatures and the average diffusivity of alloying elements in β Ti at sintering temperatures are also given in Tables 2.8 and Table 2.9, respectively.

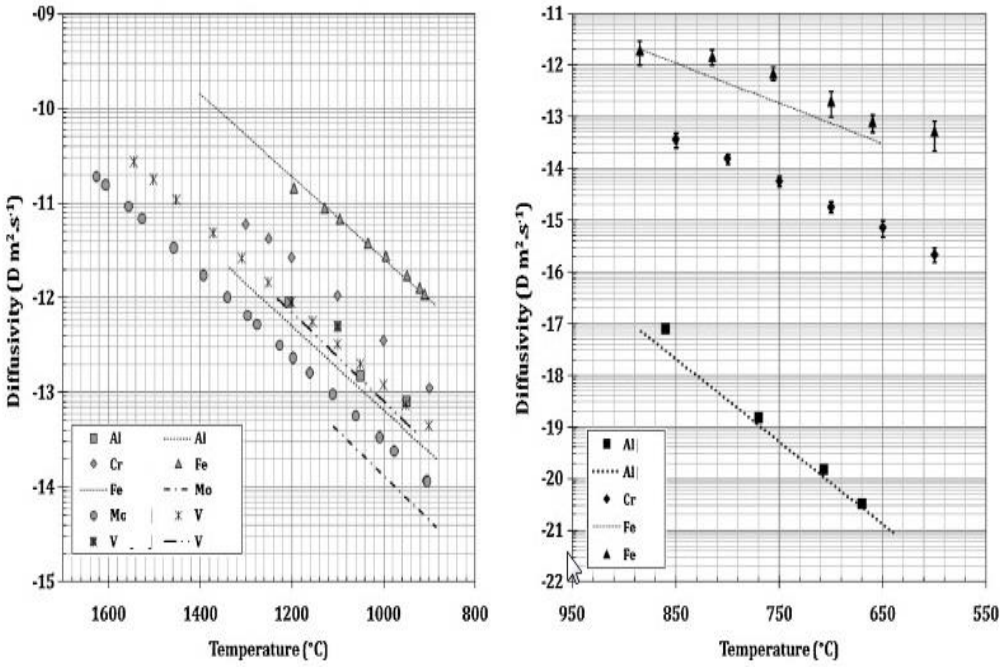

Fig.2.16 Temperature dependence of diffusion coefficients for solute diffusion in pure Ti: (a) β-Ti; (b) α-Ti [1]. Different plots for the same elements derive from different methods.

Table 2.8 Solubility of alloying elements in Ti at the temperatures of processing [61].

Temperature	Al	V	Mo	Cr	Fe
1250 °C	<27 wt.%	Not limited	Not limited	<44 wt.%	<24.7 wt.%
1020 °C	12 wt.%	Not limited	Not limited	<27 wt.%	<24 wt.%
α-Ti	6–10 wt.%	<3 wt.%	<1 wt.%	<1 wt.%	<0.047 wt.%

Table 2. 9 Average diffusivity of alloying elements in β-Ti at sintering temperatures[1].

Temperature	Al ($\times10^{-13}$ m² s⁻¹)	V ($\times10^{-13}$ m² s⁻¹)	Mo ($\times10^{-13}$ m² s⁻¹)	Cr ($\times10^{-13}$ m² s⁻¹)	Fe ($\times10^{-13}$ m² s⁻¹)
1250 °C	~12.5 ± 7.5	14 ± 01	3.25 ± 1.25	~40	~300
1020 °C	1 ± 0.2	1.25 ± 0.25	0.33 ± 0.15	~4	~30

As shown in Fig.2.13 diffusivity is primarily temperature dependent and an increase in processing temperature increases the diffusivity. This means that

higher processing temperatures help to achieve fast elemental diffusion in a titanium matrix. It is clear that Fe and Cr have the highest diffusivity both in β and α titanium, while Al has the highest diffusivity in β titanium. When the data in Table 2.8 and Table 2.9 are compared we can also conclude that the faster the diffusivity of an alloying element, the lower its solubility in titanium [1]. Some researchers [62] have shown that sintering and chemical homogenization of the titanium matrix is assisted in alloys containing faster diffusing elements (such as Fe and Al), while slower diffusing elements, such as Mo and V delay elemental homogenization.

Studies [1, 62-64] have also shown that the diffusion of alloying elements with different diffusivities can impact on the diffusion of each other, for example an α stabilizer and a β stabilizer can mutually hinder diffusion due to stabilization of corresponding phase barriers [63, 64]. This phenomenon is an important consideration when choosing the starting powders and analysis of any potentially abnormal elemental distribution is necessary in some cases. For instance, in the case of a V-Fe-Al master alloy used synthesise a Ti-10V-2Fe-3Al alloy by BEPM[64], the formation of an Al-rich area around the master alloy particles slows down the fast diffusion of Fe. So at lower temperatures the diffusion of Fe is slowed down by Al. As the Al diffuses the degree of saturation of Al in such areas is reduced, so that when the temperature increase, the fast diffusion of Fe returns. A direct result of this is that the positive effect of iron was not realised at lower temperature, where it assists in the healing of pores [1]. So based on the interaction between Fe and Al, it is better to introduce Fe as an elemental powder separately from an Al-V master alloy powder.

2.6 TMCs reinforced by TiB

TiB has been identified as probably the most compatible and effective discontinuous reinforcement for a Ti matrix due to both its thermodynamic and mechanical stability (generating minimal residual stresses) and good bonding with a Ti matrix with very clean interfaces [65]. The characteristics of TiB, which support its application as a reinforcement phase in titanium, are a similar thermal expansion coefficient and density to titanium. The coefficient of thermal

expansion of TiB is 9.0×10^{-6} K^{-1} while that of Ti is 8.6×10^{-6} K^{-1}, the density of TiB is 4.56 g/cm^3 while that of Ti is 4.57g/cm^3. This section reviews previous work on TiB reinforcement in Ti composites and includes the reactions occurring during in-situ synthesis of TiB, composite processing technology, the properties of TiB reinforced composites and the obstacles to be addressed.

2.6.1 The in-situ technology and reacting mechanism during the processing of TiB reinforcement

For TiB reinforcement, an in-situ preparation technique has become attractive for producing particulate reinforced titanium matrix composites because this approach overcomes the interfacial reactions and poor wettability between the reinforcements and the matrix. In the processing of in-situ composites, reinforcements are synthesized in the matrix by chemical reactions between elements or between elements and compounds. The merits of in-situ TMCs are thermodynamically stable reinforcements, clean reinforcement/matrix interfaces and uniformly distributed reinforcing particles [66-68], compared with conventional TMC's, which are normally made by directly adding the reinforcing particles into a matrix. In-situ technology is also safer to operate and processing eliminates any hazards associated with TiB handling. The cost of composite processing is also reduced because there is no need to use expensive TiB powder. There has been a lot of research interest aimed at improvements in the performance of Ti/TiB or Ti alloy/TiB composites using an in-situ technique.

This research has shown that different processing methods, powder metallurgy, Self-propagating High-temperature Synthesis (SHS), Reactive Hot Pressing (RHP), etc., can be used to produce a composite containing almost pure TiB reinforcing particles with a clean TiB/Ti interface. [69,70]. Some authors have studied and summarized the reaction between Ti and B during composite processing [71,72]. From their work it has been shown that there are three possible exothermic reactions in the Ti-B system as follows:

$$Ti+B = TiB \quad (1)$$

$$Ti+2B = TiB_2 \quad (2)$$

$$TiB_2+Ti = 2TiB \quad (3)$$

Based on thermodynamic analysis using thermodynamic data given in reference

[71], the reaction formation enthalpy ΔH and Gibbs free energy ΔG of reactions (1) - (3) have been calculated and the results are shown in Figs. 2.14 and 2.15. Fig. 2.14 indicates that all the above reactions are thermodynamically feasible because ΔG for the three reactions are negative. ΔG for reaction (1) is less than that for reaction (2) when titanium is in excess. This indicates that reaction (1) is more likely to take place and TiB forms in preference to TiB_2 throughout the temperature range. As shown in Fig. 2.15, the reaction formation enthalpy ΔH of the above three reactions is also negative, which indicates that the three reactions are all exothermic. According to Le Chatelier's principle, a decrease in temperature causes the equilibrium position for exothermic reaction (3) to be shifted to the right. Also, if there is excess titanium, reaction (3) will take place, which means that TiB_2 cannot exit in the final synthesised product in a Ti-B system with excess Ti. So only the thermodynamically stable TiB phase can be detected by X-ray diffraction. But a little TiB_2 phase was found in synthesised TiB70-Ti, TiB80-Ti and TiB100 products. There are two possible reasons for this. Firstly, any inhomogeneity in the powder mixture causes an inhomogeneous reaction to take place; secondly, the synthesised TiB_2 phase does not have enough time to fully react with Ti before too much cooling has occurred , so it is kept in the final product [71-72].

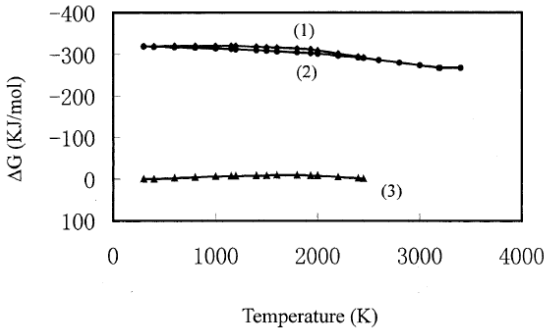

Fig.2.14 The change of Gibbs free energy ΔG as a function of temperature for reactions (1) – (3) [71]

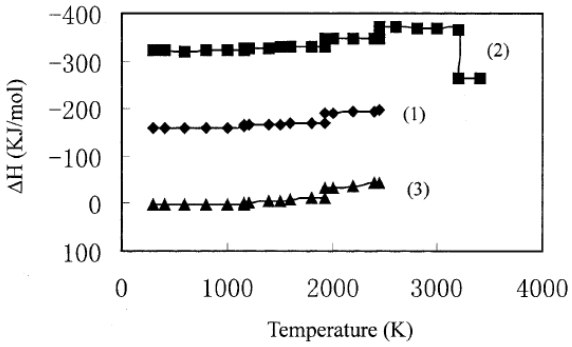

Fig.2.15 The change of formation enthalpy ΔH as a function of temperature for reactions (1)–(3)[71]

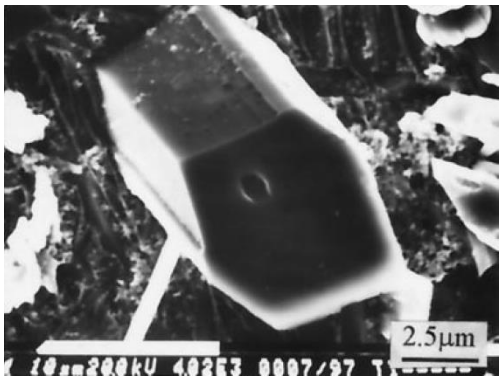

Fig.2.16 A typical SEM morphology image of TiB[73]

Some studies have also investigated the growth and structural detail of TiB formed in the solidification process. A typical SEM image showing the morphology of TiB is shown in Fig. 2.16 [73].

2.6.2 Processing technology of the composites

From the above analysis it can be concluded that in order to achieve good bonding between the reinforcing phase and the Ti matrix with a clean interface, a finely mixed powder must be prepared, with an even distribution consisting of Ti/Ti alloy and pure TiB as the final products. Varying volume fractions of the TiB-Ti composite constituents should also be taken into account. No matter which powders are involved, whether it be elemental boron or TiB_2, a fine distribution of these with full contact in the Ti powder must be achieved in the final mixing stage. This can be easily accomplished using mechanical alloying (MA). During mechanical milling, reinforcing particles are easily embedded into the titanium particles to generate a homogenously distribution of reinforcing particles within a continuous Ti matrix which are fully surrounded by Ti. Another advantage of using MA is the generation of defect structures within the Ti–TiB_2 or Ti–TiB

composite particles which enhance diffusion during high temperature processing.

Feng et al. used a planetary mill to mix Ti, TiB_2 and FeMo (β-Ti stabilisers) powders for ten hours with a ball to powder ratio of 10:1[74]. This study was successful in generating composite powders with TiB_2 dispersed in the Ti, and after spark plasma sintering generated a 0.1 volume fraction of TiB in the titanium matrix. It was reported that faster diffusion during the high temperature sintering process was facilitated by defects introduced into the milled powders. In a separate publication, up to 0.2 volume fraction of TiB was formed from mechanically alloyed mixtures of B, Ti and FeMo (β-Ti stabilisers), followed by vacuum hot pressing. There were no reported by-products at the interfaces after high temperature consolidation [75]. It is also important to point out that no alloying occurs during mechanical milling, but rather this process creates intimate mixing, so that composite particles consisting of the elemental constituents, are generated from the milling conditions used. But until now no work has been reported on the generation of higher volume fractions of TiB-Ti composites by MA. This presents an opportunity to examine the possibility of forming whiskers at high volume fraction, rather than the reported clustered/rounded particles of TiB that often occur at high TiB volume fractions (as discussed in this section).

Furthermore there are also some disadvantages associated with MA processing such as the low productivity of high energy ball milling, powder contamination from the milling balls or vial and decomposition of any process control agent (PCA) used. In view of the merits of preparing powder mixtures, microstructural control, near net shape processing and minimum material waste, the most recent publications have largely focused on powder metallurgy (PM) or powder based technology. Table 2.10 illustrates some of the work based on powder metallurgy or a powder based route along with results obtained. Based on the scope of this thesis, the selected works focus on those papers which use pure B as the boron source and Ti-6Al-4V or Ti as the matrix.

Table 2.10 Selected reported work on TiB reinforced composites.

TiB Vol. %	Boron Source	Matrix	Process	Properties				Ref
				VHN	Yield Strength	Ductility %	Young' Modulus(GPa)	
0	--	Ti-6Al-4V	C+E+H	----	986	--	110	76
0	--	Ti	VAR+HS	----	164	20.7	109	78
3.1	B	Ti-6Al-4V	C+E+H	----	1041	--	129	76
5	B	Ti	VAR+HS	----	639	12.5	121	78
6.5	B	Ti-22Al-27Nb	PM+HR+H	----	1068	2.3	---	77
10	B	Ti-6Al-4V	MA+HIP	----	-----	0.25	136.6	79
20	B	Ti-6Al-4V	PM+E	----	1181	0.5	170	80
20	TiB2	Ti-6Al-4V	RHP	580	--	--	--	82
20	TiB2	Ti-6Al-4V	MA+HP	----	----	0.1	145	80
34	B	Ti-6.4Fe-10.3Mo	PM+HP	----	----	0.5	163	81

PM=Powder Metallurgy, MA=Mechanical Alloying, C=Compaction, E=Extrusion, H=Heat Treated, HP=Hot Pressing, VAR=Vacuum Arc Remelting, HS=Hot Swaging, HR=Hot Rolling, HIP=Hot Isostatic Pressing, RHP=Reactive Hot Pressing, VHN=Vickers Hardness Number

Some researchers have attempted to use other technologies to produce TiB-Ti or TiB-Ti64 composites with satisfactory results. T.Yamamoto et al. produced TiB/Ti by SHS and the results showed that the Vickers hardness and fracture stress of the composites were 5.6-7.1 and 2.1-2.3GPa respectively [69]. Zhang et al. used the same processing technology and found that the size of TiB grains decreased with an increasing amount of metal addition, with the addition of 40 wt% Ti resulting in a drastic increase in the bending strength, tensile strength, compression strength and fracture toughness [83]. That can be a very useful support for the TiB/Ti synthesis technology.

2.6.3 The mechanical properties of Ti-TiB composites

An effect of reinforcement by TiB particles or whiskers is an increase in elastic modulus in a composite. It has been reported [80] that the Young's modulus of Ti-B composites with aligned TiB in the extrusion direction is 169 GPa compared with 159 GPa for randomly orientated TiB with the same 0.2 volume fraction of TiB. When the TiB volume fraction is 0.4, the Young's modulus in the extrusion direction increases to 205 GPa. TiB additions also increase the creep resistance of titanium [84, 80]. There are also reports of increases in tensile strength, fatigue strength and wear resistance with increasing TiB volume fraction [85], but ductility is sacrificed with increased strength. More work is needed to increase our understanding of the relationship between mechanical properties and volume fraction of TiB.

2.6.4 The impact of TiB volume fractions on the properties of composites

Ti-TiB composites with varying TiB volume fractions and morphologies have been produced using different approaches and it has been reported that the volume fraction of elemental boron influences the final TiB morphology and the properties of MMCs. Tsang et al carried out an in-depth study of the effect of TiB volume fraction on the properties of MMC [86]. A summary of their findings is shown in Table 2.11. It was reported that with increasing TiB volume fraction the size and amount of blocky TiB increases and the amount of needle-type TiB decreases. The effect of this is a linear increase in yield strength and a linear decrease in the ductility of the MMC, as shown in Fig. 2.17. Observations of failed tensile specimens used in this study show that a large reinforcing phase with a high aspect ratio promotes a linking of cracks between reinforcements and this dominates the fracture of a composite. Hence, increasing volume fractions and size of blocky TiB are detrimental to ductility.

Table 2.11 Tensile Properties of Pure Ti and in-situ TMC[86]

Sample	Y.S.(MPa)	U.T.S.(MPa)	Elon.(%)	Modulus(GPa)
Pure Ti	164	179	20.7	109
5%TiB/Ti	639	787	12.5	121
10% TiB/Ti	706	902	5.6	131
15% TiB/Ti	842	903	0.4	139
22%(TiB+TiC)/Ti	471	635	1.2	----

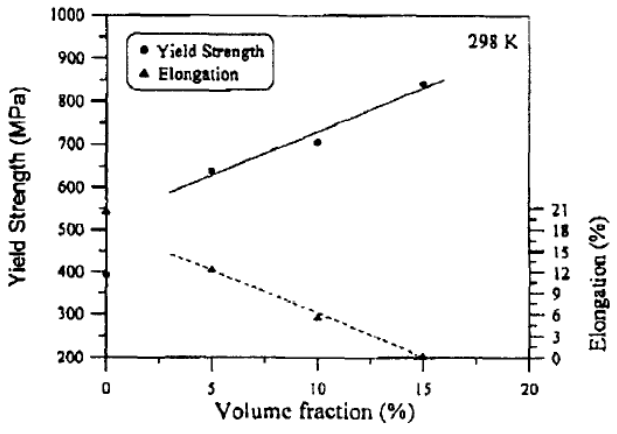

Fig.2.17 Change in yield strength and elongation to fracture with volume fraction of in-situ TiB [86].

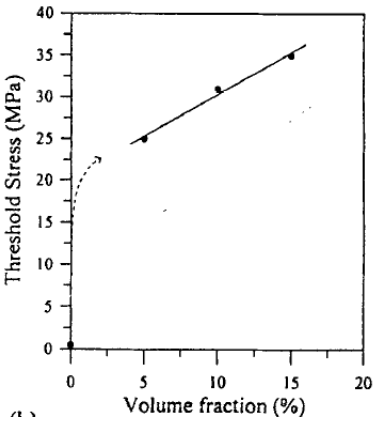

Fig.2.18 dependence of threshold stress on the volume fraction of TiB [86]

The data in fig. 2.18 shows that the threshold stresses for composites with 5%, 10% and 15% TiB/Ti are 25, 31 and 35 MPa respectively. At 5% volume fraction of TiB in a Ti matrix, there is a significant increase in threshold stress from zero to 25 MPa. However, additional 5% increases in TiB volume fraction give much smaller increases in threshold stress of about 5 MPa per 5% addition.

Although many of the relationships between TiB volume fraction and mechanical properties of Ti based MMC's are understood, further work to determine an applied mechanism for producing the best quality MMCs with TiB reinforcement is needed. Future work can depends the indeed apply conditions of MMCs to produce the desirable material with optimum TiB volume fraction, and focus on microstructure optimization. Furthermore with the increasing of TiB reinforcement volume, the tailorability of Ti-TiB composites also need to be taken into account which can be illustrated by the mechanical response of the developed composites.

2.7 Contribution and hypotheses of present thesis

The aim of this study is to use a BEPM method to prepare both an Timetal551 alloy and TiB/Ti6Al4V composites and to study the influence of processing parameters on microstructure and mechanical properties. To achieve this target the main contributions of this thesis are:

An optimisation of processing parameters through a better understanding of the effects of these on elemental diffusion and microstructure.

Determining a relationship between microstructure and mechanical properties for Timetal551 alloy and investigating the effect of different starting powders on microstructure and mechanical properties.

Investigating the effect of different heat treatments on structure and mechanical properties of Timetal551 produced by a BEPM method.

For TiB/Ti6Al4V composite material, an understanding of the effects of starting powder characteristics and an optimisation of the processing parameters. To gain a better understanding of the effects of processing parameters on the morphology of the reinforcement and the mechanical properties of TiB/Ti6Al4V composites.

It is hoped that this study will provide constructive ideas and guidance for the preparation of other titanium alloy or TMCs with complex elemental components using a BEPM method.

References

[1] A. Carman, L. Zhang, O. Ivasishin, D. Savvakin, M. Matviychuk, E. Pereloma, Materials Science and Engineering: A, 528 (2011) 1686-1693.
[2] F. Froes, Advanced materials&processes, 170 (2012) 16-22.
[3] C. McCracken, Euro PM Conference, (2009).
[4] M. Qian, Materials China, 30 (2011) 50-53.
[5] R. Supati, N. Loh, K. Khor, S. Tor, Materials Letters, 46 (2000) 109-114.
[6] F. Yang, D.L. Zhang, B. Gabittas, H.Y. Lu, Key Engineering Materials, 551 (2013) 67-72.
[7] H. Lu, D. Zhang, B. Gabbitas, F. Yang, S. Matthews, Journal of Alloys and Compounds, 606 (2014) 262-268.
[8] G. Adam, D.L. Zhang, J. Liang, I. Macrae, Advanced Materials Research, 29 (2007) 147-152.
[9] D. Zhang, Z. Cai, G. Adam, JOM, 56 (2004) 53-56.
[10] S.M.A.e. al., Affordable PIM Titanium - Microstructure, Properties, Products, MPIF Conference, (2011).
[11] P.M.a.J.O.n. SML Sastry, Metall. Trans. A, 15 (1984) 1451-1463.
[12] R.M. German, John! Wiley & Sons, Inc, 605 Third Ave, New York, NY 10016, USA, 1998. 496, (1998).
[13] S. Lee, K. Kim, Powder Technology, 186 (2008) 99-106.
[14] F.G.H. H.G. Rutz, Advances in Powder Metallurgy and Particulate Materials, 5 (1994) 117-133.
[15] F. Hanejko, Euro PM, (2007).
[16] Y.T. F.Chagnon, Advances in Powder Metallurgy and Particulate Materials, 3 (1995) 106-126.
[17] B.J. U.Engstrom, Advances in Powder Metallurgy and Particulate Materials, 3 (1995) 106-126.
[18] W. Eisen, B. Ferguson, R. German, R. Iacocca, P. Lee, D. Madan, K. Moyer, H. Sanderow, Y. Trudel, ASM handbook Volume 07: Powder Metal Technologies and Applications, ASM international, USA (1998).
[19] Z. Hu, T. Dean, Journal of Materials Processing Technology, 111 (2001) 10-19.
[20] H. Hahn, J. Logas, R.S. Averback, Journal of Materials Research, 5 (1990) 609-614.
[21] Y.B. Kim, H.M. Park, W.Y. Jeung, J.S. Bae, Materials Science and Engineering: A, 368 (2004) 318-322.
[22] P. Kollár, J. Bednarčík, S. Roth, H. Grahl, J. Eckert, Journal of magnetism and magnetic materials, 278 (2004) 373-378.
[23] K.I. Moon, H.S. Park, K.S. Lee, Journal of alloys and compounds, 325 (2001) 236-244.
[24] J. Rawers, G. Slavens, R. Krabbe, J. Groza, Nanostructured Materials, 9 (1997) 197-200.
[25] Hyunho Shin, High-Temperature Behavior of Silicon Carbide Fibers in a Si-Al-Ca-O-N Ceramic Matrix, J.A. Ceram, 78 (1995) 3153-3156.
[26] J. Fogagnolo, M. Robert, J. Torralba, Materials Science and Engineering: A, 426 (2006) 85-94.
[27] A.J.G. T.N.Baker, Powder Metallurgy, 39(3) (1996) 223-229.
[28] L.J.-a. XIE Jian-xin, Beijing: Metallurgical Industry Press, 2004.

[29] F. Yu-hang, Tube production of titanium and titanium alloy, Titanium Industry Progress, 1994.
[30] J.M.-s. CHEN Shi-qing, Die forging and extrusion of titanium, Beijing: National Defence Industrial Press, 1982.
[31] 贾如雷, 计波, 吕维洁, 王宗宝, 中国有色金属学报, 20 (2010) 897-901.
[32] Y. Chen, Q. Wang, J. Peng, C. Zhai, W. Ding, Journal of materials processing technology, 182 (2007) 281-285.
[33] L. Wen, Z. Ji, X. Li, Materials Characterization, 59 (2008) 1655-1660.
[34] S.H. Hong, K.H. Chung, C.H. Lee, Materials Science and Engineering: A, 206 (1996) 225-232.
[35] T. Murai, S.-i. Matsuoka, S. Miyamoto, Y. Oki, Journal of Materials Processing Technology, 141 (2003) 207-212.
[36] L. Li, K. Rao, Y. Lou, D. Peng, International Journal of Mechanical Sciences, 44 (2002) 2415-2425.
[37] T. Shin, Y. Lee, J. Yeom, S. Chung, S. Hong, I. Shim, N. Park, C. Lee, S. Hwang, Computer methods in applied mechanics and engineering, 194 (2005) 3838-3869.
[38] L.H.-f. HE Tie-ning, 3D thermo-mechanical couple numerical simulation of the titanium alloy extrusion process, Forging Technology, 2006.
[39] D. Damodaran, R. Shivpuri, CIRP Annals-Manufacturing Technology, 46 (1997) 179-182.
[40] A. Mukhtar, D. Zhang, C. Kong, P. Munroe, Journal of materials science, 45 (2010) 4594-4605.
[41] F. Yang, D. Zhang, B. Gabbitas, H. Lu, C. Wang, Materials Science and Engineering: A, 598 (2014) 360-367.
[42] F. Yang, D.L. Zhang, H.Y. Lu, B. Gabbitas, Key Engineering Materials, 520 (2012) 70-75.
[43] D. Zhou, D. Zhang, C. Kong, P. Munroe, Materials Science and Engineering: A, 584 (2013) 67-72.
[44] Z. Gronostajski, P. Bandoła, T. Skubiszewski, Archives of Civil and Mechanical Engineering, 9 (2009) 47-57.
[45] C. Leyens, M. Peters, Wiley-VCH, 2003, pp. 18.
[46] V.A. Joshi, Titanium alloys: an atlas of structures and fracture features, CRC Press, 2006.
[47] V.N. Moiseyev, Titanium alloys: Russian aircraft and aerospace applications, CRC press, 2005.
[48] I. Kornilov, Metal Science and Heat Treatment, 8 (1966) 92-96.
[49] M.J. Donachie, Titanium: a technical guide, ASM international, 2000.
[50] G. Welsch, R. Boyer, E. Collings, Materials properties handbook: titanium alloys, ASM international, 1993.
[51] G. Lütjering, J.C. Williams, Titanium, 2 ed., Springer, 2003.
[52] A. Huntz, S. Tsai, Journal of materials science letters, 13 (1994) 821-825.
[53] M. Koiwa, Materials Transactions, JIM, 39 (1998) 1169-1179.
[54] Z. Liu, G. Welsch, Metallurgical Transactions A, 19 (1988) 1121-1125.
[55] H. Nakajima, M. Koiwa, ISIJ International, 31 (1991) 757-766.
[56] H. Nakajima, K. Ogasawara, S. Yamaguchi, M. Koiwa, Materials Transactions, JIM, 31 (1990) 249-254.
[57] G. Neumann, C. Tuijn, Self-diffusion and impurity diffusion in pure metals: handbook of experimental data, Elsevier, 2011.
[58] R. Pérez, F. Dyment, M. Behar, Materials Letters, 57 (2003) 2670-2674.

[59] R.A. Perez, H. Nakajima, F. Dyment, Materials Transactions, 44 (2003) 2-13.
[60] R. Seebold, DTIC Document, 1964.
[61] H.O. T.D. Massalski, P.R. Subramanian, L. Kasprzak (Eds.), Binary Alloys Phase Diagrams, ASM International, Materials Park, OH, USA 1990.
[62] E.V. Pereloma, D.G. Savvakin, A. Carman, A.A. Gazder, O.M. Ivasishin, Key Engineering Materials, 520 (2012) 49-56.
[63] O.M. Ivasishin, D. Eylon, V. Bondarchuk, D.G. Savvakin, Defect and Diffusion Forum, Trans Tech Publ, 2008, pp. 177-185.
[64] O.M. Ivasishin, D.G. Savvakin, Key Engineering Materials, 436 (2010) 113-121.
[65]Ma ZY, Tjong SC, Gen L (2000) Scripta Mater 42:367
[66]J.F.Li and Z.Zhang, The in-situ preparation of metal matrix composites, Mater. Sci. Eng., 20(2002), No.3, p.453
[67] P.B.Joshi, Reactive synthesis of titanium matrix composite powder, Mater.Lett., 56(2002),p332.
[68] Lifang Cai, Yongzhong Zhang, Journal of University of Science and technology Beijing, 13(2006),p.551.
[69] T.Yamamoto and A. Otsuki, Synthesis of near net shape high density TiB/Ti composites,Mater. Sci. Eng., A239-240(1997), p.1997
[70] S.Gorsse and Y. Le Petitcorps, Investigation of the Young's modulus of TiB needles in situ produced in titanium matrix composites, Mater. Sci. Eng., A340(2003), p.80
[71] L.Yingjiao, C.Yinchang, Notebook of thermodynamic Data of Inorganic, East-North University Press, Shengyang,1996,pp.60-383
[72] Z. Xinghong, X. Qiang, et al., Self-propagating high temperature combustion synthesis of TiB/Ti composites. Mater. Sci. Eng., A348(2003)41-46
[73]Weijie Lu, Di Zhang, et al., HREM study of TiB/Ti interfaces in a Ti-TiB-TiC in situ composite, Script. Mater. 44 (2001) 1069-1075.
[74]. Feng H, Jia D, Zhou Y (2005) Composites Part A 36(5):558
[75]. Feng H-B, Jia D-C, Zhou Y, Hou J (2004) Mater Sci Tech 20(9):1205
[76] Soboyejo WO, Shen W, Srivatsan TS (2004) Mech Mater 36(1–2):141
[77] Emura S, Yang SJ, Hagiwara M (2004) Metall Mater Trans A 35A(9):2971
[78] Tsang HT, Chao CG, Ma CY (1997) Scripta Mater 37(9):1359
[79] Godfrey TMT, Wisbey A, Goodwin PS, Bagnall K, Ward-Close CM (2000) Mater Sci Eng A282(1):240
[80] Gorsse S, Miracle DM (2003) Acta Mater 51(9):2427
[81] Panda KB, Ravi Chandran KS (2003) Metall Mater Trans A 34A(6):1371
[82] Gorsse S, Chaminade JP, Petitcorps YL (1998) Composites Part A 29(A):1229
[83] Z. Xinghong, X. Qiang, et al.. Self-propagating high temperature combustion synthesis of TiB/Ti composites. Mater. Sci. Eng., A348(2003) 41-46
[85]. Ranganath S (1996) ''Discontinuously reinforced titanium matrix composites via combustion-assisted synthesis in Inorganic matrix composites'', Advanced Scientific Research and the Structural Materials division of TMS, the Indian Institute of Science,Bangalore, India.March 8–11,1996 (edited by M.K. Surappa), p. 227
[86]. Saito T, Takamiya H, Furuta T (1998) Mater Sci Eng A A243(1–2):273
[87] H.T. Tsang*, C.G. Chao* and C.Y. Ma. Effects of volume fraction of reinforcement on tensile and creep properties of in-situ TiB/Ti MMC.Scripta Materialia, Vol. 37, No. 9, pp.1359-1365, 1997

Chapter 3 Experimental details

3.1 Introduction

The experimental methodologies, equipment and materials used in this research work for synthesis of Ti-4%Al-4%Mo-4%Sn-0.5%Si alloy are described in this chapter, the specific experimental details for the synthesis of TiB/Ti6Al4V composite will be described in Chapter 8 separately from this chapter for conveniently reading. A description of powder compaction and powder compact extrusion is given, followed by the heat treatments used for as-extruded samples and sample characterization.

3.2 Metal powders and Powder mixing

All powder compaction and extrusion experiments were conducted using hydride-dehydride (HDH) Ti, gas-atomized (GA) Ti and other elemental powders used for alloying including Mo, Al, Sn and Si powders. The morphologies of the HDH Ti and GA Ti powders are shown in Fig. 3.1. The particle sizes and purity of the powder are shown in Table 3.1.

Table 3.1 Particle sizes and purity of powders used in this study.

	Gas atomized Ti	HDH Ti	Al	Mo	Sn	Si
Particle size	-200mesh	-200mesh	d_{50}=40μm	-100mesh	-325mesh	-100mesh
Purity	Oxygen =0.15wt%	Oxygen =0.3wt%	99.9%	99.9%	99.99%	99.95%

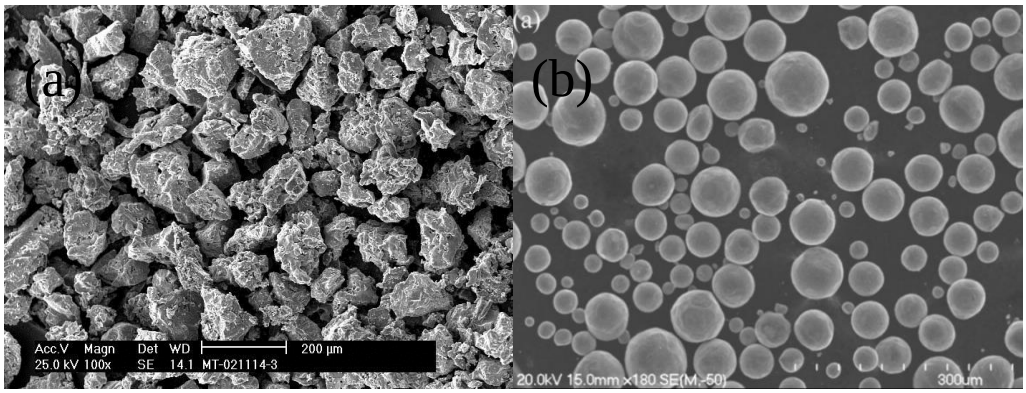

Fig.3.1 SEM photomicrograph of (a) HDH titanium powder (Courtesy of Metal Titanium Co., Ltd, China) and (b) GA titanium powder.

The powder blending was carried out for 24 hours in a roller mill with the container rotating at 200rpm. The elemental homogeneity of the blended powder was determined by XRD, by taking three 5g samples of blended powder at random time intervals. If the three XRD results were almost similar or identical, this indicated good homogeneity of the blended powder.

Because GA Ti powder has a spherical shape it is hard to deform and therefore difficult to cold compact. To make compaction of GA powder easier, another approach for powder mixing using mechanical milling was used. A combination of powders was mixed at 100rpm for 24h. Mechanical milling at 400 rpm for 6 hours was then used to produce a homogenous elemental distribution and to deform the GA Ti powder.

Fig.3.2 High energy mechanical milling machine (Retsch PM100)

3.3 Powder Compaction

In this study cold powder compaction was the preferred compaction method, rather than warm compaction, because of the Sn content in the alloy. Although warm compaction normally gives a higher green compact density, because Sn melts at 232ºC, during warm compaction at about 300ºC, the high pressure and temperature causes the liquid Sn to be squeezed from the inside of a compact and solidify on the compact surface. This phenomenon leads directly to Sn loss and this is unacceptable for the alloy preparation in this study.

The blended powders were compacted at room temperature in either a 40mm diameter or a 56mm diameter die under a pressure of 718MPa and 366MPa, respectively. The 40mm diameter compacts were extruded using a 100 vertical ton press and 56mm diameter compacts were extruded using a 300 horizontal ton press. Images of the die and a typical powder compact are shown in Fig. 3.3, and the 100 ton press and 300 ton presses used in this work are shown in Fig.3.4. To determine the relative density of the powder compacts their volume was measured using a 3D scanner and Archimedes principle.

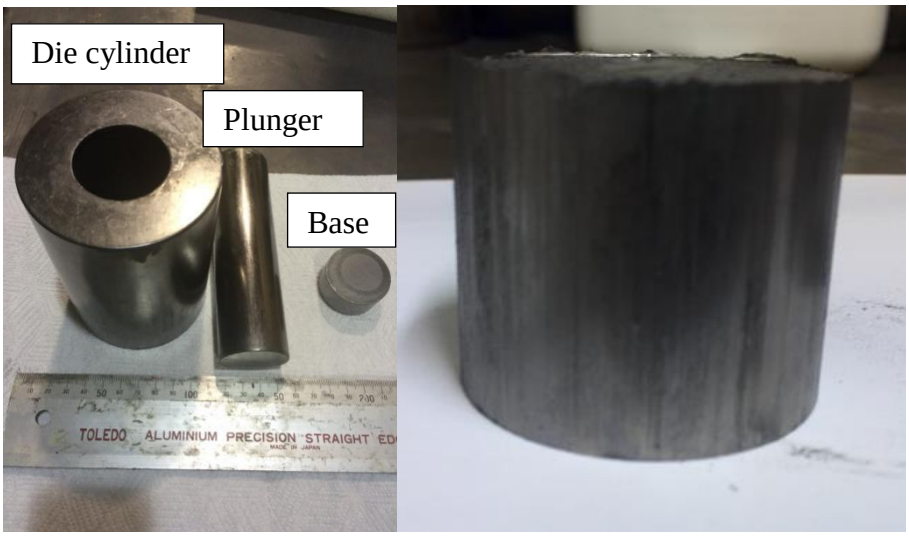

Fig.3.3 A 40 mm diameter compaction die (left) and a 40 mm diameter green compact (right)

Fig.3.4 100ton press (left) and 300ton press (right)

3.4 Compact sintering and extrusion

For compact sintering and extrusion two processing routes were used, depending on the extrusion press used for extrusion. When a 100ton press was used for extrusion, powder compacts were heated to the extrusion temperature using an induction coil with a designated holding time and then extruded at maximum pressure of 707MPa. The extrusion cylinder and die were heated to 500^{o}C prior to extrusion and the extrusion ratio was 9:1. The powder compact heating and

extrusion was done in an argon atmosphere with an oxygen content <200ppm. Larger powder compacts were extruded using a 300 ton press. In this case a powder compact was sintered at a designated temperature with a holding time of 5min at temperature before hot pressing. A 58mm diameter die was used for hot pressing with a maximum pressure of 342MPa. The hot pressing was carried out under an argon atmosphere with an oxygen content <200ppm. Hot pressed compacts were induction heated in air to a designated extrusion temperature and then extruded with an extrusion ratio of 9:1. Prior to extrusion the extrusion die was heated to 400^{o}C. Images of the induction furnace power supply and induction coils used for induction heating are shown in Fig.3.5. Images of as-extruded rods are shown in Fig.3.6.

Fig.3.5 Images of induction furnace power generator (left) and coils (right).

Fig.3.6 Images of as-extruded rod extruded by 100 ton press (upper) and 300 ton press.

3.5 Microstructure characterization

3.5.1 Sample preparation

All the as-extruded samples were cut to a designated shape using a wire cutter, or a diamond blade and then, if needed, they were subsequently mounted in resin. The powder and as-extruded samples for analysis were embedded in epoxy resin and hardened for 24 hours. The mounted specimens were ground using 160, 320, 600, 1000/1200, 2000 and 4000 grit SiC papers, followed by polishing using an alumina suspension (0.3μm agglomerated alumina).

3.5.2 Optical microscopy (OM) and Etching

An Olympus BX60 optical microscope was used for sample characterization and metallography. To observe the microstructures, samples were etched using Krolls reagent which contains 92ml distilled water, 6ml of HNO_3 and 2ml of HF. A typical etching time was 2-5 seconds.

3.5.3 Scanning electron microscopy (SEM) and Energy dispersive x-ray analysis (EDX)

A Hitachi S-4000 scanning electron microscope, at an operating voltage of 20KV and Energy Dispersive X-ray analysis (EDX) with a Kevex microanalyser attachment were used for microstructural characterisation of powder particles, mounted samples and the fracture surfaces of tensile test samples.

3.5.4 X-Ray diffractometry (XRD)

X-ray diffraction analysis (XRD) was performed to determine the phase constituents in both powder and coating samples using an X'pert diffractometer (Philips, the Netherlands) with Cu Kα radiation. The XRD patterns were obtained using a 0.02° step size averaging 5 seconds per increment, with a voltage of 40KV and a current of 40mA.

3.5.5 Thermogravimetic analysis (TGA) and differential thermal analysis (DTA)

Thermogravimetic analysis (TGA) and differential thermal analysis (DTA) were used to evaluate the phase transformation temperatures of as-extruded samples, using a simultaneous SDT 2960 analyser under flowing argon at a rate of 150 ml/sec. The heating rate was at 10℃/min from room temperature to a selected temperature.

3.5.6 Chemical composition

Testing for carbon (infrared detection) and oxygen content (detected by LECO TC300) was done at the Materials Analysis and Testing Centre, Northwest Institute for Non-ferrous Metal Research, China.

3.6 Mechanical tests of the final parts

Tensile testing was carried out using a 4204 INSTRON universal testing machine with dog-bone shaped specimens with a rectangular cross-section of 2mm x

2.5mm and a gauge length of 20mm. The strain was measured using an extensometer with a gauge length of 10mm. A strain rate of $1\times10^{-4}s^{-1}$ was used for tensile testing.

For elevated temperature tensile test, the strain was measured using an extensometer with a gauge length of 10mm. The strain rate was $1.4\times10^{-4}s^{-1}$. The elevated temperature tensile testing was conducted in a temperature controlled furnace mounted on the testing machine.

Chapter 4 Effect of the extrusion temperature on the microstructure and mechanical properties of as-extruded Ti-4Al-4Sn-4Mo-0.5Si alloy

4.1 Introduction

The specific alloying additions and their effect on microstructure are two important factors which determine the overall mechanical properties of a titanium alloy. However, when a BE approach is used, the microstructure is influenced by the distribution and degree of dissolution of the alloying elements. The scope of this chapter is firstly to investigate the effect of extrusion temperature on the dissolution and distribution of alloying elements, in order to optimize the processing parameters for preparing a Ti-4%Al-4%Mo-4%Sn-0.5Si titanium alloy with satisfactory mechanical properties. Secondly, the relationship between microstructure and mechanical properties was also investigated.

4.2 Experimental details

The starting materials used in this section include, HDH Ti powder (particle size -200mesh, oxygen content: 0.3wt%), aluminum powder (particle size: d_{50}= 40μm, 99.9% purity), molybdenum powder (particle size: -100mesh, 99.9% purity), tin powder (particle size: -325mesh, 99.99% purity) and silicon powder (99.95% purity). The powder blending was carried out for 24 hours in a roller mill with the container rotating at 200rpm. The elemental homogeneity of the blended powder was determined by XRD, by taking three 5g samples of blended powder at random time intervals. If the three XRD results were almost similar or identical, this indicated good homogeneity of the blended powder.

The blended powders were compacted at room temperature in a 40mm diameter die under a pressure of 718MPa. Because of the Sn content in the alloy, cold compaction, rather than warm compaction, was the preferred compaction method. Although warm compaction normally gives a higher green compact density [9], because Sn melts at 232^{o}C, during warm compaction at about 300^{o}C under high pressure and temperature, the liquid Sn is squeezed from the inside of a compact

and solidifies on the compact surface (as shown in Fig.4.1 (b)). This phenomenon leads directly to Sn loss and this is unacceptable for the alloy preparation in this study.

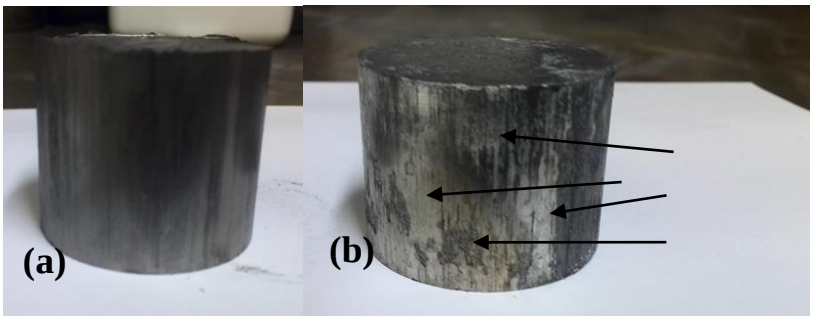

Fig.4.1 Images of the compacts produced by (a) cold compaction and (b) warm compaction, respectively. Arrows indicate Sn-rich areas on the surface of the compact after warm compaction.

To determine the relative density of the powder compacts their volume was measured using a 3D scanner. For powder compact extrusion, the powder compacts were heated to temperatures in the range of 1250-1350^{o}C using an induction coil with a designated holding time and then extruded with maximum pressure of 707MPa. The extrusion cylinder and die were heated to 500^{o}C prior to extrusion and the extrusion ratio was 9:1. All the powder compact heating and extrusion was done in an argon atmosphere with oxygen content <200ppm. Four extrusion samples were made using different extrusion temperatures and holding times, as given in Table 4.1.

Table 4.1 Ti powder types and extrusion temperatures for making the extrusion samples.

Sample name	Starting powders	Extrusion temperature, ^{o}C
Sample 1	HDH Ti+4%Al+4%Mo+4%Sn+0.5%Si	1250
Sample 2	HDH Ti+4%Al+4%Mo+4%Sn+0.5%Si	1300
Sample 3	HDH Ti+4%Al+4%Mo+4%Sn+0.5%Si	1350
Sample 4	HDH Ti+4%Al+4%Mo+4%Sn+0.5%Si	1350 with a holding time 5min

The microstructures of the extruded samples were characterized by optical microscopy (Olympus BX60), X-ray diffractometry (XRD) (Philips X' Pert system) and scanning electron microscopy (SEM) (HITACHI S4000). The tensile tests were carried out on a 4204 INSTRON universal testing machine using dog-

bone shaped specimens with a rectangular cross-section of 2mm x 2.5mm and a gauge length of 20mm. The strain was measured using an extensometer with a gauge length of 10mm. A strain rate of $1\times10^{-4}s^{-1}$ was used for tensile testing.

4.3 Results and Discussion

4.3.1 Microstructure

The elemental homogeneity of the blended powder was determined by XRD, by taking three randomly selected 5g samples of the blended powders for XRD evaluation. The XRD patterns are shown in Fig.4.2. From the three XRD results we can see that they have almost identical peaks and intensities, which means that the three batches of randomly selected powder have almost the same constitution. This indicates that the powder homogeneity is satisfactory after blending for 24hrs using a roller mixer. However, the micro-scale homogeneity of the mixed powder cannot be guaranteed due to limitations of the XRD method. In other words, there may still be localised inhomogeneous distribution of alloying additions.

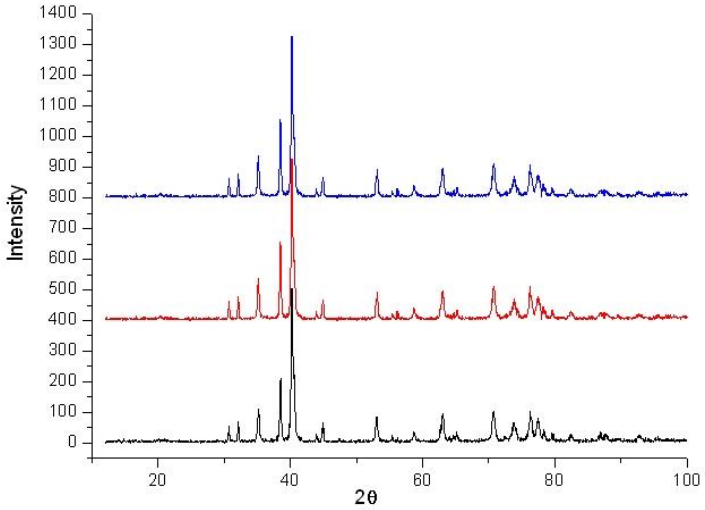

Fig.4.2 XRD patterns of randomly selected powder samples from a blended elemental powder mixture.

Table 4.2 shows oxygen analyses for the titanium powder and as-extruded samples. The oxygen content of HDH titanium powder, the main constituent of the starting powder, was 0.3wt.%. After extrusion, the oxygen content of samples shown in table 4.1was 0.36 wt.% or 0.44 wt.%. Using different extrusion temperatures had no evident impact on the oxygen content of samples, only when the extrusion temperature was 1350 ℃, with a holding time 5min, was there a slight increase in oxygen content. These are acceptable results and indicate that

the designed process for producing Ti-4%Al-4%Mo-4%Sn-0.5%Si titanium alloy is reasonable for avoiding large quantities of oxygen pick up during thermos-mechanical processing.

Table 4.2 Oxygen content of the Ti powder and as-extruded samples using the processing conditions given in Table 4.1

Sample	HDH Ti	Sample1	Sample2	Sample3	Sample4
Oxygen Content (wt.%)	0.3	0.36	0.36	0.36	0.44

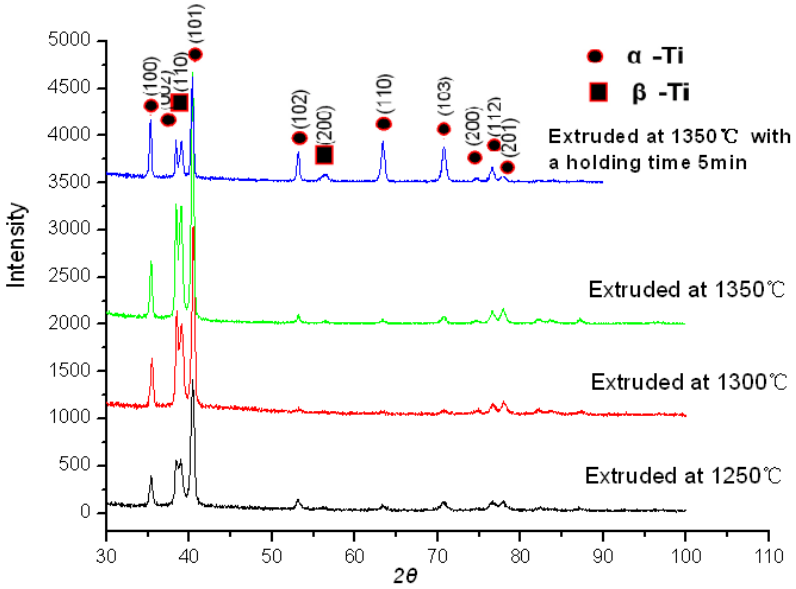

Fig.4.3 XRD patterns of the as-extruded samples

All the extruded samples had nearly full density. The XRD patterns of the as-extruded samples are shown in Fig. 4.3, with sample 1 at the bottom and sample 4 at the top. It is evident that all four samples consisted of α and β phases. It can be seen from the intensities that the volume fraction of β phase in sample 4 was smaller than that found in the other three samples. This may be because a 5min. holding time at the extrusion temperature, prior to extrusion at 1350°C, caused the Mo, which is a β stabilizer, to diffuse faster and become more homogenous. A more homogenous distribution resulted in a lower β stabilizer concentration overall, which was insufficient to preserve the β phase during cooling causing a lower amount of this phase. On the another hand, a higher extrusion temperature also helped the diffusion of α stabilizers such as Al and was beneficial to the precipitation of α phase. This would have led directly to a higher amount of α

phase after cooling.

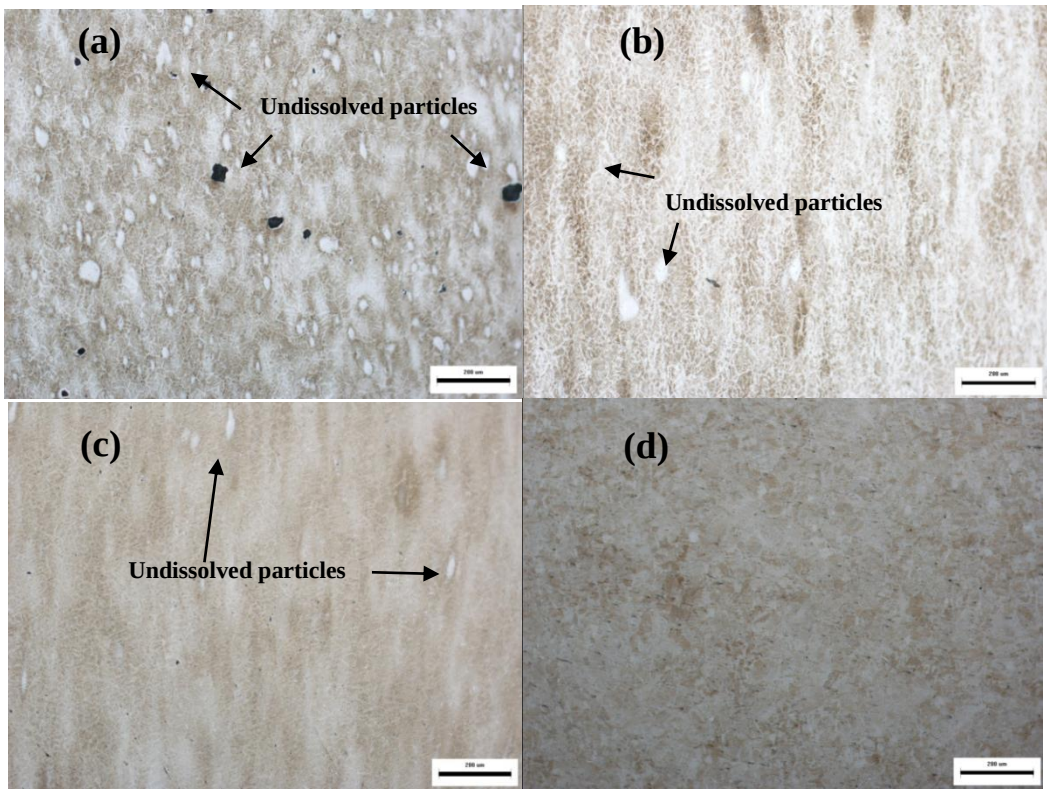

Fig.4.4 Optical micrographs showing the microstructures of as-extruded samples: (a) Sample 1; (b) Sample 2; (c) Sample 3; and (d) Sample4, the length of the scale bar is 200µm. White and dark spots are the undissolved elemental particles.

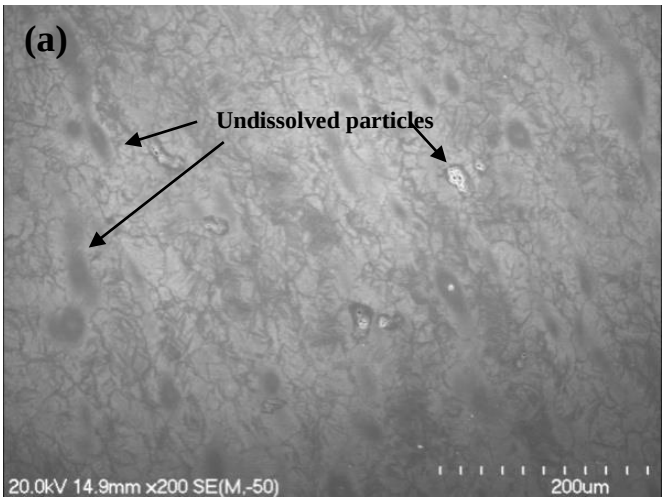

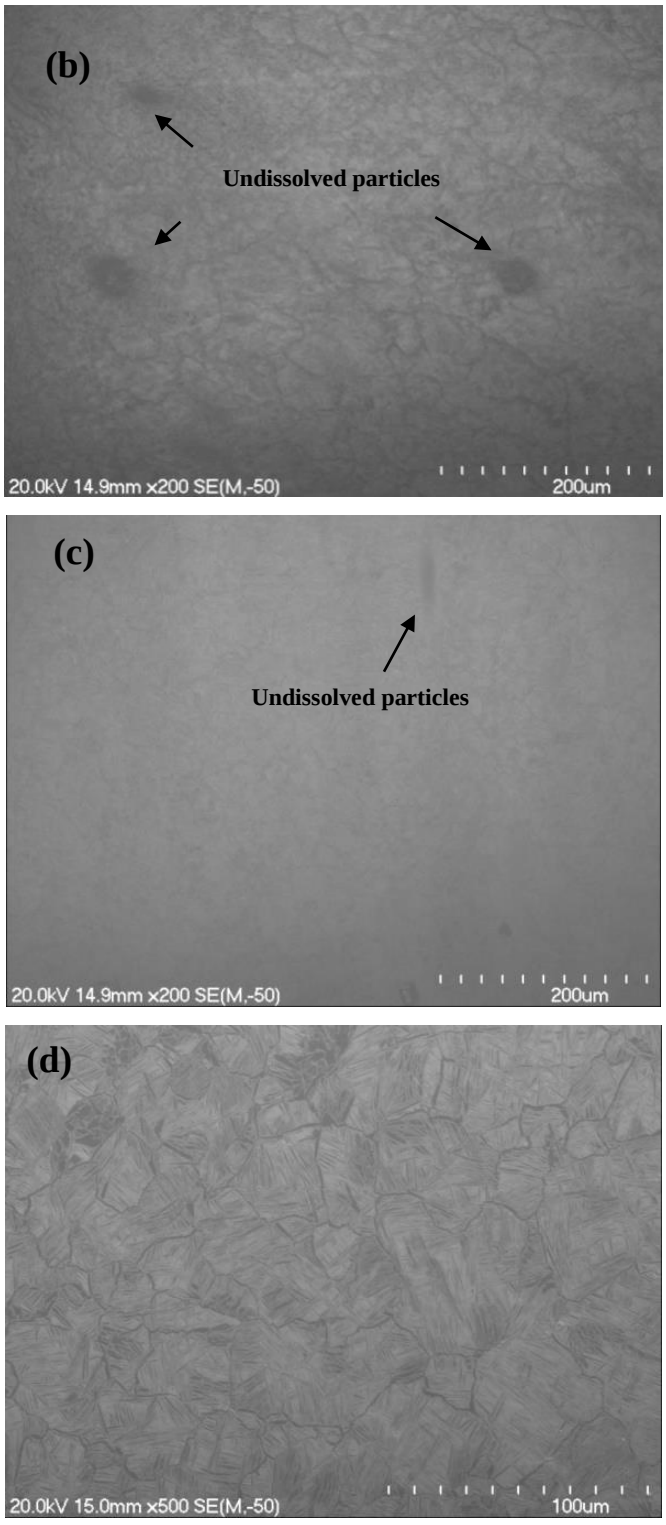

Fig.4.5 SEM images of microstructures of (a) Sample 1; (b) Sample 2; (c) Sample 3; and (d) Sample4. White and dark spots are the undissolved elemental particles.

Both optical and SEM micrographs of etched lengthwise-sections of samples 1-3 (Figs. 4.4 and Figs. 4.5) show the microstructures of as-extruded samples at higher magnification. Clearly, a large number of undissolved elemental particles are evident in the microstructure of samples 1-3, but it also can be seen that the

volume fraction and size of undissolved particles in the microstructure decreased dramatically with increasing extrusion temperature from 1250^{o}C-1350^{o}C. There were no apparent defects or undissolved elemental particles present in the microstructure of sample 4 which was extruded at 1350^{o}C with a holding time of 5min. The above observations indicate that the extrusion temperature significantly affects the degree of dissolution of the elemental particles. The evidence from the micrographs from samples 1-3, for extrusion temperatures in the range of 1250^{o}C-1350^{o}C, indicates that increasing extrusion temperature improves the dissolution of elemental particles. Finally, when a compact is treated at 1350^{o}C with a holding time of 5min, all the undissolved elemental particles are completely dissolved in the matrix.

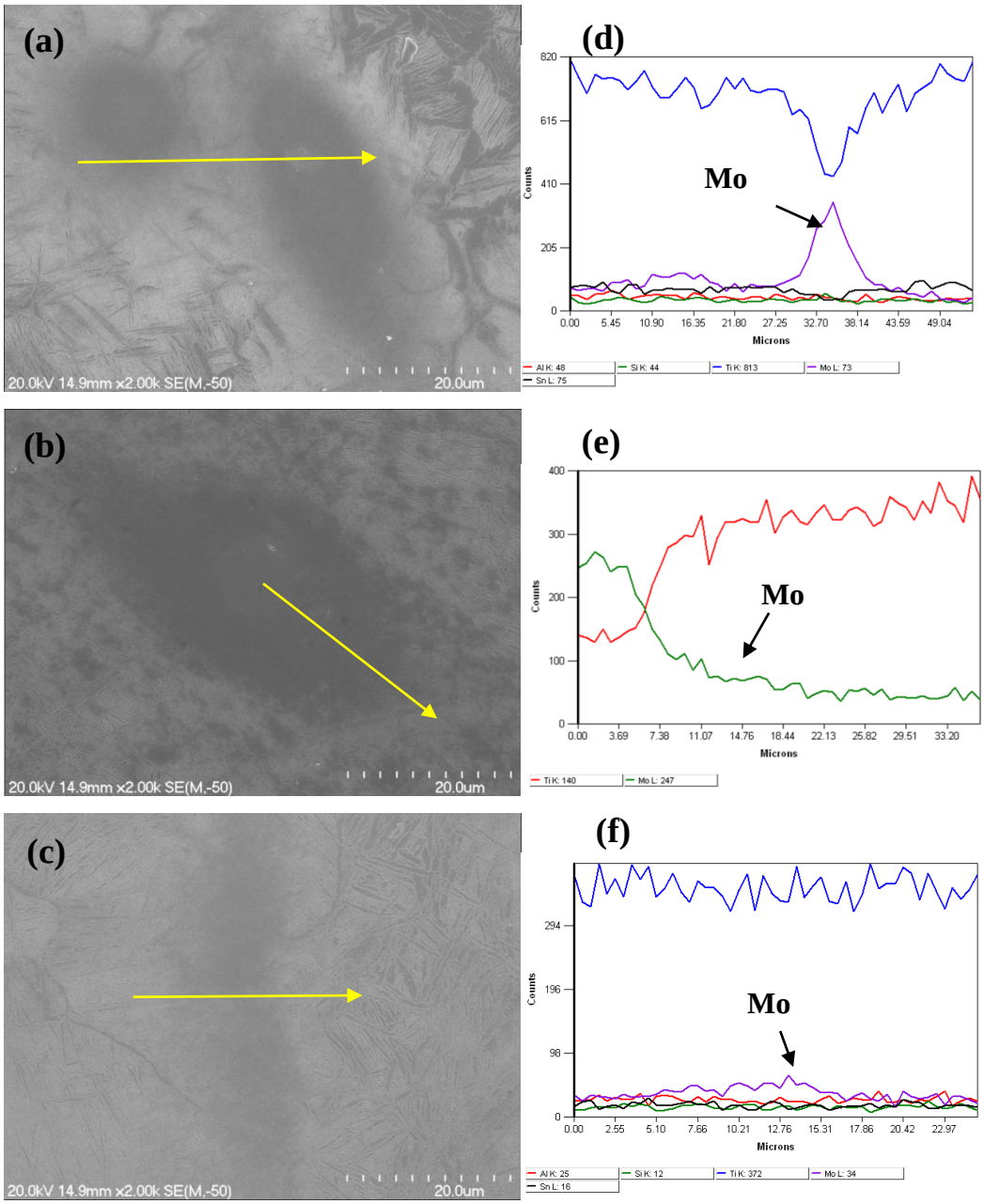

Fig.4.6 High magnification SEM images and corresponding X-ray line scans of a residual undissolved Mo particle in the microstructure of as-extruded samples 1-3. Micrographs (a), (b) and (c) show the morphologies of Mo present in the microstructure of samples 1, 2 and 3, respectively. Micrographs (d), (e) and (f) show the corresponding X-ray line scans of (a), (b) and (c), respectively. The yellow arrows indicate the routes and directions of the X-ray line scans.

It was established by EDS analysis that the undissolved element observed in the microstructures were undissolved Mo rich particles and Si rich particles. This is understandable because Mo has a very high melting point (2617^{o}C) while Si has low density and is easy to become agglomerated. Therefore, for different reasons, both these elements are hard to dissolve in a titanium matrix, especially when using a blended elemental powder metallurgy approach. Fig.4.6 shows high

magnification SEM images and the corresponding X-ray line scans of typical residual undissolved Mo particles existing in the microstructures of as-extruded samples 1-3. The high magnification SEM image and X-ray line scan in Figs. 4.6(a) and (d) respectively, indicate a distinct interface between a Mo particle and the matrix, which means that only a small part of the outer layer of the Mo particle has been dissolved. In Figs. 4.6 (b) the interface between a Mo particle and the matrix is less obvious and this is confirmed by the reduced slope in the X-ray line scan in Fig. 4.6 (e). The scattered dark spots around the Mo particles show that some parts of a Mo particle have dispersed further. With increasing extrusion temperature from 1250^{o}C to 1300^{o}C, the dissolution of Mo particles into the matrix is significantly improved. For a compact extruded at 1350^{o}C, Figs. 4.6 (c) and (f) show a Mo particle which is mostly dissolved in the matrix, with only a narrow and long Mo rich area remaining. The shape of this Mo rich area probably derives from the metal flow during extrusion. It is can therefore be concluded that the extrusion temperature has a significant effect on the degree of dissolution of Mo particles, and even when the extrusion temperature is increased to 1350^{o}C and most of the Mo particles have dissolved in the matrix, there are still some Mo rich areas present in the matrix.

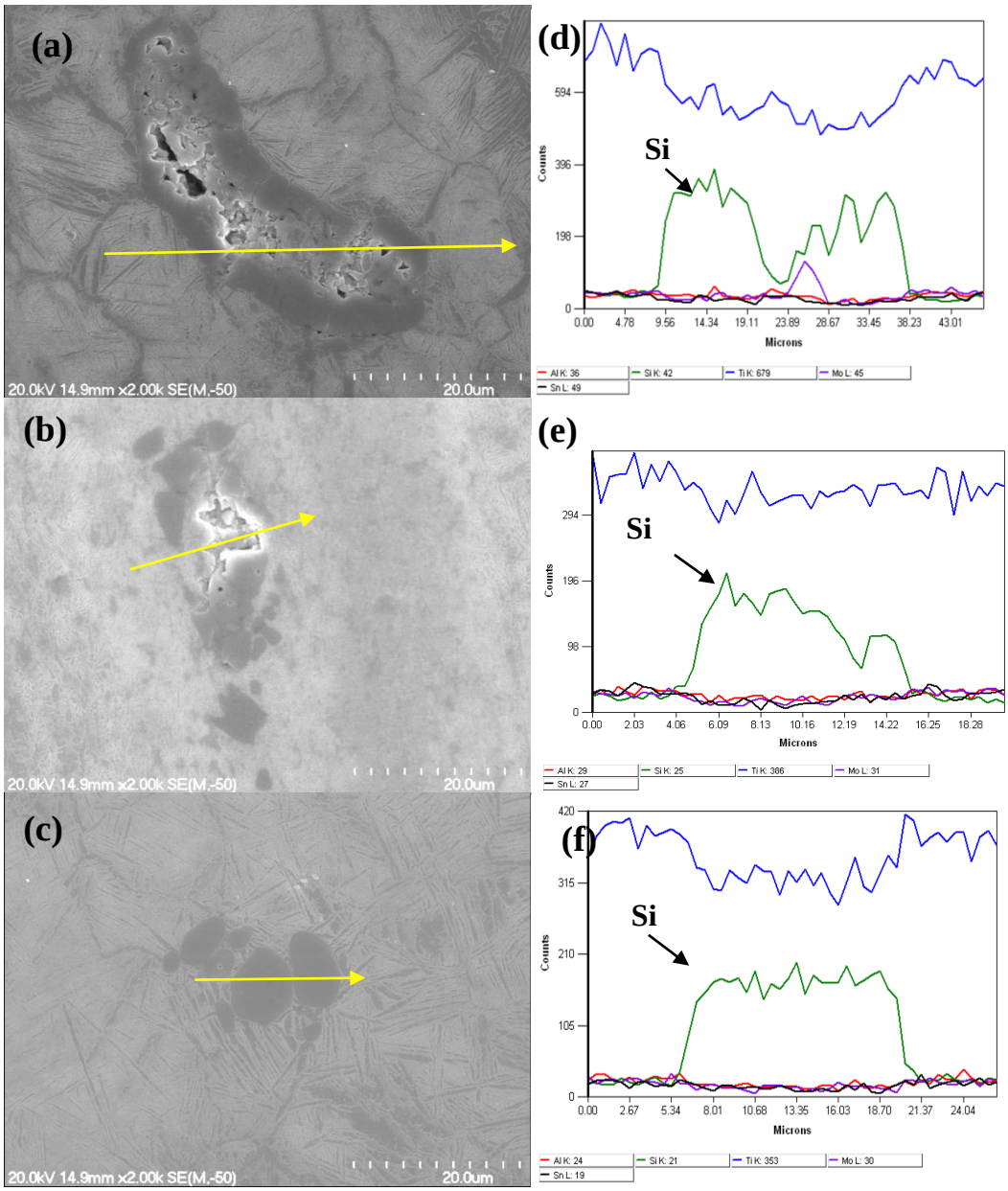

Fig.4.7 High magnification SEM images and corresponding X-ray line scans of residual undissolved Si particles in the microstructure of as-extruded samples 1-3; (a), (b) and (c) show the morphologies of undissolved Si particle present in the microstructures of sample 1, 2 and 3, respectively, (d), (e) and (f) show the corresponding X-ray line scans of (a), (b) and (c), respectively. The yellow arrows indicate the routes and directions of the X-ray line scans.

Fig.4.7 shows high magnification SEM images and corresponding X-ray line scans from typical residual undissolved Si particles existing in the microstructure of as-extruded samples 1-3. For a compact extruded at 1250^{o}C, the SEM image and X-ray line scan in Figs. 4.7 (a) and (b) respectively show that in the

microstructure there are large residual Si rich areas with associated pores. The formation of large and long Si rich areas in the microstructure is most likely caused by the low density of Si and its tendency to agglomerate. On the other hand, Si agglomerations are loosely bound to the matrix, and therefore the cavities observed in Si rich areas are caused by the removal of undissolved Si and Mo particles during etching or grinding. Figs. 4.7 (b) and (c) indicate that increasing extrusion temperature causes increased dissolution of Si so that the Si rich areas shrink. However an extrusion temperature 1350^{o}C is still insufficient for the complete dissolution of Si particles in a Ti matrix, as shown in Figs. 4.7 (c) and (f). When Fig. 4.7 (c) is compared with Fig.4.5 (d), it can be seen that a 5 min. holding time prior to extrusion at 1350^{o}C, causes complete dissolution of the Si rich areas.

Fig.4.6 and Fig.4.7 demonstrate the effect of extrusion temperature on the dissolution of Mo and Si in titanium matrix. It is known that Mo is a β stabilizer and high concentrations of β stabilizer in the titanium matrix result in high stability of the titanium β phase which prevents it from decomposing during cooling. So well diffused β stabilizing elements into the titanium matrix lead directly to a drop in their concentrations and reduce the stability of the β phase during cooling. That is to say, with improved diffusion of β stabilizers, the volume fraction of the β phase decreases and becomes more homogenous. This and observations from XRD patterns, explain why a higher extrusion temperature directly leads to a relatively low volume fraction of β phase. Si is a neutral β stabilizer, so to some extent, the complete dissolution of Si has a similar function as that of Mo for the rebalance of the α and β phases. Furthermore, in the Si rich areas, a eutectic reaction between Si and Ti can occur during cooling and some brittle products will be formed (for example: β-Ti → Ti_3Si +α-Ti) [10]. So in a sense, the monitoring of Si dissolution and achieving its complete dissolution is significant to synthesize titanium alloys with a homogenous microstructure and satisfactory mechanical properties.

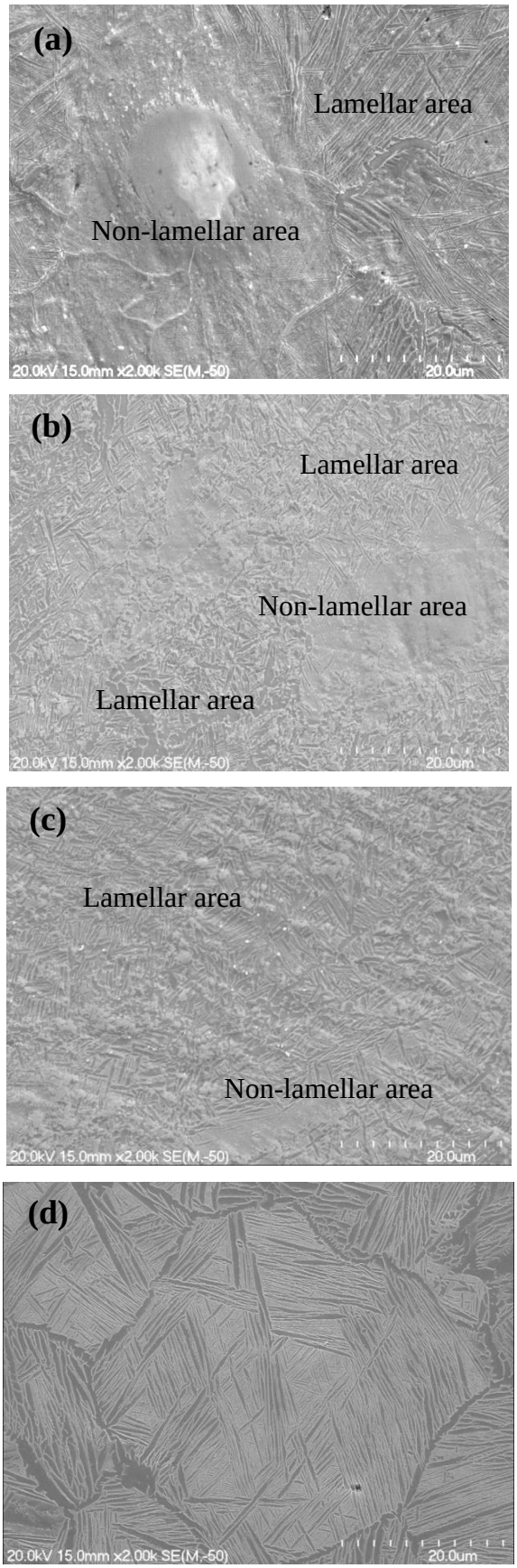

Fig.4.8 High magnification SEM images of the microstructures of as-extruded samples, (a) sample 1 extruded at 1250ºC, (b) sample 2 extruded at 1300ºC, (c) sample 3 extruded at 1350ºC and (d) sample 4 extruded at 1350ºC with a holding time 5min.

Fig.4.8 shows high magnification SEM images of the microstructures of as-extruded samples. Apparently samples 1-3 exhibit inhomogeneous microstructures due to the existence of undissolved elemental particles and an inhomogeneous elemental distribution, while sample 4 shows a homogenous microstructure with clear grain boundaries. The SEM images indicate that undissolved particle free areas in samples 1-3 have a lamellar structure, while the areas with undissolved particles shows a non-lamellar phase morphology. It is easy to understand why a non-lamellar phase morphology exists in locations where undissolved particles are present, because a high concentration of β stabiliser prevents the decomposition of the β phase during cooling. It also hinders the redistribution of α stabiliser, such as Al, into this area, so the β phase remains around the undissolved particles or the area with a high concentration of β stabilizers. This leads directly to the formation of a non-lamellar phase area.

The lamellar microstructure in sample 1 (Fig. 4.8(a)) shows coarse and long α lamellae precipitated from the prior β grain boundaries or inner prior β grains, while the microstructures for samples 2 and 3 (Figs. 4.8(b) and (c)) show fine and short α platelets with random orientations. So an increase in the extrusion temperature also leads to a finer microstructure. It is accepted that the concentration and distribution of different elements has a great impact on phase transformation and resulting microstructure. An α stabiliser, such Al, has a low melting point and diffusion into those areas with low concentration of β stabiliser elements is easy. Therefore the α phase, with a coarse morphology, can readily precipitate from such areas. This explains why coarse and long α lamellae have formed in the lamellar area shown in Fig.4.8 (a). With further dissolution of β stabilisers, such as Mo into the Ti matrix, the relative concentration of β stabiliser becomes higher in some areas and this hinders and slows down the formation of the α phase and directly results in a finer α with a shorter morphology as shown in Fig.4.8 (b) and (c).

In contrast to the microstructures for samples 1-3, the microstructure of sample 4 consists of primary β grains and colonies of a fine α/β lamellar structure, as shown in Figs.4.8 (d). The average grain size of sample 4 was approximately 50μm and

its microstructure was a typical Widmanstätten structure [11]. No undissolved particles from the prior elemental powder particles and no apparent defects were found in the microstructure. This strongly indicates that an extrusion temperature of 1350^{o}C with a holding time 5min is adequate to allow the complete dissolution of Mo and Si particles in the powder compact. It is also likely that the width of α platelets in the lamellar colonies is influenced by precipitation of silicides at the α-platelet/β phase interfaces [4]. Si is one of the common α stabilizers and Si additions can cause some Si compounds to precipitate with titanium along the α-platelet/β phase interfaces or the β grain boundaries. These precipitated silicides are normally of a nano-scale size. If they are precipitated at the α-platelet/β phase interfaces, the nano-scale silicides effectively hinder the growth of α-platelets in the cross-sectional direction, and are effective in refining the α-platelets. If they are precipitated along the β grain boundaries, not only can they help to prevent grain growth during hot working, but they also effectively segregate the dislocations and prevent dislocation climb, which improves the creep behaviour of material. This is why small amount of Si are always introduced into alloys. However, if Si is precipitated with titanium or other elements around the Si rich area, due to localized inhomogeneous elemental distribution, an extensive formation of silicides or other compounds could be a serious drawback. This is because of their brittle nature and the creation of poor bonding interfaces between them and the titanium matrix. This issue will be discussed in the next section.

4.3.2 Mechanical properties and fracture surfaces

Typical tensile engineering stress-strain curves of specimens cut from samples 1-4 are shown in Fig. 4.9. Tensile specimens from samples 1, 2 and 3 fractured prematurely at stresses of around 800MPa to 900MPa, respectively, before yielding. The improvement in the mechanical properties by increasing the extrusion temperature is not obvious for samples 1, 2 and 3. One tensile specimen from Sample 4 showed a yield strength, ultimate tensile strength and elongation to fracture of 1288MPa, 1423MPa and 5.1%, respectively, in which the strength is better than that found in material produced using a more traditional metallurgical method. For the latter material, the tensile strength is in the range 1200MPa-1300MPa with an elongation of 8% [12]. It was found that two tensile specimens

from Sample 4 exhibited poor mechanical properties and fractured prematurely at just under 500 MPa, with no ductility. That is to say, we can get high mechanical strength with reasonable ductility in a tensile test, but this was not repeatable among all the samples tested.

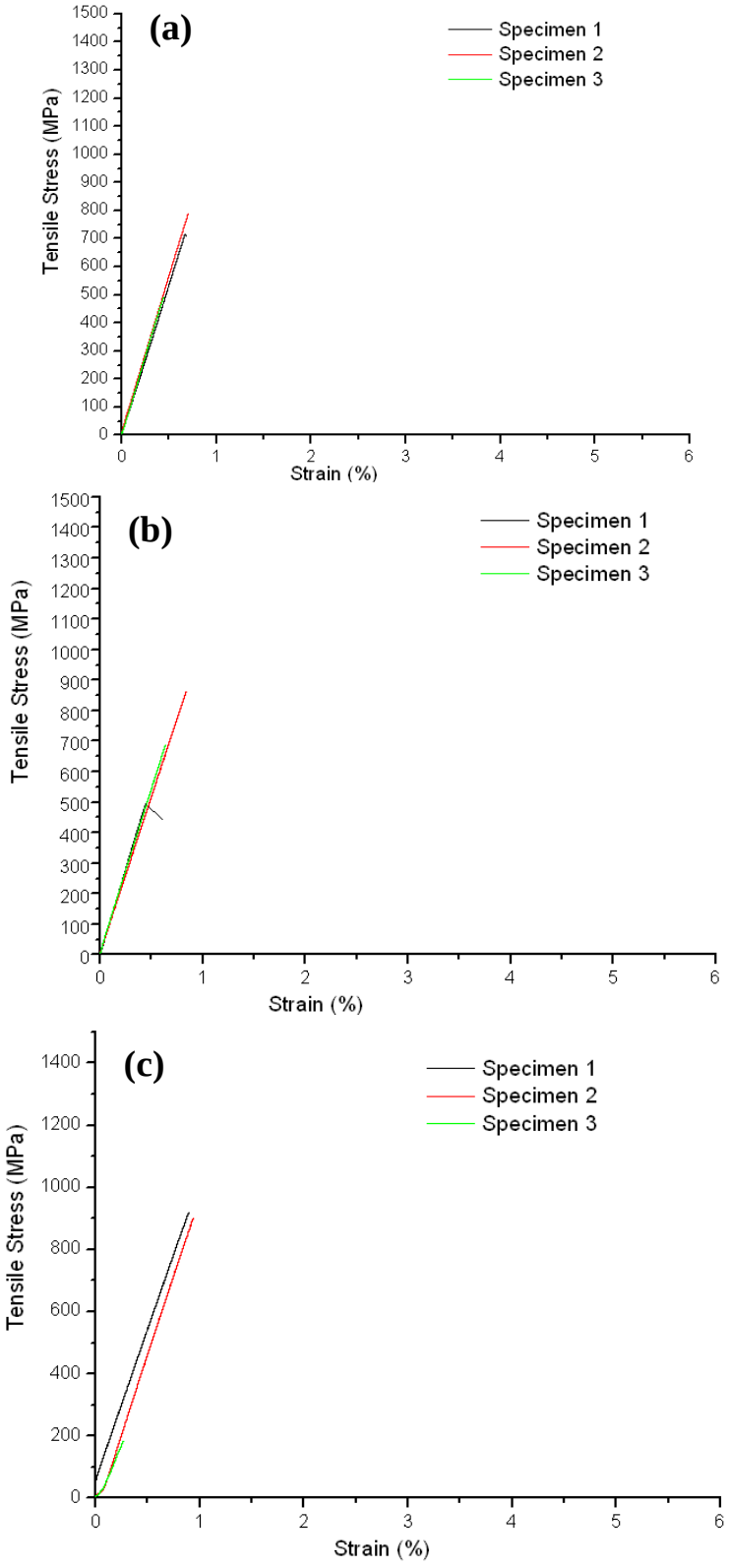

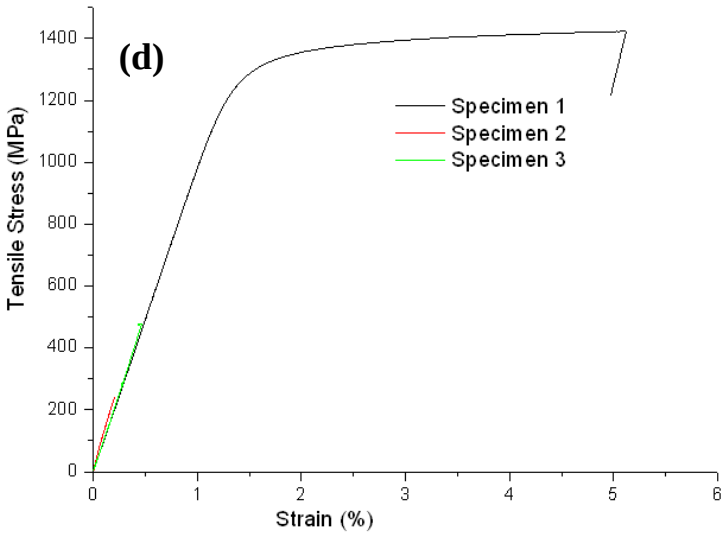

Fig.4.9 Tensile engineering stress-strain curves of as-extruded samples, (a) sample 1, (b) Sample 2, (c) Sample 3 and (d) Sample 4.

Fig.4.10 shows fracture surfaces for the broken tensile specimens. A fracture surface for sample 1 is not illustrated due to its similarity with those for samples 2 and 3. Figs. 4.10 (a) and (b) show a typical cleavege mode of fracture with obvious porous areas (as shown in Fig. 4.10 (a)) and a well defined crack growth direction shown in the cleavage fracture shown in Fig. 4.10 (b)). The pores, which were caused by undissolved elemental particles (because all as-extruded samples showed nearly full density), are clearly shown in the high magnification images in Figs. 4.10 (a)' and (b)'. It is clear from Fig.4.10 (a) that the cracks were generated and developed from porous areas associated with agglomerations of undissolved elemental particles, which led to fracture and failure. The river pattern cleavage characteristics in the fracture shown in Fig.4.10 (b) also shows that cracks were generated in and developed from a localised area, and then propagated from this area leading to failure. SEM examination of this localised area showed that it was also full of pores caused by undissolved particles like the one shown in Fig.4.10 (b)'. So the premature fracture of the tensile specimens cut from sample 1-3 could have been initiated by undissolved elemental particles. There are two possible explanations for the failure initiated by undissolved elemental particles during a tensile test. Firstly, the bonding interface between undissolved particles and the titanium matrix is weak and similar to that from mechanical interlocking; secondly, pores always exist where undissovled particles aggomerate together. The weak

interfaces between particles and matrix and the presence of porosity creates stress concentrations and a likely crack initiation site. This leads directly to brittle failure of the specimen during a tensile test.

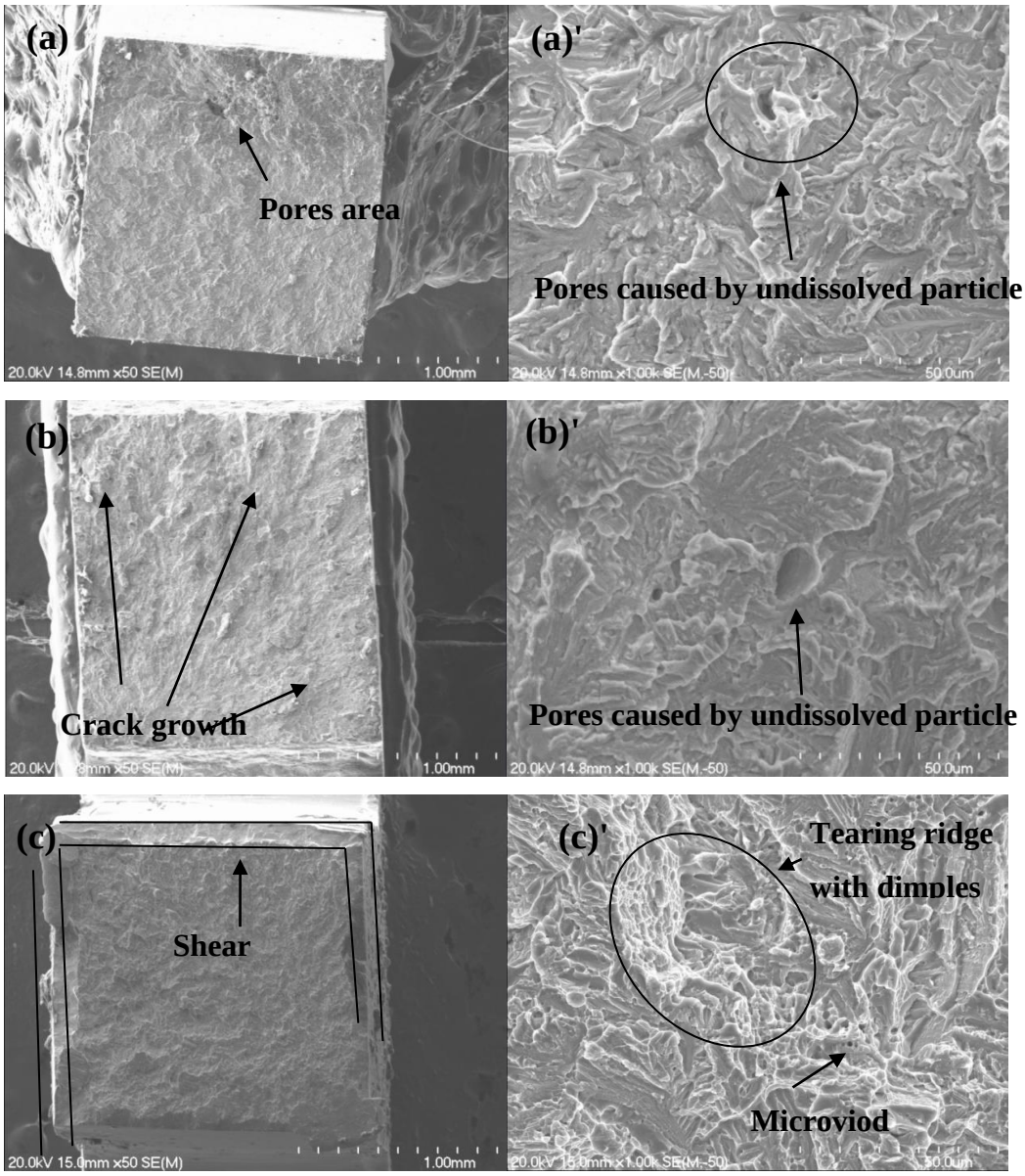

Fig.4.10 SEM images of the fracture surfaces of the tensile test specimens cut from the as-extruded samples; (a) sample 2, (b) sample 3; (c) sample 4, the high magnification SEM images (a)', (b)' and (c)' show typical fracture surface area from (a), (b) and (c), respectively.

Fig.4.10 (c) and (c)' show the fracture surface of a specimen with good ductility, cut from sample 4. The image 4.10 (c) shows a flat fracture surface without any cleavage steps and a shear region is clearly observed around the edge of fracture surface. High magnification SEM images shown in Fig.4.10 (c)' and Fig.4.11

reveal a mixture of trans-lamellar cleavage fracture of α/β lamellae and ductile fracture of grains as reflected by the tearing ridges with fine dimples. The grains which exhibited ductile fracture are most likely primary β grains. Microvoids (indicated by arrows in Fig.4.10 (c)') can also be seen on the lamellar structure and this seems to also contribute to the enhancement of the fraction of ductile fracture in the specimens. In contrast to the fracture mechanism for tensile specimens from samples 1-3, much better elemental dissolution and a relatively homogenous microstructure contributes to the good mechanical properties obtained from tensile specimens taken from sample 4.

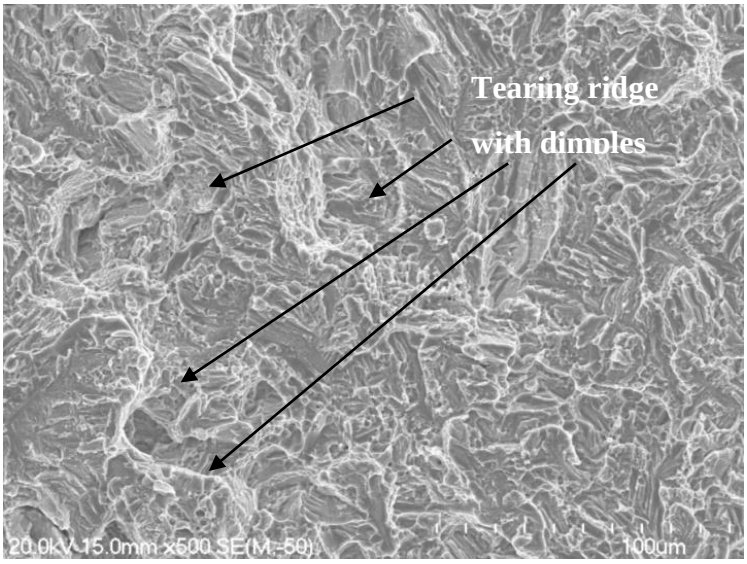

Fig.4.11 SEM image of a typical fracture surface from a specimen with good mechanical properties which was cut from sample 4.

On the other hand, as shown in Fig.4.9 (d), two specimens, prepared using an extrusion temperature of 1350℃ with a holding time 5min have poor mechanical properties. This reflects the presence of inhomogeneities in samples 4. Fig.4.12 shows a typical fracture surface for a tensile specimen with bad properties taken from sample 4. There are clearly identifiable porous areas on the fracture surface, which are in disagreement with an observation of a relatively homogenous microstructure without any visible defects. These porous defects were probably formed during tensile testing. The features in Fig.4.12 (b) show that the porous area is actually filled with dendrites having a pagoda-like appearance. Elemental quantitative analysis on the pagoda-like dendrites indicates that they consist of the

elements Ti, Al and Si. That is to say, some compounds are precipitated during cooling after high temperature processing; this is accordance with the discussion in section 4.3.1, namely that dendrites are easily precipitated in the Si rich areas at a certain cooling rate and these turn out to be a potential hazard to the overall quality of alloys. This phenomenon is critical to the properties of this material, so knowledge about how the dendrites are formed and avoidance of the large scale formation of dendrites is an important issue to be addressed.

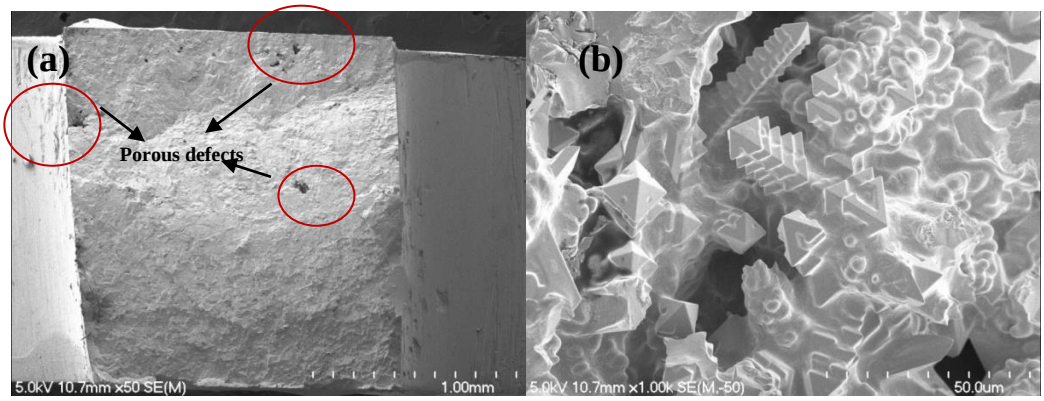

Ti	Al	Si
95.94wt.%	2.58wt.%	1.49wt.%

Fig.4.12 Typical SEM fracture surface images of the tensile specimens (from sample 4) which showed poor tensile properties with no ductility, (a) a low magnification image and (b) a high magnification image revealing the typical morphologies of porous defects, with a table listing an elemental quantitive analysis of the pagoda-like dendrites shown in (b).

4.3.3 Interactions between different elements during diffusion and the precipitated phase formed during high temperature processing

Different elements have different diffusion coefficients and when they are mixed together, the diffusion of one element can have an impact on the diffusion coefficients of another element [13]. So to investigate the interactions between the diffusion coefficients for different elements in a Ti-4%Al-4%Mo-4%Sn-0.5Si alloy, it is helpful to know how a localised inhomogeneous elemental distribution occurs.

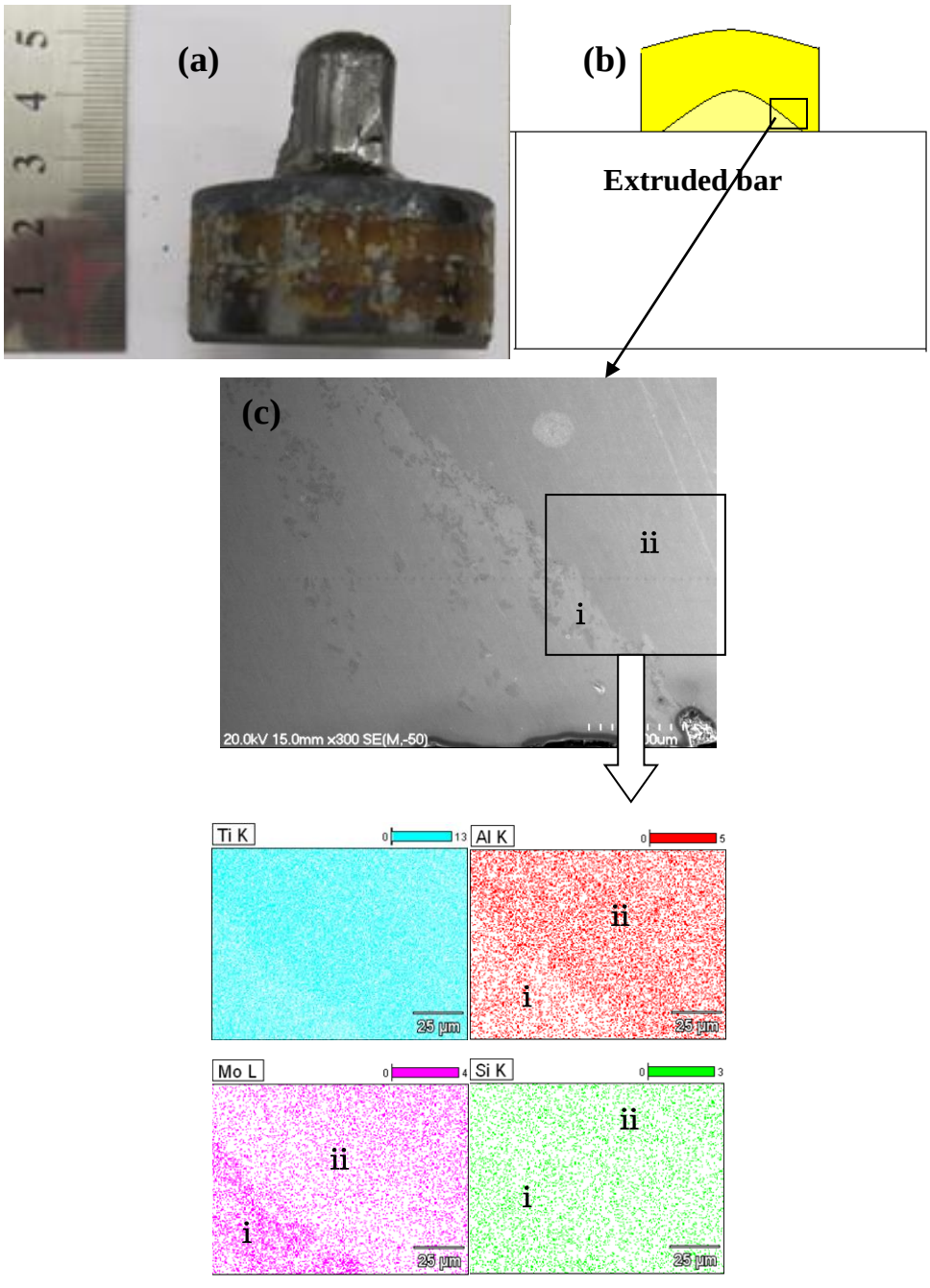

	Al-K (wt.%)	Si-K	Ti-K	Mo-L
Area i	2.01	0.96	82.50	5.73
Area ii	4.69	0.15	93.30	1.12

Fig.4.13 An investigation of the differences in elemental diffusion at the early stages of extrusion, (a) an as-extruded sample, (b) a sketch of an extruded part, showing a lengthwise cut with two distinct elemental distribution regions and (c) an SEM image showing the two distinct elemental distribution regions, along with EDS mapping and quantitative elemental analysis of these regions.

A short extrusion bar shows the early stage of extrusion with part of the extrusion

showing minimum plastic deformation and another with more severe plastic deformation. The early extrusion stage contains the original elemental distribution in the powder compact, while the more severely deformed stage shows the elemental redistribution caused by severe plastic deformation at high temperature. So to investigate the interactions between different elements, a short extrusion bar was prepared at 1350^{o}C with a holding time 5min as shown in Fig.4.13 (a). Two distinct elemental distribution regions are found in the microstructure of a lengthwise section, as shown in Fig.4.13 (c). EDS mappings and quantitative analysis clearly shows the elemental differences between each area (the mapping of Sn is not shown due to its homogenous distribution).

During extrusion, the temperature in region i is higher than that in region ii, so generally speaking the Al content in region i should be higher than that in region ii. But the measured results show quite the reverse, namely the Al content in region i is lower than that in region ii. A reasonable explanation is that at a temperature of 1350^{o}C the solubility of Mo in Ti is much higher than that of Al [13], and the high amount of Mo β stabilizer, which helps β phase retention, hinders Al diffusion and reduces its diffusion coefficient. So we can conclude that an inhomogeneous distribution of Al occurs in localised areas after high temperature processing due to the impact of other elements.

The differences in the Si and Mo content in area i and ii are larger than those found for Al which indicates that the diffusivity of Si and Mo is lower than that for Al. This is understandable because Si and Mo have a high melting temperature and Si powder easily becomes agglomerated, contributing to their low diffusivities in titanium. This phenomenon possibly contributes to the formation of localised inhomogeneous elemental distributions.

After area i was etched, some non-lamellar areas could be seen, as shown in Fig.4.14 (a) (area identified with a circle). EDX data indicated that the non-lamellar area contains only Ti, Al and Si (as shown in (b)) and an EDS point analysis shows a location with a particularly high Si content. This is evidence of the precipitation of compounds after processing due to the inhomogeneous elemental distribution in localized areas.

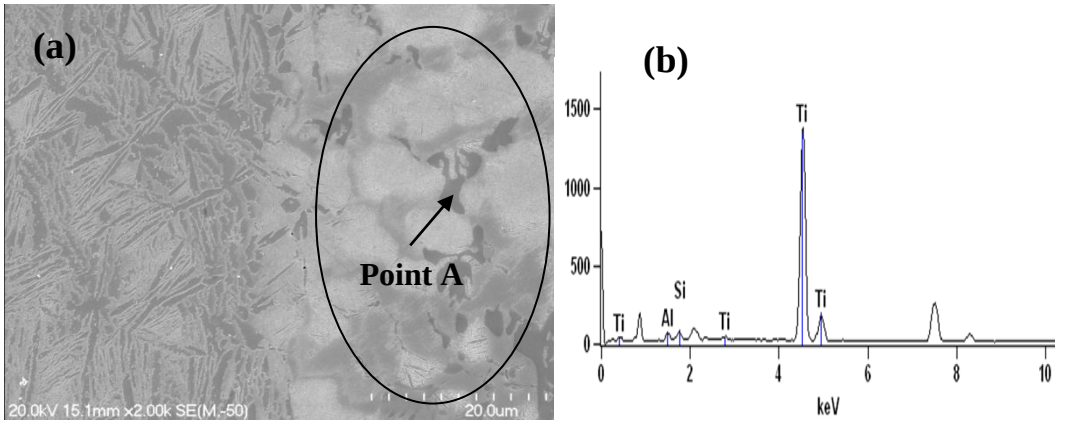

	Al-K	Si-K	Ti-K	Mo-L	Sn-L
Point A	0.91	16.12	82.97		

Fig.4. 14 A selected etched microstructure of area i shown in Fig. 4.13, (a) SEM image of the selected microstructure, (b) EDX spectra of the area marked with a black circle with a table showing a quantitive analysis of point A.

The above observations indicate that even without microstructural disruption caused by undissolved elemental particles, it is hard to find any well diffused Si, and Mo. This is because of their low diffusivities in a Ti matrix which leads to localised inhomogeneous Al distributions after high temperature processing due to the impact of other elements. Another very important reason for an inhomogeneous elemental distribution is residual elemental inhomogeneity after blending.

To ascertain the effect of an inhomogeneous elemental distribution, a batch of blended powders was analysed using an SDT test, and the result is shown in Fig.4.15. There are two exothermic peaks in the SDT trace obtained from heating the initial blended powders. This reveals that exothermic reactions (for example : β-Ti → Ti_5Si_3 +α-Ti) occur in the temperature range 500-700^oC (as shown in Fig.4.15). These observations are in accordance with those of other workers who have studied the ternary Ti-Al-Si phase [14-16]. This means that reactions have already happened with increasing temperature due to the inhomogeneous elemental distribution. No matter what outcome occurs after these reactions, they may have a further impact on further elemental diffusion.

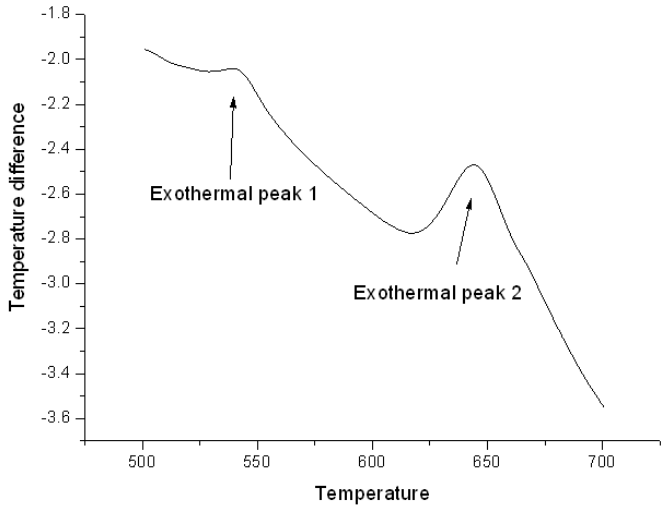

Fig.4.15 An SDT trace obtained during the heating of blended elemental powders with a composition of Ti-4%Al-4%Mo-4%Sn-0.5%Si, showing two exothermic peaks.

Fig.4.16 shows high magnification SEM images of the dendrites found in the fracture surface of a tensile test specimen from sample 4, with bad properties. There are clearly two different kinds of dendrite, each with a different composition, precipitated during cooling after preparation. The dendrites have a significantly different Si content, one is 1.49wt% and another one is 23.52wt%. If we check the phase diagram for the Ti-Si system, when the liquid is slowly cooling down from 1330°C, which is lower than the extrusion temperature 1350°C, a region with a high concentration of Si could liquify causing Ti_5Si_3 to form and be retained down to room temperature, while a lower Si concentration of about 2wt% could lead to a β Ti phase dendrite. So the pagoda-like dendrite most likely consists of β Ti which is formed with the help of Si and the other kind of dendrite is probably Ti_5Si_3.

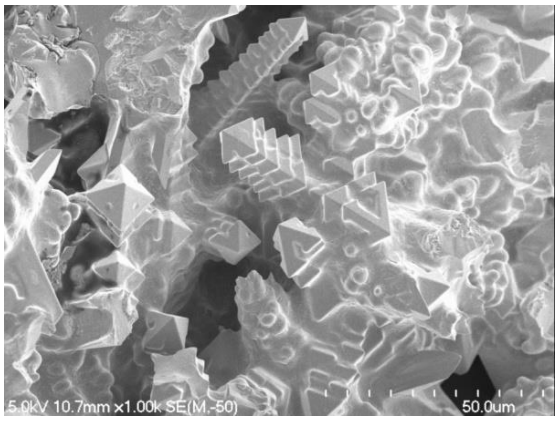

Ti	Al	Si
95.94wt.%	2.58wt.%	1.49wt.%

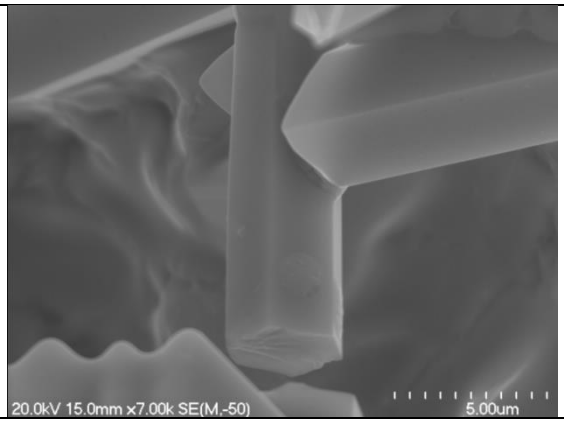

Ti	Al	Si
74.96wt.%	1.52wt.%	23.52wt.%

Fig.4.16 Two different kinds of dendrite (SEM images) and EDS analysis results found from the fracture surface of the specimen with bad properties from sample 4.

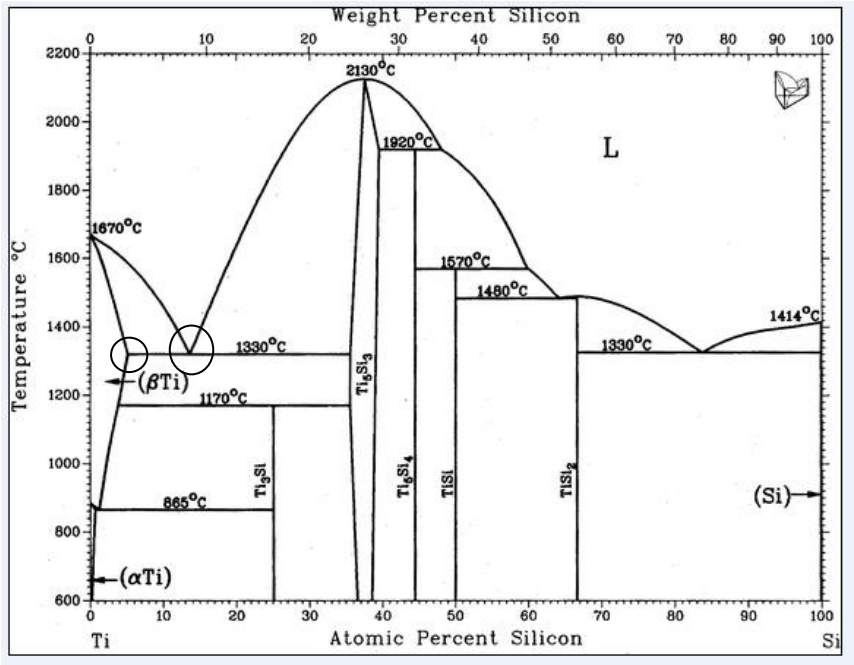

Fig.4.17 Phase diagram of the Ti-Si system[17], circles indicates two different precipitations could occur.

4.4 Conclusions

(1) The extrusion temperature has a significant effect on the degree of elemental dissolution. An increase in the extrusion temperature significantly improves the dissolution of Si and Mo. However, an extrusion temperature 1350^{o}C is still not enough to achieve complete dissolution of the elemental particles, especially Si and Mo particles. By using an extrusion temperature 1350^{o}C with a holding time 5 min prior to extrusion, elemental dissolution was much improved and a relatively homogenous microstructure was achieved.

(2) As-extruded bars with undissolved elemental particles showed low tensile strength without any ductility, while those samples without any inhomogeneities in the microstructure caused by undissolved particles and defects showed an ultimate tensile strength and elongation to fracture of 1423MPa and 5.1%, respectively.

(3) After achieving dissolution of the elemental particles, some localized areas with an inhomogeneous elemental distribution still existed. These most likely derive from non-uniform blending during powder mixing and the diffusion interactions between different elements during high temperature processing.

(4) Ti_5Si_3 and β Ti dendrites grew during cooling due to the local elemental

inhomogeneities. These dendrites are detrimental to the mechanical properties of the alloy, being the main reason for premature failure during tensile testing, leading to a large variation in tensile properties.

References

[1] P. Esteban, L. Bolzoni, E. Ruiz-Navas, E. Gordo, PM processing and characterisation of Ti‐7Fe low cost titanium alloys, Powder Metallurgy, 54 (2011) 242-252.
[2] D. Eylon, P.R. Smith, S.W. Schwenker, F.H. Froes, Status of Titanium Powder Metallurgy, ASTM STP, 830 (1984) 48-65.
[3] T. Fujita, A. Ogawa, C. Ouchi, H. Tajima, Microstructure and properties of titanium alloy produced in the newly developed blended elemental powder metallurgy process, Materials Science and Engineering: A, 213 (1996) 148-153.
[4] M. Hagiwara, S. Emura, Blended elemental P/M synthesis and property evaluation of Ti-1100 alloy, Materials Science and Engineering: A, 352 (2003) 85-92.
[5] F. Froes, D. Eylon, Developments in Titanium P/M, Moscow, ID: University of Idaho website, (2005).
[6] F. Froes, M.A. Imam, Cost Affordable Developments in Titanium Technology and Applications, Key Engineering Materials, 436 (2010) 1-11.
[7] M.T. Jia, D.L. Zhang, B. Gabbitas, Comparison of blended elemental (BE) and mechanical alloyed (MA) powder compact forging into Ti-6Al-4V rocker arms, Key Engineering Materials, 520 (2012) 82-88.
[8] F. Yang, D.L. Zhang, H.Y. Lu, B. Gabbitas, Preparation, Microstructure and Properties of Ti-6Al-4V Rods by Powder Compact Extrusion of Powder Mixture, Key Engineering Materials, 520 (2012) 70-75.
[9] A. Simchi, G. Veltl, Behaviour of metal powders during cold and warm compaction, Powder Metallurgy, 49 (2006) 281-287.
[10] Y. Zhan, X. Zhang, J. Hu, Q. Guo, Y. Du, Evolution of the microstructure and hardness of the Ti–Si alloys during high temperature heat-treatment, Journal of Alloys and Compounds, 479 (2009) 246-251.
[11] E. Borisova, G. Bochvar, M.Y. Brun, Metallography of Titanium Alloys, Metallurgiya, Moscow, (1980) 464.
[12] R. Boyer, E. Collings, Materials properties handbook: titanium alloys, ASM international, 1993.
[13] A. Carman, L. Zhang, O. Ivasishin, D. Savvakin, M. Matviychuk, E. Pereloma, Role of alloying elements in microstructure evolution and alloying elements behaviour during sintering of a near-β titanium alloy, Materials Science and Engineering: A, 528 (2011) 1686-1693.
[14] C. Azevedo, H. Flower, Experimental and calculated Ti-rich corner of the Al-Si-Ti ternary phase diagram, Calphad, 26 (2002) 353-373.
[15] X.-G. Chen, M. Fortier, TiAlSi intermetallic formation and its impact on the casting processing in Al–Si alloys, Journal of Materials Processing Technology, 210 (2010) 1780-1786.
[16] Z. Guan, T. Pfullmann, M. Oehring, R. Bormann, Phase formation during ball milling and subsequent thermal decomposition of Ti–Al–Si powder blends, Journal of Alloys and Compounds, 252 (1997) 245-251.
[17] H. Okamoto, Desk handbook: phase diagrams for binary alloys, ASM international, 2000.

Chapter 5 The effect of different starting powders on the microstructure and mechanical properties of an as-extruded Ti-4%Al-4%Mo-4%Sn-0.5%Si alloy

5.1 Introduction

Defects directly affect the overall performance of materials, particularly for small samples, which are sensitive to the slightest defects occurring during processing. Therefore, during materials' preparation, it is important that the impact of defects is minimised. As shown in Chapter 4, although good performance is generally obtainable for different extrusion conditions, the uniformity of mechanical properties can be variable, due to the existence of small defects, and this needs to be further improved. The purpose of this section is to describe the preparation of extrusion bars from different starting powders, intended to eliminate defects, improve the overall performance of the material, or to provide a reference and constructive suggestion for preparing extrusion samples with good overall mechanical properties.

From the last section it was found that an extrusion temperature of 1350^{o}C and a holding time of 5min is enough to dissolve the alloying elements into the titanium matrix. As a result a high tensile strength with good ductility can be obtained but there is variability in mechanical properties caused by precipitated dendrites as a result of an inhomogeneous elemental distribution in localised areas. To eliminate localised inhomogeneous elemental distributions, as-milled elemental powders and gas atomized (GA) titanium powder were introduced into this study. Three samples were prepared for this study, namely sample 4 which was prepared from HDH titanium powder blended with other elemental powders, sample 5 prepared from HDH titanium powder blended with other as-milled elemental powders and sample 6 prepared from GA titanium powder blended with other elemental powders. An introduction of as-milled Ti-Al-Mo-Sn-Si powders is expected to achieve more homogeneity in the elemental distribution, which will reduce the possibility of dendrite precipitation during hot processing. The introduction of gas

atomized titanium powder aims to achieve a relatively homogenous elemental distribution. This is because the lower oxygen content and thinner oxide layer on GA titanium powder, compared with HDH titanium powder, increases the potential for more homogenous elemental diffusion. The microstructures and mechanical properties were investigated and the effect of elemental diffusion on these is also discussed in this section.

5.2 Experimental details

The starting materials used in this study were almost the same as those used in the last section except that gas atomized (GA) Ti powder was used here. The particle size and purity of the powders is given in Table 5.1. For samples 4 and 6, the blending of elemental powders was carried out for 24 hours in a roller mill with the container rotating at 200 rpm. For sample 5, a powder mixture of Mo+Al+Sn+Si was milled using a planetary milling machine at a speed of 400pm for 2hr and then the as-milled powder was blended with HDH titanium powder in the roller mill at a speed of 200rpm for 24hr. The starting powders used for all the samples were mixed with a nominal composition of a Ti-4%Al-4%Mo-4%Sn-0.5%Si alloy. The morphologies of the different starting powders used in this study are shown in Fig.5.1.

Table 5.1 Starting powders used in this study

	Gas atomized Ti	HDH Ti	Al	Mo	Sn	Si
Particle size	-200mesh	-200mesh	d_{50}=40μm	-100mesh	-325mesh	-100mesh
Purity	Oxygen= 0.15wt%	Oxygen= 0.3wt%	99.9%	99.9%	99.99%	99.95%

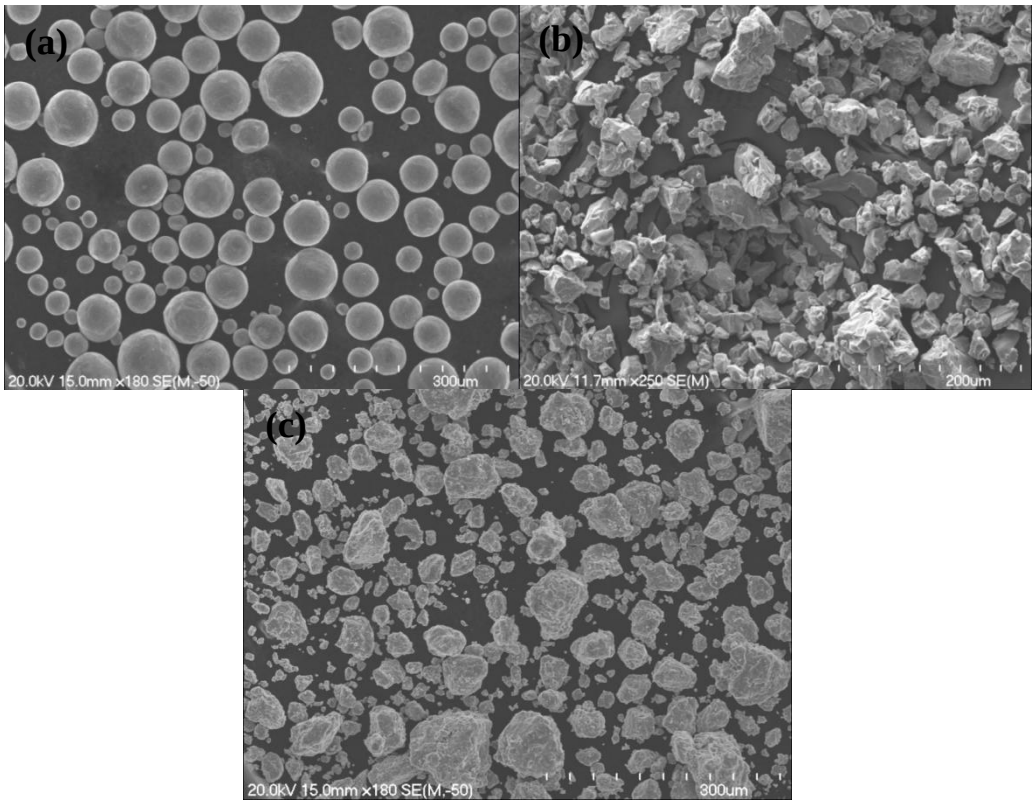

Fig.5.1 The morphologies of the different powders used in this study: (a) GA titanium powder, (b) HDH titanium powder and (c) HDH Ti powder blended with as-milled Al-Mo-Sn-Si powder

The blended powders were compacted at room temperature in a 40mm diameter die under a pressure of 718MPa, then the powder compacts were heated to temperatures in the range of 1250-1350℃ using an induction coil with a designated holding time and extruded using a maximum pressure of 707MPa. The parameters used for the different Ti powder types and the extrusion temperature, are given in Table 5.2.

Table 5.2 Ti powder types and extrusion temperatures for making the extrusion samples.

Sample name	Starting powders	Extrusion temperature, ℃
Sample 4	HDH Ti+ Al+Mo+Sn+Si	1350 with a holding time 5min
Sample 5	HDH Ti +as-milled powder mixture of Al+Mo+Sn+Si	1350 with a holding time 5min
Sample 6	GA Ti + Al+Mo+Sn+Si	1250

The microstructures of the extruded samples were characterised by optical microscopy (Olympus BX60), X-ray diffraction (XRD) (Philips X' Pert system), and scanning electron microscopy (SEM) (HITACHI S4000) with an attached

EDS elemental analysis detector. Tensile testing was carried out using a 4204 INSTRON universal testing machine with dog-bone shaped specimens having a rectangular cross-section of 2mm x 2.5mm and a gauge length of 20mm. The strain was measured using an extensometer with a gauge length of 10mm. The strain rate used during tensile testing was $1\times10^{-4}s^{-1}$.

5.3 Results and discussion

5.3.1 Microstructure

Fig.5.2 shows the results of XRD analysis of as-extruded samples. The XRD peaks indicate that all three samples are typically two phase alloys, consisting of α and β phases and no other phases precipitated during cooling were detected (in all cases the cooling conditions were the same, namely air cooling after extrusion). Compared with the other two samples, there was a lower volume fraction of β phase in sample 6, which indicates that in this case the α phase was almost completely precipitated during β phase decomposition. We know that the mechanical properties of an alloy are not only determined by phase composition, but also by microstructure [1, 2]. As a result of a lower β volume fraction, which can be easily distinguished from the much lower peaks for the β phase in sample 6, compared with those for samples 4 and 5, we might expect the strength of sample 6 to be lower than that of sample 4 and 5, but with a relatively higher ductility [3, 4]. A similar phase compositions in samples 4 and 5 might lead to them having a similar tensile strength and ductility. Furthermore, a well precipitated α phase in sample 6, during β phase decomposition also indicates that an α stabilizer, such as Al, is well distributed or that there is a relatively higher concentration of α stabilizer along the β grain boundaries [4]. This is because the α phase nucleates preferentially at the β grain boundaries, leading to a more or less continuous α layer along them. With continued cooling, α plates nucleate either at the interface of the continuous α layer or at the β grain boundary itself, growing into the β grains as parallel plates [4-7]. So a well distributed and relatively higher concentration of α stabilizer along the β grain boundaries aids α phase precipitation during β phase decomposition.

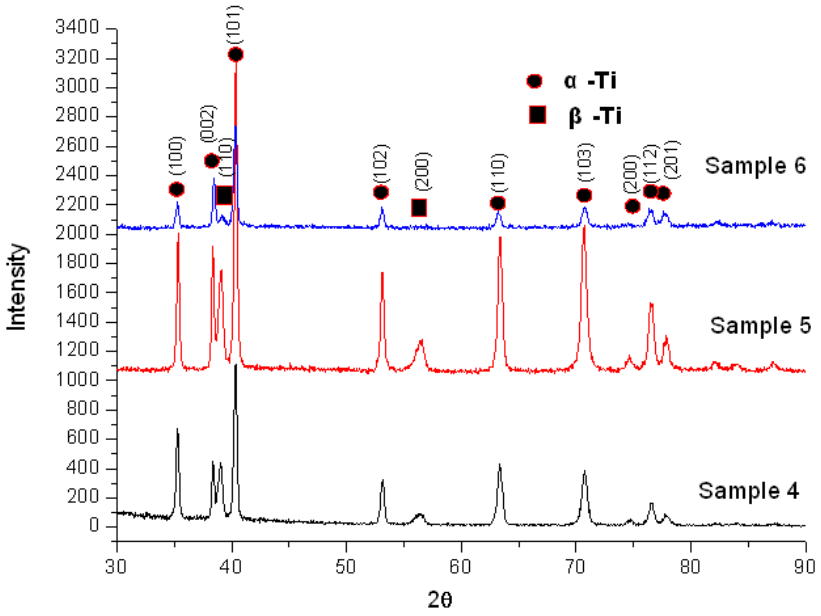

Fig.5.2 XRD patterns of as-extruded samples, sample 4 was prepared from HDH Ti with other elemental powders, sample 5 was prepared from HDH Ti with as-milled elemental powders and sample 6 was prepared from GA Ti with other elemental powders.

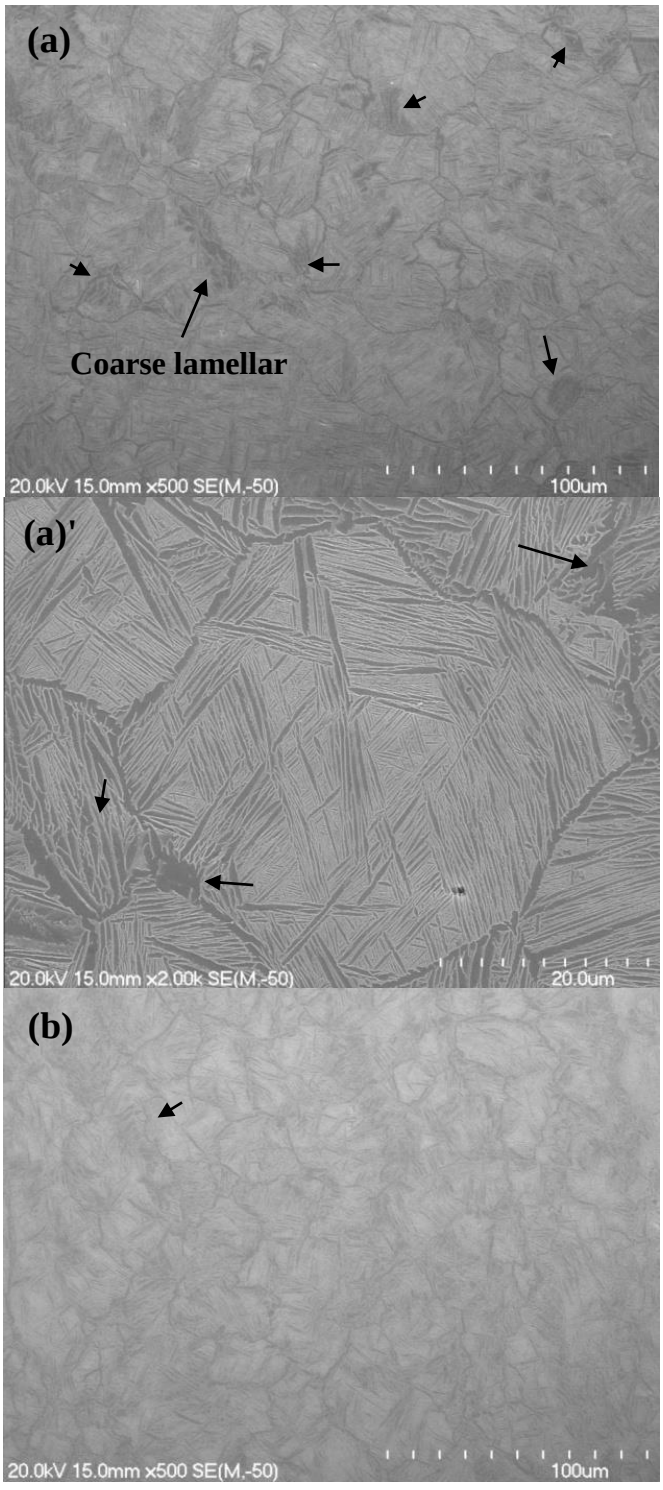
(a)
Coarse lamellar
20.0kV 15.0mm x500 SE(M,-50)
100um
(a)'
20.0kV 15.0mm x2.00k SE(M,-50)
20.0um
(b)
20.0kV 15.0mm x500 SE(M,-50)
100um

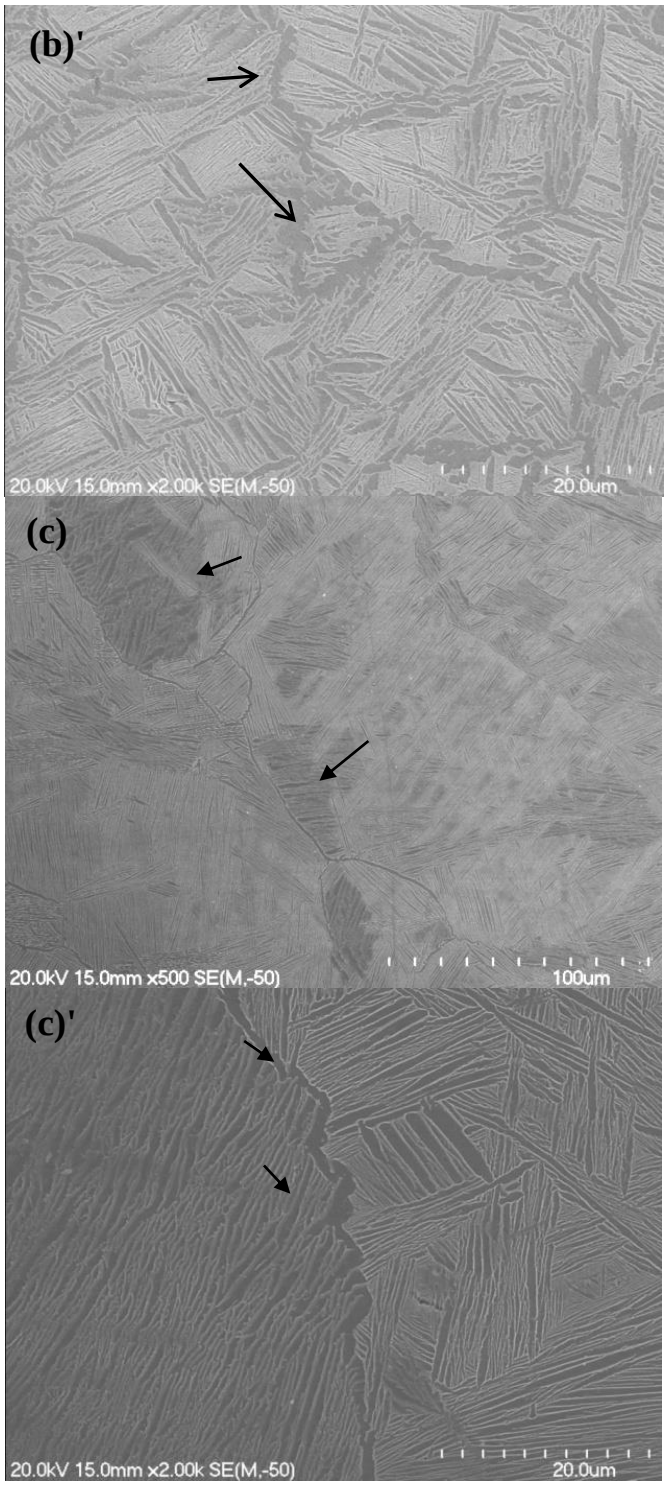

Fig.5.3 SEM images of the microstructure in as-extruded samples, (a) and (a)' sample 4 at low and high magnifications respectively; similarly (b) (b)' and (c) (c)' shows the microstructures in samples 5 and 6, respectively. Coarser lamellar areas are pointed out by black arrows.

Fig.5.3 shows SEM images of as-extruded samples. No undissolved elemental particles were found in any of the microstructures, indicating complete elemental dissolution in the matrix during extrusion. All the samples show a typical

Widmanstätten structure with primary β grains and α lamellar colonies. It is also easy to see from the micrographs that all the samples contain both coarse and fine lamellar areas.

The lower magnification images (a), (b) and (c), show that there is a more homogeneous lamellar structure and grain size in sample 5 compared with samples 4 and 6. Since the alloying element distribution affects the microstructure, this suggests that the distribution of alloying elemental in sample 5 is more homogenous than that in samples 4 and 6. This indicates that mechanically milling the mixture of powders used for alloying created a relatively homogenous distribution of alloying elements.

The micrographs also indicate that the lamellae in the coarser-lamellar areas in sample 4 are larger than similar areas in samples 5 and 6. However, in different areas of sample 6, there are some small differences in the morphology of the lamellar structure, but overall it is similar. Elemental quantitative analysis of the coarse lamellar areas, shown in Table 5.3, shows that the Si content is higher in these areas in samples 4 and 5 and the Si content in such areas seems close to the nominal content namely 0.5wt.%. In section 4.3.1 we have already discussed the effect of Si rich compounds, which might be precipitated in Si rich areas and their detrimental effect on tensile properties. A comparison of the lamellar structures in samples 4 and 5, suggests that they might have similar tensile strengths, and that the reproducibility of mechanical properties from sample 5 should be better than those from sample 4, because of a more homogenous lamellar distribution.

Table 5.3 EDS quantitive analysis of the relatively coarser lamellar areas of each as-extruded sample

	Al (wt.%)	*Si (wt.%)*	*Ti (wt.%)*	*Mo (wt.%)*	*Sn (wt.%)*
Sample 4	3.68	0.96	89.70	2.53	3.13
Sample 5	3.17	0.95	90.34	1.26	4.28
Sample 6	3.71	0.43	89.38	2.92	3.56

Weight % Error (+/- 1 Sigma) of each element in samples

Al	*Si*	*Ti*	*Mo*	*Sn*
+/-0.10	+/-0.14	+/-0.66	+/-0.23	+/-0.22

Table 5.4 shows a quantitative elemental analysis of the grain boundary region of each as-extruded sample. The results demonstrate that the Si content of the grain boundaries in sample 5 is much higher than that for the other two samples. In

sample 5 the Si content is 0.91wt.%, whereas the Si content at the grain boundaries in samples 4 and 6 is close to the nominal content 0.5wt.%. It is known that silicides are normally precipitated at the grain boundaries and also tend to segregate on dislocations, where they effectively prevent dislocation climb and increase the yield strength [8]. The close to nominal Si content at the grain boundaries in sample 4, explains why one tensile specimen had a high strength and fairly good ductility with a UTS of 1423MPa and an elongation to fracture of 5.1%. The Si rich areas located within the β grains resulted in the precipitation of intermetallic Si rich compounds, and this led directly to the variable tensile properties in sample 4. However, sample 6 has a similar Si content to that in sample 4, but in sample 6 the Si is well diffused with a homogenous distribution within the β grains and at the grain boundaries. This suggests that more uniform mechanical properties such as in sample 6 are more likely to be obtained, compared with the variability found in sample 4. To illustrate a potential benefit from using gas atomized titanium powders, a lower oxygen content is obtained when GA Ti powder is used instead of other kinds of starting powders.

When as-milled elemental powders were used, the resulting microstructure was more uniform, as shown in Fig.5.3 (b), but to some extent, the diffusion of Si was hindered and this resulted in some coarser lamellar areas and a higher Si content at the grain boundaries, as shown in Fig.5.3 (b)' and Table 5.4. To improve the elemental diffusion, the use of as-milled elemental powders for alloying is inefficient.

Table 5.4 EDS quantitve analysis on the grain boundaries of each as-extruded sample

	Al (wt.%)	*Si (wt.%)*	*Ti (wt.%)*	*Mo (wt.%)*	*Sn (wt.%)*
Sample 4	3.51	0.42	89.27	2.16	4.63
Sample 5	3.19	0.91	90.52	1.52	3.87
Sample 6	3.69	0.36	88.62	3.55	3.78

Weight % Error (+/- 1 Sigma) of each element in samples

Al	*Si*	*Ti*	*Mo*	*Sn*
+/-0.10	+/-0.14	+/-0.66	+/-0.23	+/-0.22

The data for Al content in Tables 5.3 and 5.4 is also consistent with that found from XRD analysis, with the existence of a relatively uniform distribution of α stabilizer and a relatively higher concentration of α stabilizer along the grain boundaries in sample 6. This directly aids α phase precipitation during the β phase

decomposition process, so that a relatively higher α phase volume fraction was achieved in sample 6. In sample 6, the elemental composition at the grain boundaries is close to the nominal composition values, even in the coarse lamellar areas. However, the Mo content in the coarse lamellar areas is lower than the nominal amount and this might derive from an inhomogeneous Mo elemental distribution caused by the mechanical mixing process. That is to say, the use of gas atomized titanium powders greatly contributes to a more homogenous elemental distribution. This kind of homogenous elemental distribution should helped by the thinner oxide layer on atomized titanium powders compared with that on the surface of HDH titanium powder, as shown in Fig.5.4.

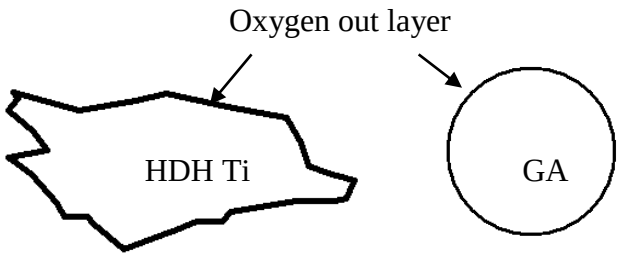

Fig.5.4 The schematic illustration of oxygen out layer of HDH Ti and GA Ti.

5.3.2 Mechanical properties and fracture surfaces

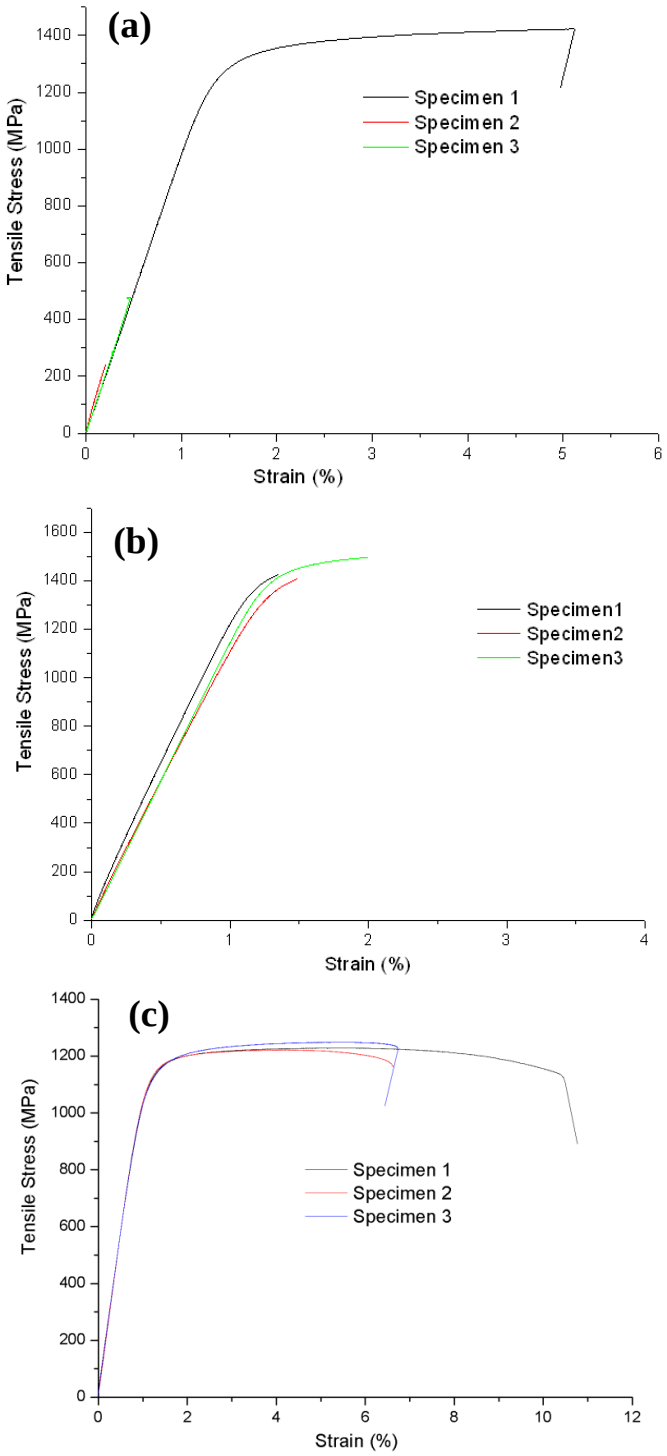

Fig.5.5 Tensile test results for as-extruded samples, (a) sample 4, (b) and (c) samples 5 and 6, respectively.

Table 5.5 Tensile test results in specific details

		UTS (MPa)	YS (MPa)	Elongation %
Sample 4	Specimen 1	1423	1288	5.1
	Specimen 2	242	-	-
	Specimen 3	480	-	-
Sample 5	Specimen 1	1427	-	-
	Specimen 2	1410	1404	1.5
	Specimen 3	1498	1446	2
Sample 6	Specimen 1	1230	1117	11
	Specimen 2	1222	1120	7.4
	Specimen 3	1250	1107	7

Fig.5.5 shows room temperature tensile properties of as–extruded samples and Table 5.5 shows specific values. Clearly, a higher UTS is exhibited by samples 4 and 5 compared with sample 6, but the tensile properties in different test-pieces from sample 5 are more uniform compared with those for sample 4. Ductility was sacrificed for this uniformity in properties, as shown in Fig.5.5 and Table 5.5, where low elongations to fracture of less than 2% are found in sample 5. The tensile results for sample 6 show a good combination of tensile strength and ductility.

In sample 5 the use of as-milled Al-Mo-Sn-Si powder improves the elemental distribution of each element and this significantly enhances the strength and gives more uniformity in the mechanical properties, but due to a relative high concentration of Si in the coarse lamellar areas and at the grain boundaries, the ductility is largely decreased because silicides or intermetallic Si rich compounds of large size are easily precipitated in these localised areas. This was also discussed in chapter 4. For sample 6, a relatively lower oxygen content and better elemental distribution either in coarse lamellar area or at grain boundaries is beneficial for achieving better tensile properties and good ductility.

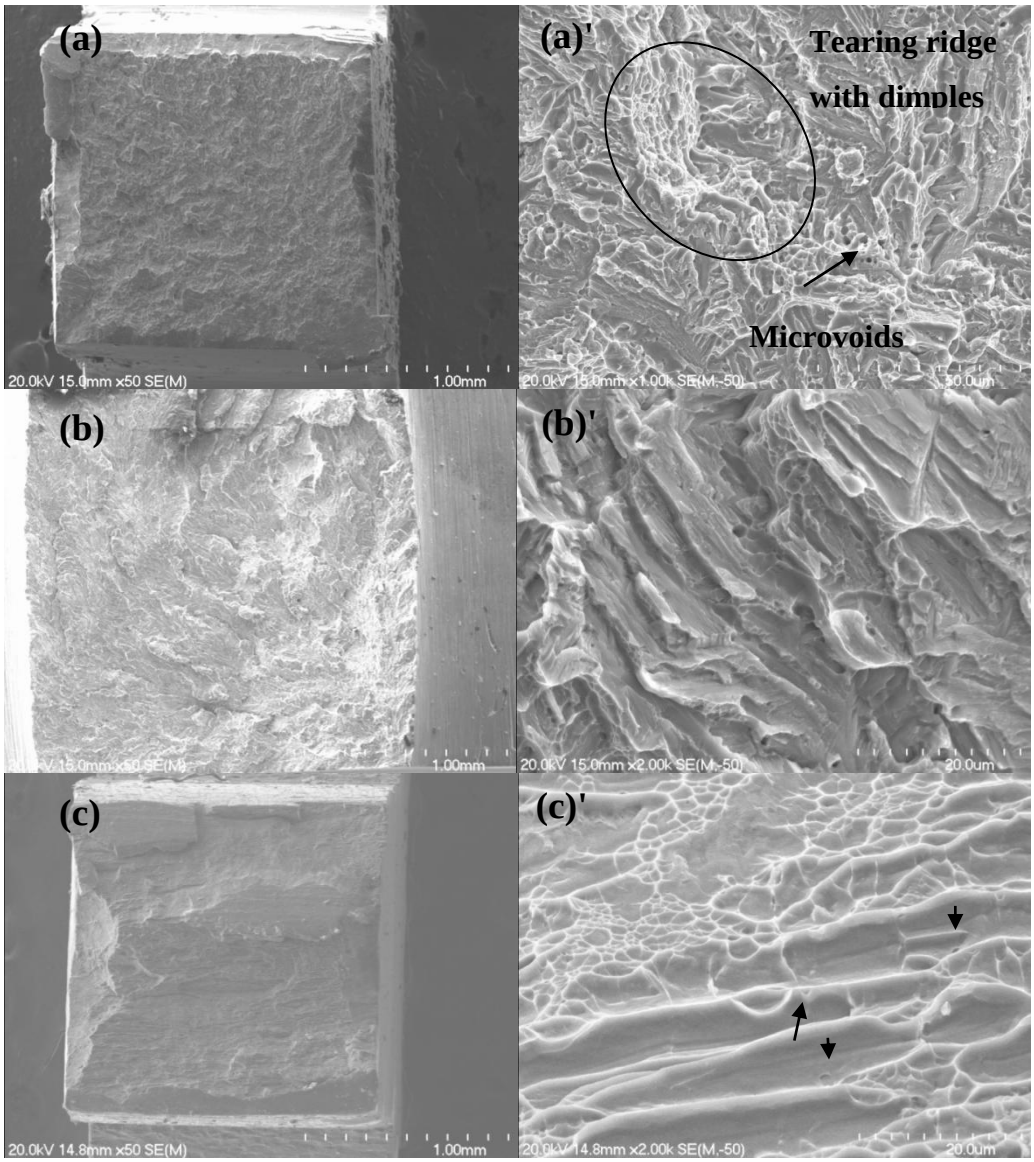

Fig.5.6 SEM images of the fracture surfaces of tensile test specimens cut from as-extruded samples; (a) sample 4, (b) sample 5; (c) sample 6. The high magnification SEM images (a)', (b)' and (c)' show typical fracture characteristics for (a), (b) and (c), respectively.

The relationship between the mode of fracture and the resulting tensile properties for sample 4 has been discussed in Section 4.3.1. For a test-piece with good tensile strength and ductility, the fracture surface consists mainly of translamellar fracture, as shown in Fig.5.6. The dependency of strength and ductility on microstructure can be explained in terms of the elemental distribution, especially the distribution of Si. The grain boundary Si content of sample 4 is close to the nominal value and we know silicide precipitation at the grain boundaries prevents dislocation climb and plays a significant role in enhancing the tensile strength and improving the ductility. That is why a high tensile strength with satisfactory

ductility was evident in one of the specimens from sample 4. But the overall inhomogeneous distribution of Si in sample 4 directly caused variability in mechanical properties That is to say the precipitation of larger sized silicide particles prompted initial cracking which led to premature failure of the specimen.

Figs.5.6 (b) and (b)' show a rougher surface morphology indicating that the specimen also failed by translamellar fracture. There was no evidence of tearing ridges with dimples and the fracture surface showed little or no ductility. This fracture phenomenon can be explained by the elemental quantitive analysis of the grain boundaries in sample 5, which shows that there is almost 1wt.% Si at the grain boundaries. A much higher Si content could result in the precipitation of more silicides or intermetallic compounds. An agglomeration of either of them at grain boundaries has a detrimental effect on the tensile strength and especially on ductility. So an overall homogenous elemental distribution contributes to the high tensile strength and uniformity of mechanical properties in sample 5, whereas an inhomogeneous elemental diffusion with high Si content, especially at grain boundaries, directly leads to a low ductility of less than 2% in sample 5.

On the other hand the tensile test specimens cut from sample 6 showed a mixture of translamellar cleavage of the α/β lamellae and ductile fracture of grains as reflected by the fine dimples (Fig. 5.6 (c) and (c)'). The grains exhibiting ductile fracture are most likely the primary β grains. Microvoids (indicated by arrows in Fig. 5.6(c)') can also be seen between α lamellae, showing that the ductile fracture of the thin layers of β phase between the lamellae of α phase probably also contributed to an enhancement of the fraction of ductile failure in the specimens, leading to good ductility. Based on the microstructure and elemental distribution analysis, we know that a good combination of tensile strength and ductility in sample 6 definitely derives from the relatively homogenous elemental distribution, with no Si or Mo rich areas or phases within the β grains or at the grain boundaries. This means that the use of GA titanium powder has a beneficial effect on the homogenous elemental diffusion during hot processing and cooling.

5.4 Conclusions

(1) When as-milled alloy powders were blended with HDH titanium powder to

prepare as-extruded samples, the uniformity in tensile strength improved, but ductility was sacrificed. A relatively higher Si content in the coarse lamellar area and grain boundaries should be the reason for poor tensile properties especially poor ductility.

(2) When the starting powders were dominated by gas atomized (GA) titanium powders, a good combination of tensile strength and ductility was achieved which showed a UTS of 1220-1250 MPa with an elongation to fracture of 7-11%. More uniform mechanical properties were given by this alloy when GA titanium powder was introduced.

(3) GA titanium powders have a beneficial effect on elemental diffusion and the achievement of more uniformity in mechanical properties.

References

[1] R. Filip, K. Kubiak, W. Ziaja, J. Sieniawski, The effect of microstructure on the mechanical properties of two-phase titanium alloys, Journal of Materials Processing Technology, 133 (2003) 84-89.
[2] G. Lütjering, J. Williams, A. Gysler, Microstructure and mechanical properties of titanium alloys, Microstructure and Properties of Materials, 2 (2000) 1-74.
[3] V.A. Joshi, Titanium alloys: an atlas of structures and fracture features, CRC Press, 2006.
[4] G. Lütjering, J.C. Williams, Titanium, Springer, 2003.
[5] M. Benedetti, J. Heidemann, J. Peters, G. Lütjering, Influence of sharp microstructural gradients on the fatigue crack growth resistance of α+ β and near‐α titanium alloys, Fatigue & Fracture of Engineering Materials & Structures, 28 (2005) 909-922.
[6] G. Lütjering, Influence of processing on microstructure and mechanical properties of (α+β) titanium alloys, Materials Science and Engineering: A, 243 (1998) 32-45.
[7] M. Peters, A. Gysler, G. Lütjering, Influence of texture on fatigue properties of Ti-6Al-4V, Metallurgical Transactions A, 15 (1984) 1597-1605.
[8] C. Leyens, M. Peters, Titanium and titanium alloys, Wiley Online Library, 2003.

Chapter 6 The effect of heat treatment on the mechanical properties of Ti 4%Al 4%Mo 4%Sn 0.5%Si as-extruded bar

6.1 Introduction

The purpose of heat treatment for titanium alloys is normally for reducing residual stress, optimizing special properties such as fracture toughness, fatigue strength and high temperature creep strength and producing acceptable mechanical properties with a combination of ductility, strength, machinability etc. [1]. In terms of mechanical properties improvement, especially for two phase titanium alloys, heat treatment mainly produces effects through microstructural changes and changes in the chemical composition of phases [2-6]. So a study of the effect of heat treatment on phase morphology, microstructure and phase composition is critical to revealing how mechanical properties are improved.

In chapters 4 and 5 it has been shown how a Ti-4Al-4Mo-4Sn-0.5Si titanium alloy can be successfully prepared using blended elemental powders. Among the different methods, the most cost effective approach is by using HDH titanium powder directly blended with other elemental powders without any additional powder processing. Unfortunately, there is variability in mechanical properties due to the existence of micro defects produced during hot processing. In this chapter the effect of typical heat treatments on the microstructure and mechanical properties of Ti-4Al-4Mo-4Sn-0.5Si titanium alloy, produced by the cost effective blended elemental approach was studied. This study reports on microstructural evolution, variations of phase composition and phase morphology after different heat treatments, and provides constructive suggestions for improvements in mechanical properties for this alloy such as higher yield stress, better ductility and more consistent tensile properties. The $(\alpha+\beta)/\beta$ transformation temperature and martensitic phase transformation in Ti-4Al-4Mo-4Sn-0.5Si alloy were also investigated and the results of this work is discussed.

6.2 Experimental details

The raw material used in this study was prepared from blended elemental powders (mainly containing HDH Ti powders) by powder compact extrusion, as described for sample 4 in chapter 4. For preparing sample 4, an extrusion temperature of 1350^{o}C with a 5 min. hold time at temperature, prior to extrusion was used. The oxygen content of the alloy was 0.44wt%. After extrusion, as described in chapters 4 and 5 the microstructure had a typical Widmanstätten morphology with an average grain size of approximately 50 μm, as shown in Fig.6.1. A high yield strength, an ultimate tensile strength and an elongation to fracture of 1288MPa, 1423MPa and 5.1%, respectively, can be achieved from this alloy after extrusion using blended elemental powders.

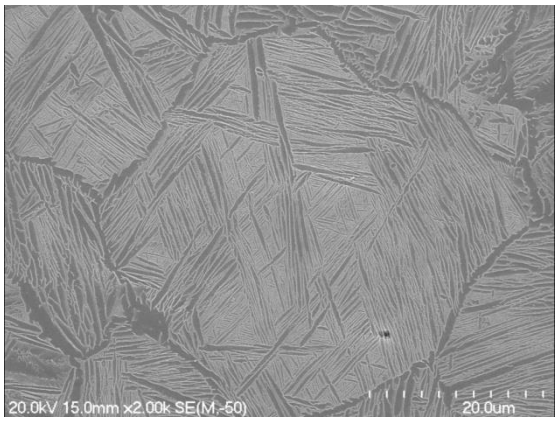

Fig.6.1 Typical high magnification SEM image of the microstructure of an as-extruded sample studied in chapter 4.

Heat treatment was conducted in an electrical tube furnace (RADATHERM FURNACE Australia, Model HTHTF7030) under a protective argon gas flow (oxygen content < 200ppm) during all the heat treatments. The rate of temperature increase during solution treatment was 10^{o}C min^{-1}. For the Timetal551 alloy, three typical heat treatments were investigated in this study, so three heat treated samples were prepared. The parameters of each heat treatment are summarised in Table 6.1.

Table 6.1 Heat treatment methods and samples

Samples	Heat treatment methods
HT-1	1 hour solution at 925^{O}C, water quenched, and then 500 ^{O}C ageing for 24hrs, air cooling
HT-2	1 hour solution at 925^{O}C,air cooling, and then 500 ^{O}C ageing for 24hrs, air cooling
HT-3	1 hour solution at 925^{O}C, furnace cooling, and then 500 ^{O}C ageing for 24hrs, air cooling

The microstructure was characterised using optical microscopy (Olympus BX60), X-ray diffractometry (XRD) (Philips X' Pert system) and scanning electron microscopy (SEM) (HITACHI S4000). The software Image Pro Plus was used to analyse the volume fraction of different phases in the microstructures. Tensile testing was carried out using a 4204 INSTRON universal testing machine with dog-bone shaped specimens having a rectangular cross-section of 2mm x 2.5mm and a gauge length of 20mm. The strain was measured using an extensometer with a gauge length of 10mm. The strain rate during tensile testing was $1\times10^{-4}s^{-1}$.

6.3 The (α+β)/β transformation temperature and Martensitic phase transformation in a Ti-4%Al-4%Mo-4%Sn-0.5Si alloy

The (α+β)/β phase transformation temperature in titanium alloys is important for determining processing temperature and suitable heat treatment temperatures [7]. The β transus temperature for any single material may vary within a certain temperature range due to differences in processing. In this section the (α+β)/β transformation temperature of Ti-4%Al-4%Mo-4%Sn-0.5Si alloy will be discussed and then determined using three methods, namely an equation computation method, the SDT thermal method and by metallography. The metallographic method can be regarded as the most effective method for measuring the phase transformation temperature [7] while the results of the SDT thermal method and the computation method provide a proper temperature range for metallographic investigations.

In the computational method the phase transformation temperature is calculated by considering the effects of chemical composition. The equation used in this method can be expressed by a linear model [7]

$$\mathrm{T}\ ((\alpha+\beta)/\beta\ \text{transformation temperature}) = t_0 + \sum_{i=1}^{n} k_i C_i$$

where t_o is the (α+β)/β transformation temperature of pure titanium, k_i denotes the coefficient that characterizes the changes in the temperature of the (α+β)/β transformation upon the introduction of 1 wt.% of each alloying element into the alloy; C_i indicates the content of the alloying elements in mass percent. Table 6.2 shows the effect of alloying elements on the β transus temperature in α/β titanium alloys. So taking the (α+β)/β transformation temperature of pure titanium to be 890°C and introducing an oxygen content of 0.44wt.%, after calculation the transition temperature T=1023.5°C. Normally if there are some impurities and the differences between real elemental content and nominal content is taken into account, this computed transformation temperature is lower than the real one.

Table 6.2 The effect of alloying elements on the β transus temperature [7].

Element	Al	Mo	Sn	Si	O
Change in β transus temperature upon introduction of 1 wt.% element)	22	-10	0	-5	2°C /0.01wt.%

Fig. 6.2 (a) shows the SDT trace for the as-extruded alloy. An endothermic peak ranging from 1030°C to 1072°C is clearly shown. The first derivative of the SDT trace is illustrated in Fig.6.2 (b). When the value of the first derivative of the SDT trace is zero, the corresponding temperature is 1040°C, which means that the phase transformation temperature determined by thermal difference analysis is 1040°C.

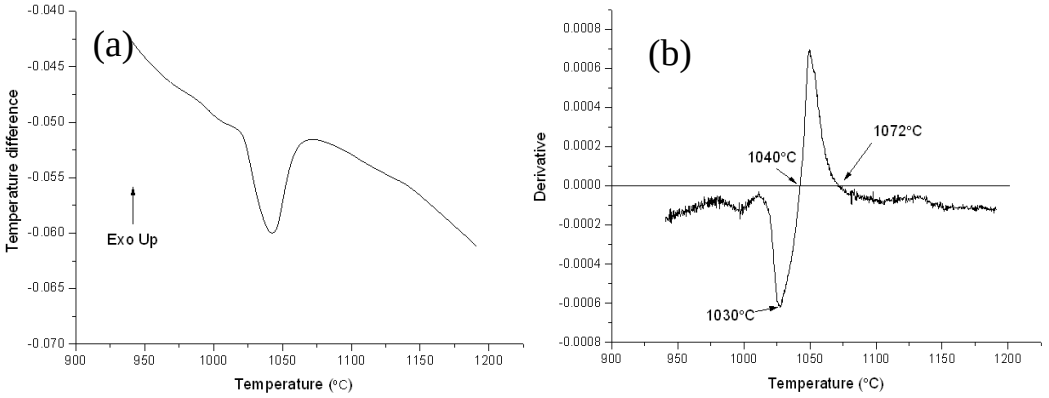

Fig.6.2 SDT trace (a) and the derivative of the SDT curve is illustrated in (b).

Based on the previous analysis using SDT and the computation method, and bearing in mind that the β transus is given as between 1050 ±15ºC in reference [8], the temperature range for the metallographic method should be set between 1000ºC and 1100ºC. Four temperatures were selected for the metallographic and XRD analysis to determine the phase transformation temperature, namely 1000ºC, 1050ºC, 1075ºC and 1100ºC. The as-extruded specimens were respectively solution-treated at one of the four temperatures and then water quenched. The optical micrographs and XRD results for the as-quenched specimens are shown in Fig.6.3 and Fig.6.4, respectively.

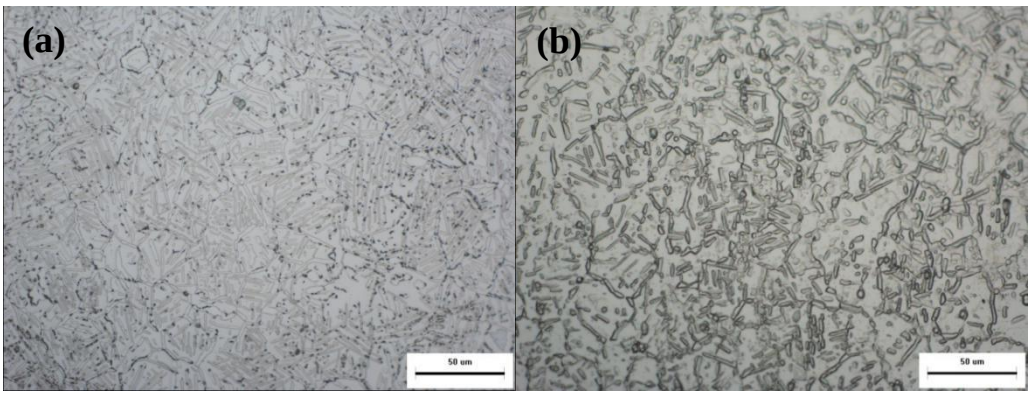

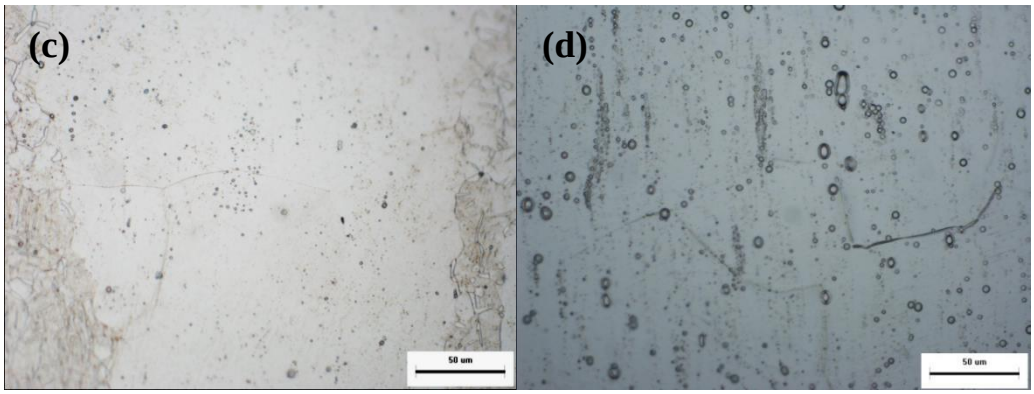

Fig.6.3 Optical micrographs of the as-extruded Ti-4%Al-4%Mo-4%Sn-0.5%Si alloy quenched from (a) 1000°C, (b) 1050°C, (c) 1075°C and (d) 1100°C, respectively. The length of the scale bar is 50μm.

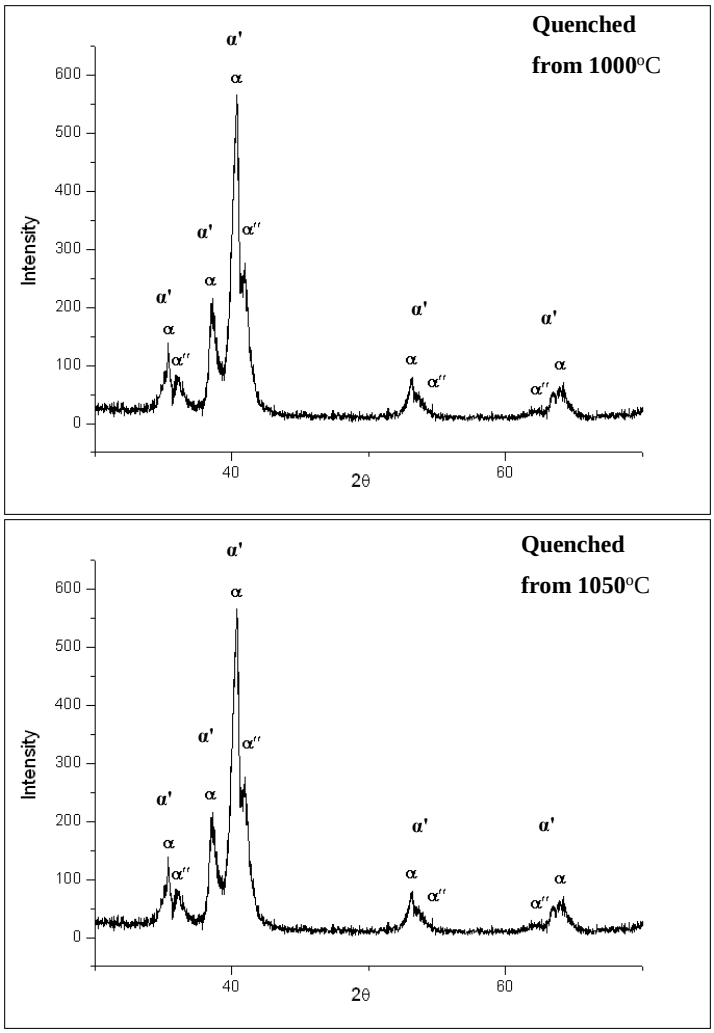

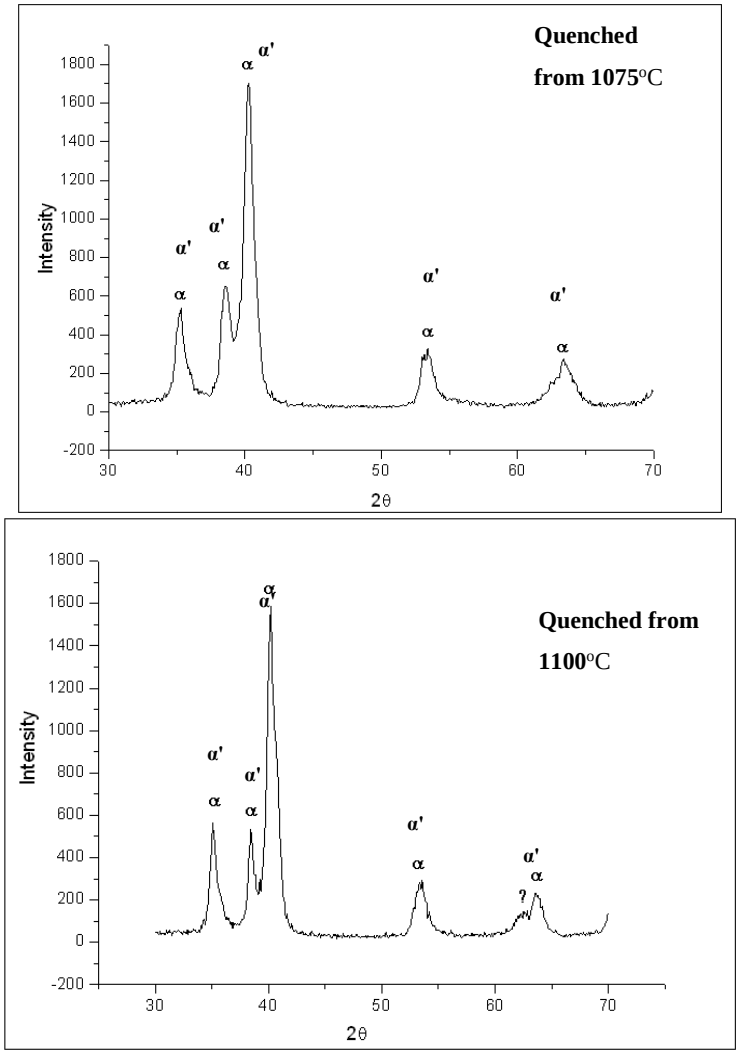

Fig.6.4 XRD patterns of the as-extruded samples quenched from different temperatures.

From the metallographic images and XRD results we can see that the as-quenched alloys consist mainly of four phases, namely α, α'， β and α" (orthorhombic structure). As shown in Fig.6.3 (a) and the corresponding XRD pattern in Fig.6.4, after quenching from 1000ºC, α, α', α" and β phases were observed. Normally when a specimen is annealed below the beta-transus temperature, only primary alpha particles and the martensitic phase (α') are detected [9-13]. When the temperature is further increased, but still within the two phase range, the α" phase (orthorhombic structure) is always precipitated after water quenching. There are two reasons: firstly, a martensitic phase transformation can easily occur at higher solution temperatures. This is because the amount of primary alpha decreases with increasing solutioning temperature and the concentration of beta stabilizer in the beta phase is reduced. This decreases the stability of the beta phase. This is

beneficial for promoting a martensitic phase transformation. Secondly, the phase mechanical stability of the beta phase decreases when the grain size increases at higher solution-treatment temperatures. So from Fig. 6.3 (a) and the corresponding XRD pattern, we can conclude that within the alpha-beta phase region at 1000^{o}C, the detected phases: α, β, α' and α" are respectively the primary alpha phase, retained beta phase and martensite phases (α', α"). This also indicates that 1000^{o}C lies at the upper end of the two phase range and is perhaps close to the transus temperature.

The results of previous work on the martensite phase α" have shown that after solution treatment followed by air cooling, alpha and beta phases are produced, but subsequent ageing at 400^{o}C resulted in α, α" and some beta phase. This suggests that the α" was precipitated during the ageing process [14] and that the phase transformation to α" is not strictly martensitic [14]. Other researchers [15] have also suggested that the exact nature of the phase transformation and decomposition of beta to the α" phase is not clear, but the α" phase has been reported to form within a certain composition range and its formation is especially dependent on the concentration of Mo in the beta phase. That means that when the concentration of Mo in the beta phase remains in a certain range after quenching from the solution treatment temperature, the formation of α" phase is possible. The evidence from the work described above also agrees with the observations from this study. When a specimen was quenched from 950^{o}C (as shown in Fig.6.5), α" phase was not observed and when the specimen was quenched from 1075^{o}C, the α" phase had disappeared from the XRD pattern. Obviously the concentration of Mo in the beta grains varies with the solutioning temperature and impacts on the formation of the α" phase.

Based on the above analysis we can say that the precipitation of α" phase is highly sensitive to the solution treatment temperature and is closely related to the concentration of β stabilizer, especially Mo in this kind of alloy. These conclusions give us some meaningful suggestions for the synthesis and heat treatment of this alloy. Some authors [14] have used a step-quenching method to produce a high strength alloy containing retained α" and α' phases. The existence of α" is beneficial for enhancing strength but is detrimental to ductility. On the

other hand, α" is an unstable phase and easily decomposes at a certain temperature, which directly impacts on the mechanical property stability of the alloy. So even though higher strengths can be achieved with the precipitation of α" phase, its presence in the microstructure should be avoided. Hence monitoring the formation and full decomposition of the α" phase during processing and heat-treatment is critical for achieving satisfactory mechanical properties from this alloy.

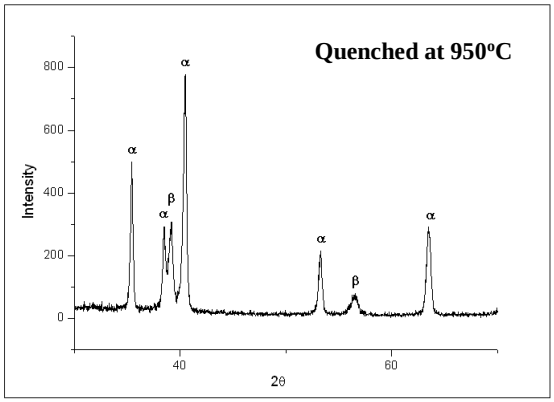

Fig.6.5 XRD patterns of the as-extruded sample quenched at 950°C

When the specimens were quenched from 1075°C and 1100°C only the alpha and martensite phases were detected. The alpha phases appearing in the two XRD patterns for the two temperatures are secondary alpha, which is the product of decomposition of the beta phase and the martensite phase α', which is also transformed from beta. Optical micrographs show that at 1075°C and 1100°C only secondary α exists in the matrix. The grain boundaries are not clear due to the nearly complete transformation to α' from the beta phase. This is especially the case after solution treating at 1100°C, when some grain boundaries could only be distinguished by the precipitation of secondary α phase along the boundaries. The optical micrographs and XRD patterns indicate that when solution treating above 1075°C, the alloy is in the single phase range, and a temperature of 1075°C should be the α+β→β phase transformation temperature.

Based on the above analysis, we can conclude that: (1) the solutioning temperature and the concentration of beta stabilizer, especially the concentration of Mo in the beta matrix has a significant effect on the martensite phase transformation; (2) since the α" phase can easily precipitate in this alloy, monitoring the formation and full decomposition of the α" phase during

processing and heat treatment is crucial for good mechanical properties; (3) using three methods, a beta transus temperature of 1075°C was confirmed.

6.4 The effect of heat treatments on the microstructure and mechanical properties of as-extruded bar

After confirming a beta transus temperature of 1075°C, a solution treatment temperature of 925°C is within the two phase region and was set according to the recommendation in the heat treater's guide [16]. The processing route for the three different heat treatment methods is illustrated in Fig.6.6, including a solution treatment (recrystallization in this study) and aging process. We know that the only difference between each method is the cooling rate after high temperature solutioning. It is known that cooling rate has a great effect on the microstructure after solution treatment. With increasing cooling rate the width of α lamellae and their colony size becomes smaller. Furthermore, with higher cooling rates the beta grains are prone to be unstable and become divided into smaller sized beta grains. So this is why a choice of different cooling rates is the key parameter between the different heat treatments.

After solution treatment in the two phase alpha - beta range, the aim is to obtain α', α and metastable β phases. It is hoped that with phase decomposition and elemental diffusion during high temperature solutioning, some intermetallic compounds formed after extrusion will be dissolved into the matrix again and the defects introduced by these kinds of intermetallic compounds will be eliminated. The goal to be achieved from aging is decomposition of the martensitic and metastable beta phases into a fine dispersion of alpha or intermetallic particles, so that the matrix is dispersion strengthened and the overall mechanical properties of alloy dramatically improved.

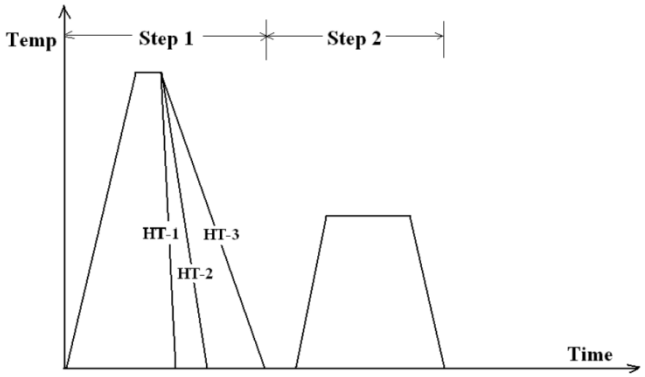

Fig.6.6 Processing route for the three heat treatment methods used. Step 1 is solution treatment, namely a recrystallization process and step 2 is an aging process.

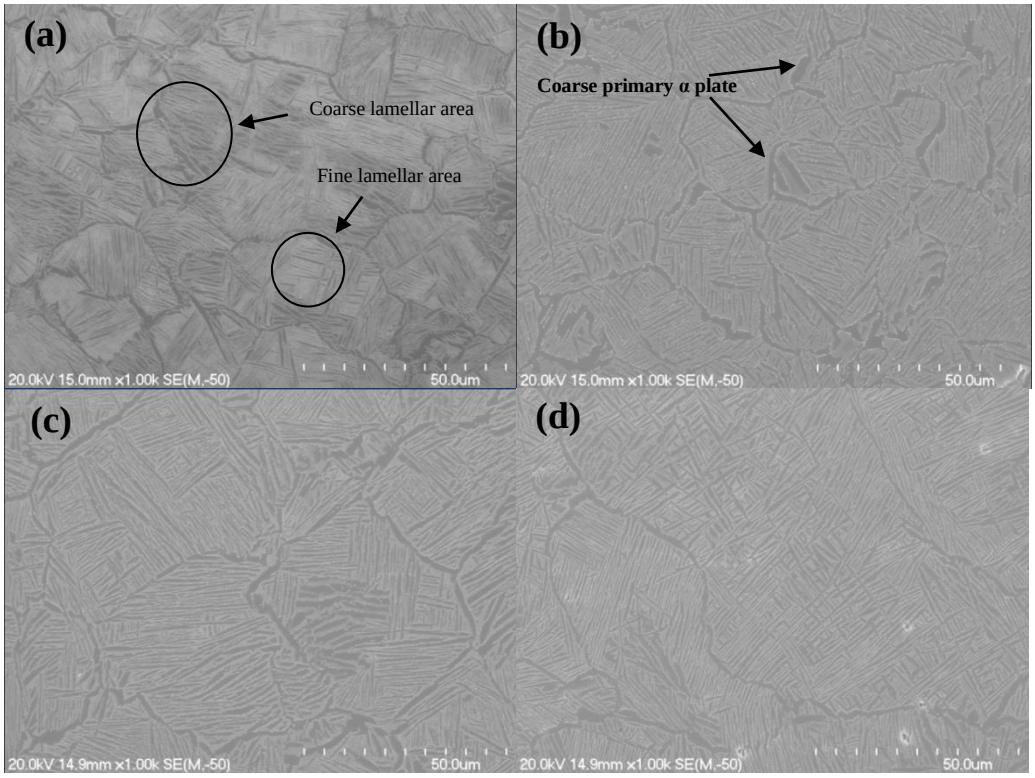

Fig.6.7 SEM images of the samples before and after heat treatment, (a) before heat treatment (b) HT-1, (c) HT-2 and (d) HT-3.

The microstructures obtained before and after the heat treatments are shown in Fig.6.7. It is clear that after cooling at different cooling rates from the solution treatment temperature, HT-1 to HT-3, the grain size gradually increases as the cooling rate decreases. Before heat treatment, there were two distinctive lamellar areas in the microstructure, described as coarse and fine areas, due to the localized inhomogeneous elemental distributions. This has already been discussed in Chapter 4. After heat treatment the microstructure is more homogeneous and this is an indication that the mechanical properties will be more uniform.

The micrographs in Fig.6.7 show that slow cooling after solution treatment, such as cooling in air or furnace cooling (Figs.6.7 (c) and (d)), the amount of coarse α lamellae is more than that found in specimen HT-1 (water cooling, Fig.6.7 (b)). A similar observation is also made for α colonies. A smaller grain size and α colony size are beneficial for improving yield strength, because colony boundaries provide obstacles for microcrack propagation [6]. So with a smaller grain size, a finer α lamellae and finer α colony size the yield strength of material in condition HT-1 should be higher than that for samples from HT-2 and HT-3.

It also can be seen from the micrographs in Fig.6.7 that the grain boundaries in material which has undergone heat treatment HT-1 are coarser and more discontinuous compared with those in material after heat treatments HT-2 and HT-3. It should also be mentioned that there are more of the coarser primary α plates after heat treatment HT-1. This can be explained as deriving from a coarsening of the primary α during high temperature solutioning, which is retained after fast cooling and long but relatively low temperature aging. During solutioning the existence of coarser primary α plates is beneficial for the diffusion of α stabilisers but hinders the diffusion of β stabilizers. This means that during fast cooling, there is precipitation of discontinuous and coarse α layers from the beta phase. An elemental quantitative analyses shows that the Al content at the grain boundaries in material after HT-1 is higher than that after HT-2 and HT-3, as shown in Table 6.3. After slower cooling rates, as in heat treatments HT-2 and HT-3, the primary α phase has a longer time to dissolve allowing elements such as Al, an α stabilizer, time to diffuse into the β phase. This means that during an air or furnace cool, there is less of the coarse primary α phase retained. The diffusion of α stabilisers from the primary α into the β phase also promotes the precipitation of secondary α from the β grains. This kind of relatively homogenous elemental diffusion results in finer and more continuous α layers precipitated along the beta grains and also gives a hint that the volume fraction of the α phase after heat treatments HT-2 and HT-3 should be greater than that after heat treatment HT-1.

After heat treatment HT-1 the beta grains are finer and this microstructure helps to impede the development and propagation of microcracks and therefore enhances the material's tensile strength. A microstructure with relatively coarse and

discontinuous grain boundaries is prone to the initiation of microcracks, which decreases the ductility. On the other hand, after heat treatments HT-2 and HT-3, there is an improvement in ductility deriving from a well precipitated fine α phase at the grain boundaries. The tensile properties are also affected by Si content and a quantitative analysis of the grain boundary silicon content after the three heat treatments is shown in table 6.3. The Si content after heat treatment HT-1 is lower than the nominal value and higher after heat treatments HT-2 and HT-3. A Si content which is close to the nominal compositional value favours the precipitation of nano-scale silicides along the β grain boundaries [17] and these can act to prevent grain growth. When the Si content is greater than the nominal compositional value, the amount of silicide precipitated can be a serious drawback because of their brittle nature and the creation of a poor bonding interface between them and the titanium matrix.

Table 6.3 EDS quantitve analysis on the grain boundaries of samples before and after HT

	Al (wt.%)	*Si (wt.%)*	*Ti (wt.%)*	*Mo (wt.%)*	*Sn (wt.%)*
Before HT	3.51	0.42	89.27	2.16	4.63
HT-1	3.64	0.34	89.06	3.50	3.46
HT-2	2.94	0.62	88.37	3.82	4.25
HT-3	3.17	0.57	88.91	3.80	3.55

Weight % Error (+/- 1 Sigma) of each element in samples

Al	*Si*	*Ti*	*Mo*	*Sn*
+/-0.10	+/-0.14	+/-0.66	+/-0.23	+/-0.22

Table 6.4 gives the differences in the phase volumes after the three heat treatments. The α volume fraction increases and the beta volume fraction decreases with decreasing cooling rate after solutioning. This is consistent with the explanations given earlier for microstructure evolution. The highest α volume fraction of 66.45%- occurs after heat treatment HT-3 while the highest beta volume fraction of 62% occurs after heat treatment HT-1. This is because with increasing cooling rate the amount of retained beta phase increases while the amount of α phase precipitated from beta matrix decreases.

Table 6.4 Phase composition of the as-heat treated samples

Phase \ Samples	HT-1	HT-2	HT-3
α (%)	38	53.24	66.45
β (%)	62	46.76	33.55

In summary, a decreasing cooling rate after solution treatment creates a more homogeneous microstructure with an increase in the alpha phase volume fraction from 38% to 66.45%, while the volume fraction of the beta phase decreases from 62% to 33.55%. The α lamellae, α colony size and beta grain size become coarser and the morphology of grain boundary α becomes finer and more continuous. All these factors will impact on the mechanical properties of samples after heat treatment.

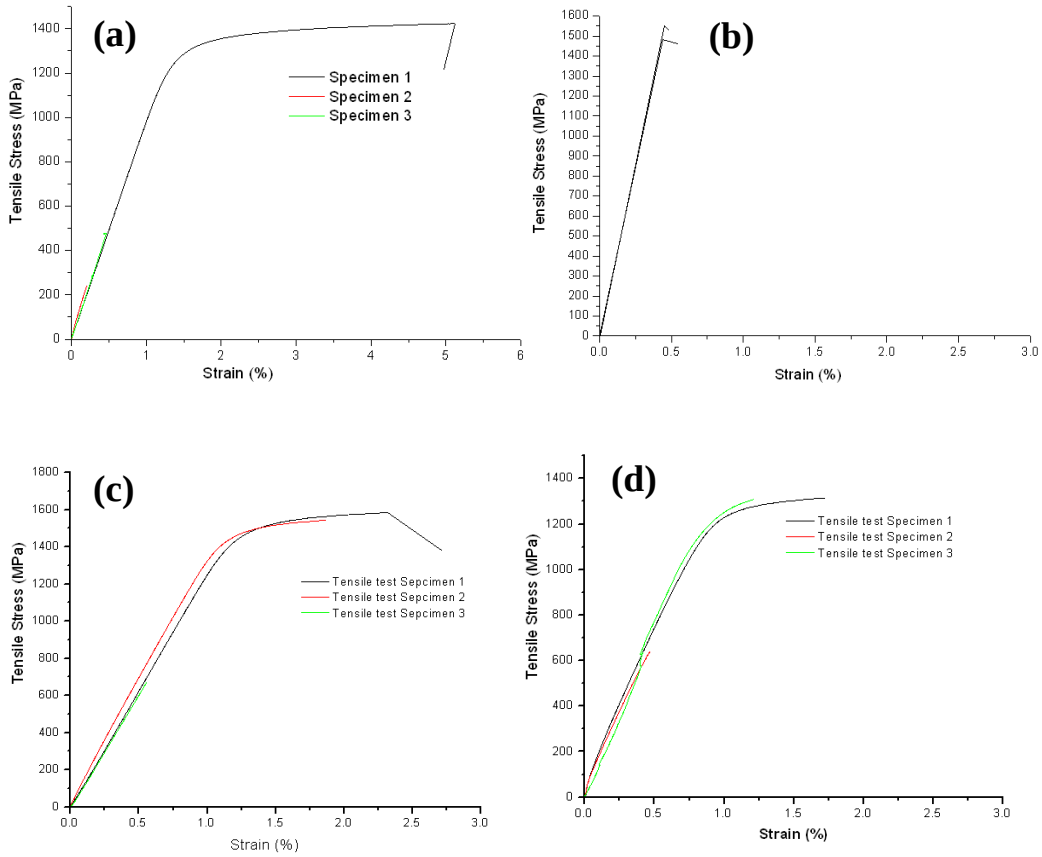

Fig.6.8 Room temperature tensile testing data for as-extruded and as-heat treated samples: (a) as-extruded sample, (b) HT-1, (c) HT-2 and (d) HT-3

Table 6.5 Mechanical properties of the as-extruded and as-heat treated samples.

		UTS (MPa)	YS (MPa)	Elongation %
Before HT	Specimen 1	1423	1288	5.1
	Specimen 2	242	-	-
	Specimen 3	480	-	-
HT-1	Specimen 1	1567	-	-
	Specimen 2	1480	-	-
	Specimen 3	-	-	-
HT-2	Specimen 1	1584	1505	2.5
	Specimen 2	1544	1486	1.9
	Specimen 3	672	-	-
HT-3	Specimen 1	1315	1255	1.7
	Specimen 2	637	-	-
	Specimen 3	1310	1257	1.2

The tensile test curves and results are shown in Fig.6.8 and Table 6.5, respectively. It is clear that after heat treatment the consistency of mechanical properties improves, because of the microstructural changes described earlier. After heat treatment HT-1 the alloy has a high fracture strength of 1567MPa and 1480MPa for two specimens tested, but no ductility. After heat treatments HT-2 and HT-3 the yield strengths were 1505MPa and 1255MPa and elongations to fracture 2.5%, 1.7%, respectively. However, although the mechanical properties are more consistent, there was one specimen from each as-heat treated sample which failed prematurely.

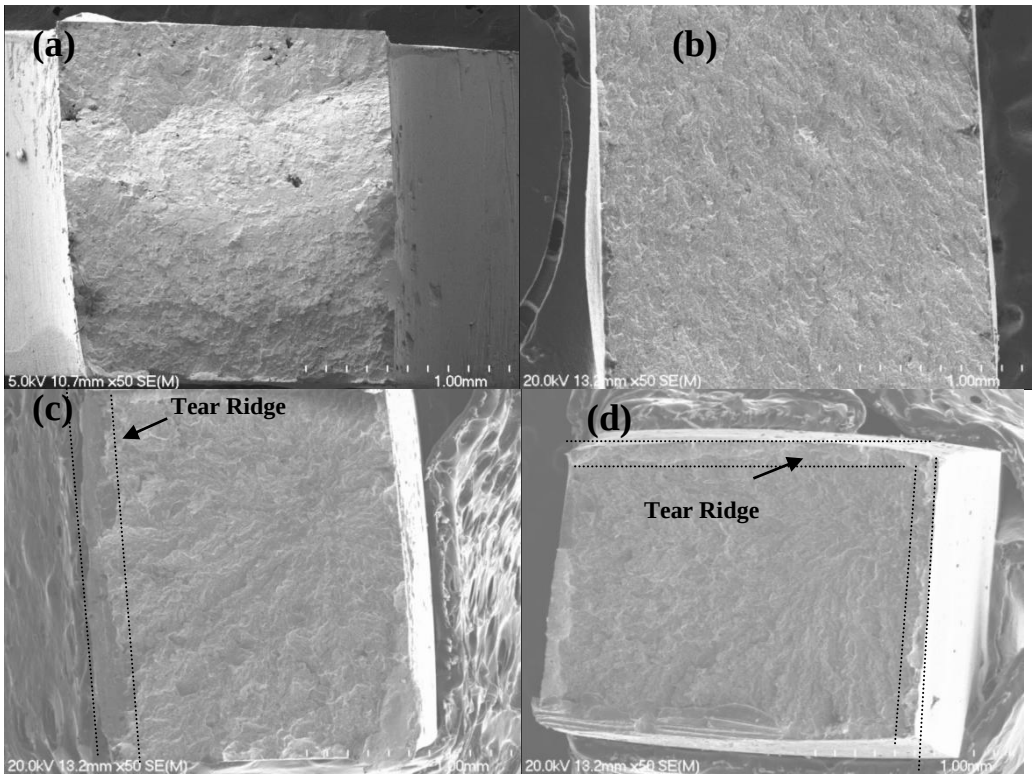

Fig.6.9 Low magnification SEM images of the fracture surfaces of as-extruded and as-heat treated samples: (a) as-extruded sample, (b) HT-1, (c) HT-2 and (d) HT-3.

Fig.6.9 shows low magnification SEM images of the fracture surfaces of broken specimens after tensile testing. The fracture mechanism of an as-extruded alloy has already been discussed in Chapter 4 and the variability in mechanical properties caused by the precipitation of large scale compounds during hot working. Fig.6.9 (b) shows that after heat treatment HT-1 the fracture surface has a flat appearance which is typical of a cleavage, transgranular fracture. A high strength fracture with little or no ductility is typical of this mode of fracture. Fig.6.9 (c) and (d) also show typical transgranular fracture modes but there are tear ridges on the fracture surface, which are evidence of some ductile fracture and these have contributed to some ductility.

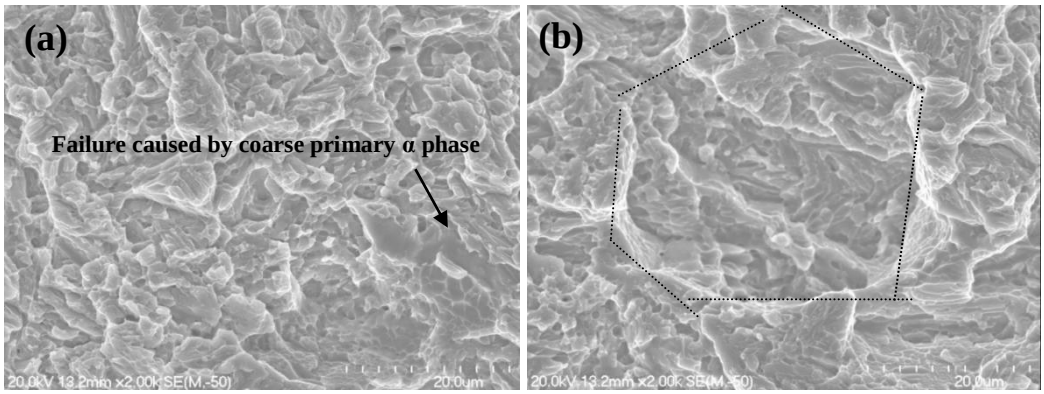

Fig.6.10 High magnification SEM images of the fracture surface of as-heat treated sample HT-1.

High magnification SEM images of a fracture surface from heat treated tensile specimen HT-1 are shown in Fig.6.10. The fracture surface contains a mixture of transgranular and intergranular fracture mode. From Fig.6.10 (a) cracking at a coarse primary α plate can be clearly seen, which contributes to the transgranular fracture mode. A coarse primary α plate is likely to be the initial source of cracking which promotes the propagation of microcracks, eventually leading to transgranular fracture. Fig.6.10 (b) clearly shows the outline caused by beta grain failure, which is another typical intergranular fracture mode after heat treatment HT-1. Based on the microstructural analyses, it is the presence of coarse α phase and the discontinuous grain boundaries which are likely the key factors leading to microcrack propagation leading to intergranular fracture.

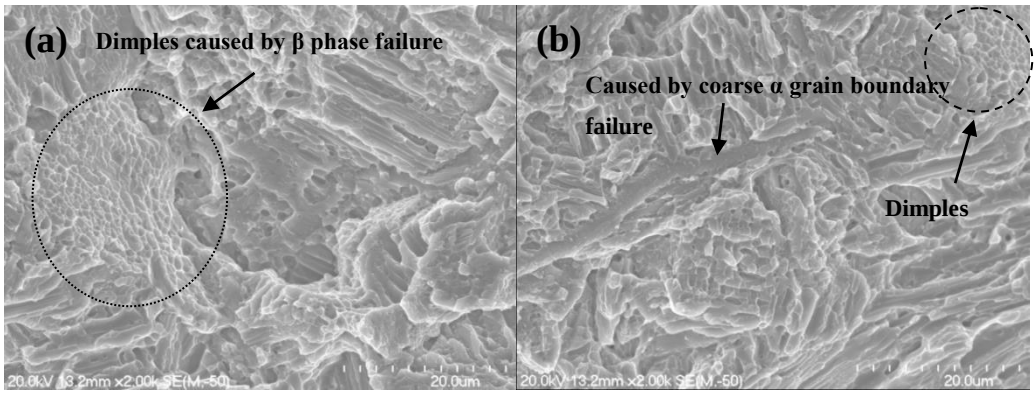

Fig.6.11 High magnification SEM images of the fracture surface of as-heat treated sample HT-2.

Fig.6.11 shows high magnification SEM images of a fracture surface from heat treated tensile specimen HT-2. The fracture surface contains a mixture of transgranular and intergranular fracture. The dimpled morphology indicated in Fig.

6.11 is caused by beta phase failure and this is most likely responsible for the improved ductility after heat treatment HT-2. On the other hand the residual coarse α phase at the beta grain boundaries (as shown in Fig.6.11 (b)) is detrimental to good ductility expected of this specimen and this limits the elongation to fracture of the specimen. Based on the microstructural evolution discussion earlier in this study, a relatively fine beta lamellar structure contributes to the dimples caused by beta phase failure and the coarser α phase grain boundaries mainly contribute to intergranular failure. So a high yield strength of 1505 MPa and an elongation to fracture of 2.5% can be achieved after heat treatment HT-2.

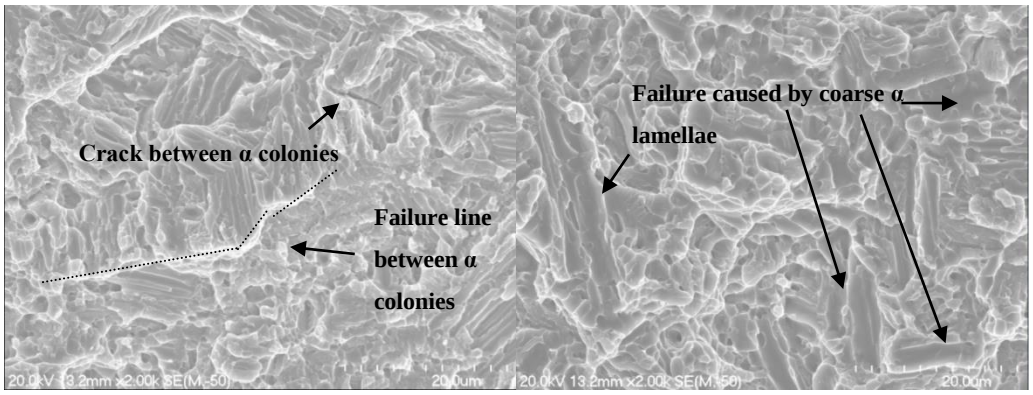

Fig.6.12 High magnification SEM images of fracture surface of as-heat treated sample HT-3.

The fracture surface in broken tensile test pieces after heat treatment HT-3 are shown in Fig.6.12. Here we can see a crack and failure line between an α colony and the residual parts left by failed coarse α lamellae. After heat treatment HT-3 a microstructural analysis shows relatively coarse α lamellae, large α colonies and a large beta grain size when compared with the other heat treated samples. These microstructural features are responsible for reduced tensile strength and ductility compared with specimens after heat treatment HT-2. This is why a lower yield strength of 1255MPa and a slightly higher elongation to fracture of 1.7% can be achieved after heat treatment HT-3, compared with heat treatment HT-2.

6.5 Conclusions

(1) A beta transus temperature of 1075^{o}C has been confirmed. The solutioning temperature and the concentration of beta stabilizer, especially Mo, in the beta

matrix has a significant effect on martensite phase transformation. Since the α" phase is easy to precipitate in this kind of alloy, a control of the formation and full decomposition of α" phase during processing and heat treatment is essential for acceptable tensile properties.

(2) After heat treatment the microstructural homogeneity and tensile properties are significantly improved. The cooling rate after solutioning plays a key role in determining the morphology of the α lamellar structure and the α colony and beta grain size. A faster cooling rate causes a decrease in the width of α the lamellae, the size of the α colonies and the beta grain size.

(3) After heat treatment HT-1, a high tensile strength of 1567MPa could be obtained but without any ductility. After heat treatment HT-2 an ultimate tensile strength of 1584MPa, a yield strength of 1505MPa and an elongation to fracture of 2.5% were obtained. After heat treatment HT-3 a tensile strength of 1315MPa, a yield strength of 1255MPa and an elongation to fracture of 1.7% were obtained.

References

[1] M.J. Donachie, Titanium: a technical guide, ASM international, 2000.
[2] Z. Du, S. Xiao, L. Xu, J. Tian, F. Kong, Y. Chen, Effect of heat treatment on microstructure and mechanical properties of a new β high strength titanium alloy, Materials & Design, 55 (2014) 183-190.
[3] D. Eylon, S. Fujishiro, P.J. Postans, F. Froes, High-temperature titanium alloys—a review, JOM, 36 (1984) 55-62.
[4] R. Filip, K. Kubiak, W. Ziaja, J. Sieniawski, The effect of microstructure on the mechanical properties of two-phase titanium alloys, Journal of Materials Processing Technology, 133 (2003) 84-89.
[5] Y.-W. Kim, Microstructural evolution and mechanical properties of a forged gamma titanium aluminide alloy, Acta metallurgica et materialia, 40 (1992) 1121-1134.
[6] G. Lütjering, Influence of processing on microstructure and mechanical properties of (α+ β) titanium alloys, Materials Science and Engineering: A, 243 (1998) 32-45.
[7] B. Kolachev, Y.B. Egorova, S. Belova, Relation between the temperature of the α+ β→ β transformation of commercial titanium alloys and their chemical composition, Metal Science and Heat Treatment, 50 (2008) 367-372.
[8] R.F. Boyer, E. Collings, Materials properties handbook: titanium alloys, ASM international, 1994.
[9] J. Qazi, J. Rahim, F.S. Fores, O. Senkov, A. Genc, Phase transformations in Ti-6Al-4V-xH alloys, Metallurgical and Materials Transactions A, 32 (2001) 2453-2463.
[10] T. Ahmed, H. Rack, Phase transformations during cooling in α+β titanium alloys, Materials Science and Engineering: A, 243 (1998) 206-211.
[11] F. Gil Mur, D. Rodriguez, J. Planell, Influence of tempering temperature and time on the α′-Ti-6Al-4V martensite, Journal of Alloys and Compounds, 234 (1996) 287-289.
[12] J. Qazi, O. Senkov, J. Rahim, F. Froes, Kinetics of martensite decomposition in Ti–6Al–4V–x H alloys, Materials Science and Engineering: A, 359 (2003) 137-149.
[13] S. Semiatin, S. Knisley, P. Fagin, D. Barker, F. Zhang, Microstructure evolution during alpha-beta heat treatment of Ti-6Al-4V, Metallurgical and Materials Transactions A, 34 (2003) 2377-2386.
[14] C. Ingelbrecht, The effect of step-quenching on the tensile properties and microstructure of the titanium alloy Ti-4Al-4Mo-2Sn-0.5 Si (IMI 550), Journal of materials science, 20 (1985) 3034-3040.
[15] K. Kharia, H. Rack, Martensitic phase transformations in IMI 550 (Ti-4Al-4Mo-2Sn-0.5 Si), Metallurgical and Materials Transactions A, 32 (2001) 671-679.
[16] H. Chandler, Heat treater's guide: practices and procedures for nonferrous alloys, ASM international, 1996.
[17] M. Hagiwara, S. Emura, Blended elemental P/M synthesis and property evaluation of Ti-1100 alloy, Materials Science and Engineering: A, 352 (2003) 85-92.

Chapter 7 Synthesis of Ti-4%Al-4%Mo-4%Sn-0.5%Si titanium alloy by powder compact extrusion from a pre-consolidated compact

7.1 Introduction

Compared with other technologies, powder metallurgy, especially blended elemental (BE) PM has a potential to produce near net shape titanium alloys at reduced cost [1-6]. For example, intake and exhaust valves produced by a BE process have already been successfully used in Toyota automobiles for more than ten years [7]. The company, Dynamet Technology Inc., also manufactures a wide range of cost-effective products which are prepared by a BE process [8]. In Chapter 4, 5 and 6 the alloy Ti-4%Al-4%Mo-4%Sn-0.5%Si was successfully manufactured using Blended Elemental Powder Metallurgy (BEPM) using a processing route consisting of powder mixing, powder compaction, induction sintering and extrusion. The aim of BEPM processing is to reduce costs especially if a secondary compaction step can be avoided.

However, if sintering and extrusion are carried out under the protection of an argon atmosphere, the increased costs mitigate against the aim of large scale, low cost titanium product manufacture. So in this study, a novel BEPM technology has been developed which enables the manufacture of larger scale titanium alloy extrusions without of the need for inert atmosphere protection. In this study the general process to synthesize Ti-4%Al-4%Mo-4%Sn-0.5%Si titanium alloy was powder mixing, powder compaction, pre-consolidation by hot pressing and then hot extrusion in air. The processing parameters, especially the extrusion temperature, were optimized, the microstructures and mechanical properties were studied and the relationship between elemental diffusion and mechanical properties was also investigated. Since alloy Timetal551 has useful tensile properties at a relatively high temperature of 400^{o}C [9], these were tensile tested at temperatures of 300^{o}C, 350^{o}C, 400^{o}C, 450^{o}C and 500^{o}C.

7.2 Experimental details

The starting materials were HDH (Hydride-Dehydride) Ti powder (particle size -200mesh, oxygen content: 0.3 wt%), aluminum powder (particle size: d_{50}= 40μm, 99.9% purity), molybdenum powder (particle size: -100mesh, 99.9% purity), tin powder (particle size: -325mesh, 99.99% purity) and Si powder (99.95% purity). The powder blending was carried out for 24 hours in a roller mill with the container rotating at 200 rpm. The blended powders were compacted at room temperature in a 56mm diameter die under a pressure of 366MPa, then the powder compact was sintered at 1350^{o}C with a holding time of 5min at temperature before hot pressing. A 58mm diameter die was used for hot pressing with a maximum pressure of 342MPa. The hot pressing was done under the protection of an argon atmosphere with an oxygen content <200ppm. Extrusion of hot pressed compacts, using a 300 ton extrusion press was done in air at different extrusion temperatures, with no holding time at the target extrusion temperature prior to extrusion. The extrusion ratio used was 9:1 and the extrusion die temperature was 400^{o}C. The general processing route for sample production is illustrated in Fig.7.1. To optimise the processing parameters, three as-extruded samples were prepared, as shown in Table 1.

Table 7.1 Samples prepared using different extrusion temperature

Sample name	Extrusion temperature, ^{o}C
HP	Hot pressed after sintering at 1350^{o}C with a holding time of 5min at the sintering temperature
Sample 1	1025 (the β transus temperature 1075^{o}C)
Sample 2	1125
Sample 3	1200

The relative density of the powder compacts was determined from their volume which was measured using a 3D scanner. The microstructures of the extruded samples were characterized by optical microscopy (Olympus BX60), X-ray diffractometry (XRD) (Philips X' Pert system) and scanning electron microscopy (SEM) (HITACHI S4000). Both the room temperature and elevated temperature tensile tests were carried out using a 4204 INSTRON universal testing machine with dog-bone shaped specimens with a rectangular cross-section of 2mm x 2.5mm and a gauge length of 20mm. The strain was measured using an

extensometer with a gauge length of 10mm. The strain rates used for the room temperature and elevated temperature tensile testing were 1×10^{-4} s^{-1} and 1.4×10^{-4} s^{-1}, respectively. The elevated temperature tensile testing was conducted in a temperature controlled furnace mounted on the testing machine. The temperatures used for high temperature tensile testing were 300°C, 350°C, 400°C, 450°C and 500°C.

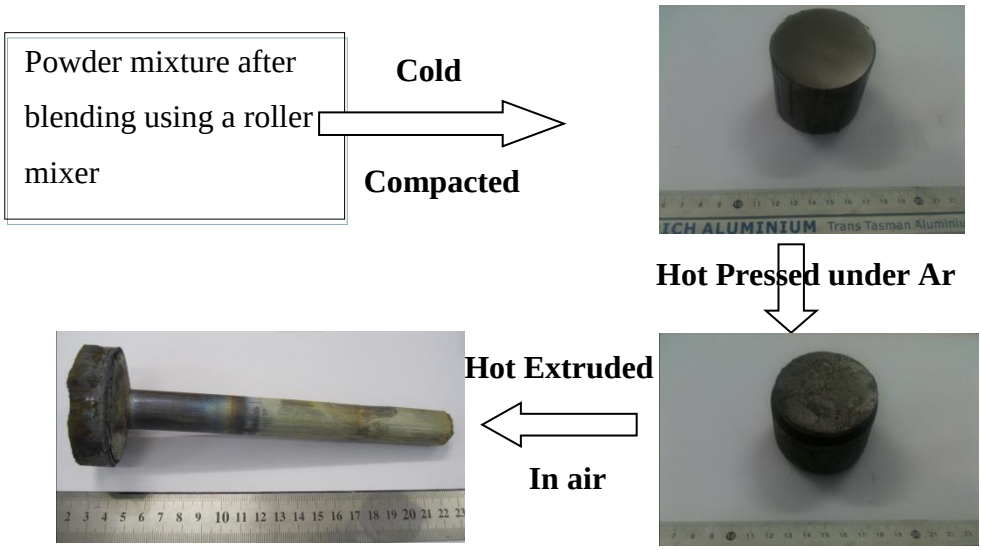

Fig.7.1 Processing route for preparing Ti-4%Al-4%Mo-4%Sn-0.5%Si titanium alloy by powder compact extrusion from a pre-consolidated compact.

7.3 Results and discussion

7.3.1 Oxygen analysis

Table 7.2 shows the results for oxygen analysis of the titanium powder and as-extruded samples. The oxygen content of the HDH titanium powder, the main constituent of the starting powder, is 0.3wt.%. After extrusion, the oxygen content of samples increased to 0.36 wt.% or 0.37 wt.%. This means that 0.06-0.07 wt.% oxygen was picked up during thermo-mechanical processing by hot pressing and extrusion. It was evident that different extrusion temperatures did not have any impact on the oxygen content of samples, except for extrusion at 1200°C, when a slight increase in oxygen content was observed. These results indicate that this thermo-mechanical processing route for Ti-4%Al-4%Mo-4%Sn-0.5%Si alloy avoids large quantities of oxygen pick up.

Table 7.2 Oxygen content of the titanium powders and as-extruded samples

Sample	HDH Ti	Sample 1	Sample 2	Sample 3
Oxygen content (wt.%)	0.3	0.36	0.36	0.37

7.3.2 Microstructural and elemental diffusion analysis

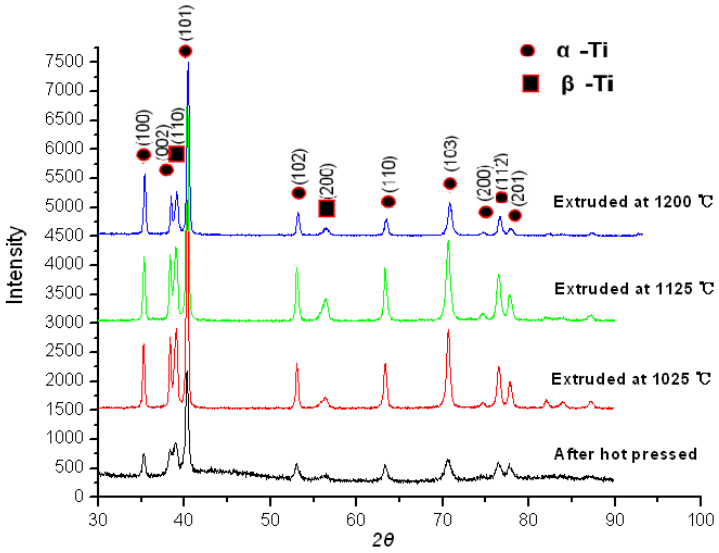

Fig.7.2 XRD patterns from the hot pressed and as-extruded samples.

Fig.7.2 shows XRD patterns for the hot pressed sample (pre-consolidated compact) and the three as-extruded samples. Clearly, all the samples are typically α+β two phase alloys. It is also can be seen from the XRD peak intensities that the amount of β phase in sample 3 has decreased compared with that in the other three samples. This is perhaps because Mo, which is a β stabilizer, diffuses faster at a higher extrusion temperature of 1200^{o}C, creating a more homogenous distribution of Mo. This leads to a lower overall Mo concentration, which is insufficient to preserve the β phase during cooling leading to a reduced amount of β phase. On the another hand, a higher extrusion temperature aids the diffusion of α stabilisers such as Al, which is beneficial to α phase precipitation. The amount of α phase after cooling is therefore increased.

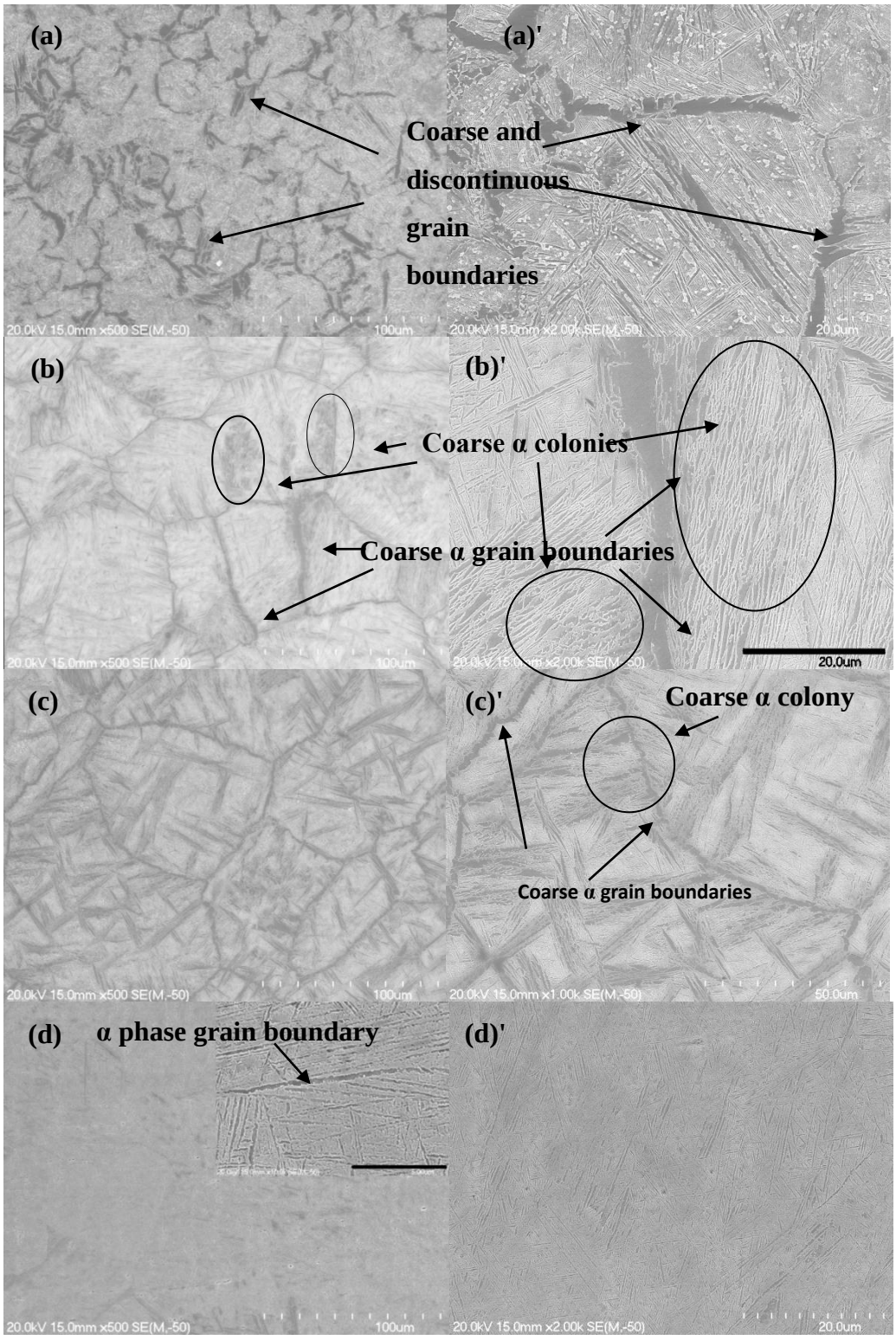

Fig.7.3 SEM images of the as-extruded samples: (a) and (a)' after hot pressing at 1350ºC with a 5 min. holding time (HP), (b) and (b)' extruded at 1025ºC (sample 1), (c) and (c)' extruded at 1125ºC (sample 2), (d) and (d)' extruded at 1200ºC (Sample 3). A higher magnification image is shown in (d) with a 5µm scale bar in the corner.

Fig.7.3 shows typical low and high magnification SEM images, of hot pressed and

extruded samples. No undissolved elemental particles could be seen in each of the microstructures. The pre-consolidated compact (sample HP) has an inhomogeneous microstructure, as shown in Fig.7.3 (a) and (a)', with distinct grain boundaries. The microstructure shows a fine grain size overall, of less than 50μm. The low density and high porosity may also have contributed to the inhomogeneous microstructure in sample HP. In the microstructure of sample HP, there are also coarse α colonies. The microstructure of sample 1 in Fig.7.3 (b) and (b)', which was extruded at 1025^{o}C, has a Widmanstätten α+β lamellae structure and a much larger grain size, with grains less than 100μm but greater than 50μm, compared with the microstructure in Fig.7.3 (a) for sample HP. The grain boundaries are clearly seen delineated and have a coarse appearance. Coarse α colonies are also visible, but not as coarse as those seen in sample HP. As the extrusion temperature is increased further, the microstructures shown in Fig.7.3 (c) and (c)' for sample 2, are more homogeneous compared with those for sample HP and sample 1, with more uniformly distributed coarse α colonies and a larger grain size (almost 100μm) compared with that for sample HP and sample 1. The microstructure in sample 2 still has a characteristic Widmanstätten structure similar to that in sample HP and sample 1. Sample 3, extruded at 1200^{o}C, has a more homogenous microstructure, as shown in Fig. 7.3 (d) and (d)'. Continuous α phase grain boundaries can be seen in the microstructure. Most of the α phase is precipitated at the grain boundaries or as fine α platelets within the β grains to form the colonies. The β grain microstructure has an acicular Widmanstätten of microstructure and is quite different from that found in sample HP, sample 1 and sample 2, while the microstructure in sample 3 still has a characteristic Widmanstätten structure.

In conclusion, with increasing extrusion temperature the microstructure and distribution of coarse α colonies becomes more homogeneous and when the alloy is extruded at 1200^{o}C the coarse α colonies disappear. The grain boundaries also change from having coarse and discontinuous alpha to a finer and continuous alpha distribution. The grain size of different samples also increases with increasing extrusion temperature: with sample HP < 50μm<Sample1<100μm≈Sample 2<Sample 3. The thickness of α phase lamellae within the β grains in extrusions produced using a 300 ton extrusion press is very

fine and normally < 1um, as shown in Fig. 7.4 (a). This is much finer than that in samples produced using a 100 ton press, as shown in Fig.7.4 (b) and described in Chapters 4, 5 and 6. This is most likely because the extrusions carried out using a 100 ton press were done in an enclosed chamber where the atmosphere in the enclosed space was warm. Therefore the cooling rate after extrusion would have been lower than that for extrusions done in air using a 300 ton press. A faster post-extrusion cooling rate would give a finer precipitated α phase.

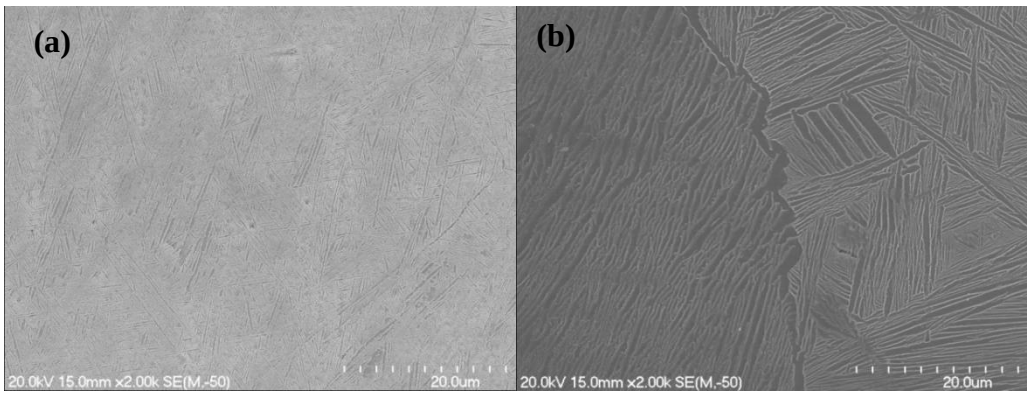

Fig.7.4 Typical α phase morphologies inner β grain of the samples extruded (a) by 300 ton press show an average phase width definitely < 1μm and (b) by 100 ton press.

It is well known that the degree of elemental diffusion and distribution directly affects microstructure. Elemental diffusion giving a uniform distribution normally results in a homogeneous microstructure. On the other hand, the microstructural distribution reflects the degree of elemental diffusion and elemental distribution. From the microstructural observations, no undissolved elemental particles could be seen in a hot pressed compact (pre-consolidated compact), but the microstructure was inhomogeneous with different phase morphologies in different parts of the microstructure. This suggests that elemental diffusion was not sufficient to achieve elemental homogeneity after hot pressing. After extruding the pre-consolidated compact at 1025^{o}C and 1125^{o}C, respectively, the elemental distribution becomes more homogenous than that in the pre-consolidated compact, but there are differences in phase morphology throughout the microstructure. There are many clusters of both short and coarse α lamellae due to the inhomogeneous elemental distribution. It is known that the fracture mechanism in a Widmanstatten α structure is mainly controlled by the effect of colony facet size on crack growth [10], so clusters of coarser α lamellae which gave coarser α

colonies are crack initiations sites which reduce tensile strength and ductility. After extruding at 1200^{o}C, better elemental diffusion gives a more homogenous microstructure. This means that the processing parameters selected, especially the extrusion temperature, meet the requirement for preparing material with a satisfactory microstructure and good mechanical properties.

Table 7.3 Quantitative element Si analysis on the coarse phase area including coarse grain boundaries of the HP and as-extruded samples.

	Sample HP	Sample 1	Sample 2	Sample 3
Si (wt.%) (average)	0.86	1.04	0.93	0.53

Weight % Error (+/- 1 Sigma): +/- 0.09

To investigate the causes for the microstructural features observed, such as the formation of coarse phases, including coarse grain boundaries, a quantitative investigation of Si distribution was carried out. The data is given in Table 7.3. It can be seen that the Si content in samples with areas of coarsened phases is significantly higher than the nominal content 0.5wt.%. Although the precipitation of silicides at the α platelet/β phase interface could control the width of the α platelets in a colony [4], from this study we can see that the Si content was far higher than the nominal content, leading to a coarsened α phase. From the results of the study described in Chapter 4, we can conclude that a Si-rich area promotes the formation of silicides, especially large sized silicides and this hinders the diffusion of the β stabilizer. In this alloy this is Mo and an elemental analysis compared Table 7.3 and Fig.7.7 shows that there is a low Mo content in Si rich areas, this directly leads to precipitation and growth of the α phase. The effect of Si content on the width of the α phase and a possible fracture mechanism is illustrated in Fig. 7.5. From the EDS analysis we can be definite that “close to nominal content” means between 0.4-0.6 wt% Si and “far beyond nominal content” refers to a content between 0.8-1.1 wt.% Si.

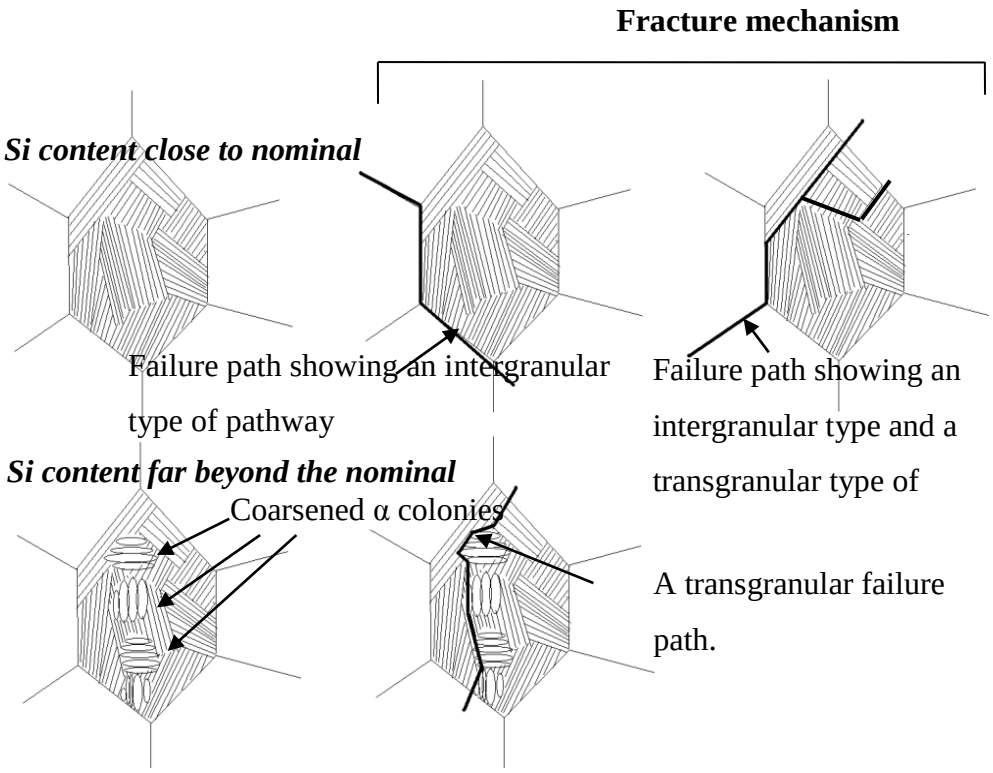

Fig.7.5 The effect of Si content on the morphology of α colonies and fracture mechanism.

In a Widmanstätten structure, grain boundary α influences the fracture mechanism [10]. Coarser grain boundaries are potential sites for cracking when there is an accumulation of microvoids [10]. Fig.7.6 shows typical high magnification SEM images of grain boundaries in each sample. It is noticeable that the width of grain boundary α phase in sample 3 is significantly finer than that in the other three samples and is hard to distinguish from the microstructure. The microstructure in sample 3 is finely acicular as shown in Fig.7.3 (d) and Fig.7.6 (d). The micrographs shown in Fig.7.5 suggest that for sample 3, the overall finer microstructure with no course grain boundary α and α colonies might give improved tensile properties.

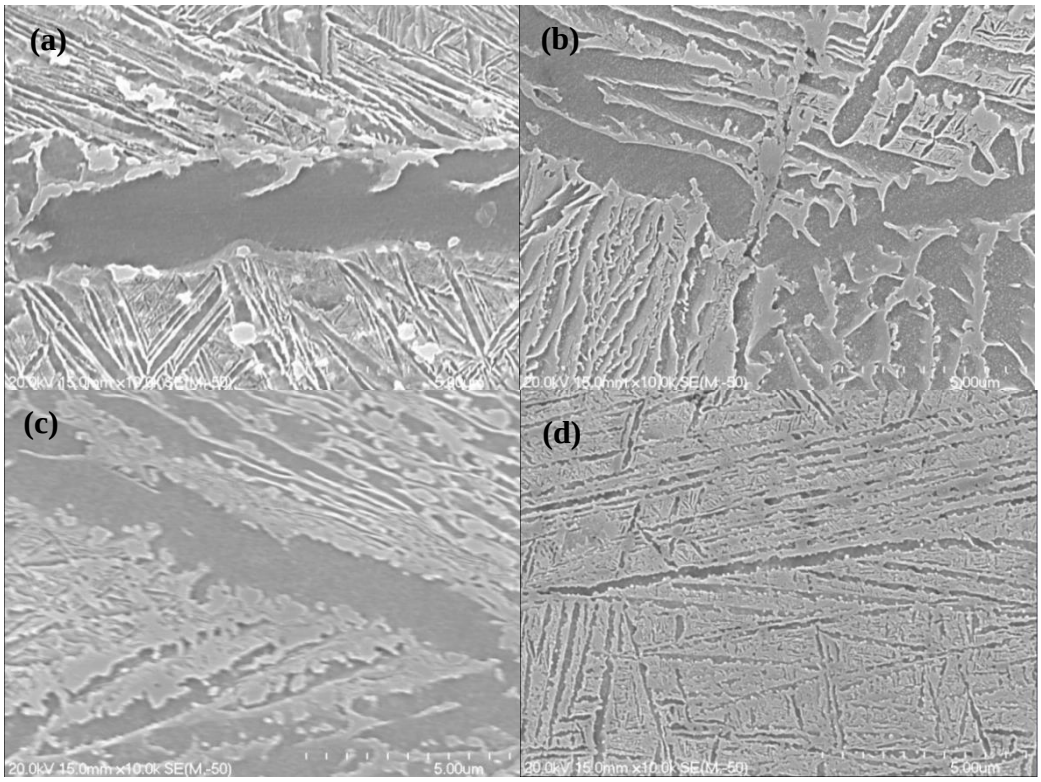

Fig.7.6 High magnification SEM images of the typically grain boundaries and textures presented in four samples, (a) the pre-consolidated sample, sample1, (b), (c) and (d) are the as-extruded sample 1 (extruded at 1025°C), sample 2 (extruded at 1125°C) and sample 3 (extruded at 1200°C), respectively.

Fig.7.7 shows elemental quantitative analysis of the grain boundaries for each sample. Compared with the Si contents given in Table 7.3, there is a significant difference in Si and Mo content. With increasing extrusion temperature the grain boundary Si content decreases and the Mo content significantly increases. The variation in Al content is relatively small. This suggests that the slower diffusion of Si impacts on the diffusion of other elements and directly leads to the precipitation of silicides, the formation of an inhomogeneous microstructure and finally unsatisfactory tensile properties. The Si rich areas are beneficial to the formation of silicides, which hinder the diffusion of β stabilizer which promotes the precipitation and growth of the α phase. Coarsening grain boundaries and coarser α colonies are likely sites for microcracking which is deleterious to tensile ductility [10].

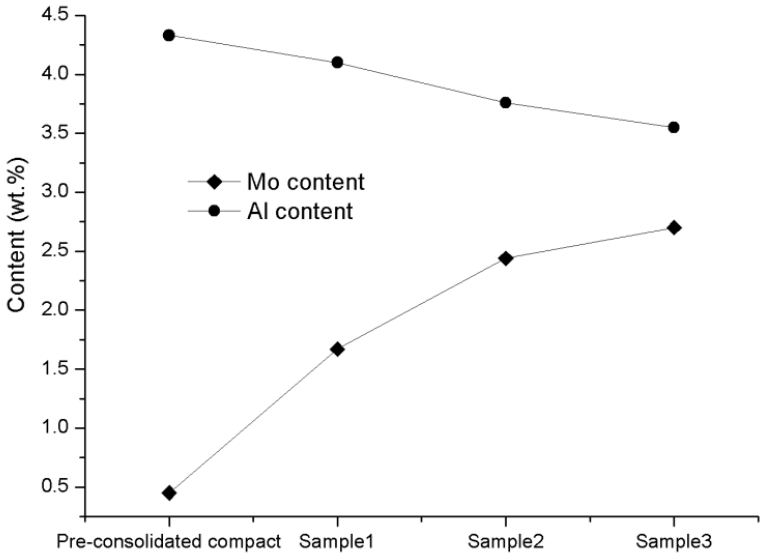

Fig.7.7 Quantitative elemental analysis on the grain boundaries of each sample.

7.3.3 Mechanical properties and fracture mechanism analysis

Fig.7.8 and Table 7.4 give the room temperature tensile stress-strain curves and tensile properties for each of the samples investigated. The results indicate that tensile specimens taken from sample HP and samples 1 and 2 failed prematurely before yielding. Test specimens from sample 1 gave a very small elongation to fracture of about 1% and a yield strength of 1200MPa. The microstructures of these samples, as described in section 3.2, had coarse features which most likely accounted for the poor ductility. Tensile test pieces taken from sample 3, which had a fine and relatively homogeneous microstructure, had satisfactory mechanical properties with a yield strength, UTS and elongation to fracture of 1278 MPa, 1421 MPa and 7.2% respectively. These properties are better than those obtained for alloy Timetal551 produced from ingot material by forging. This material has a UTS between 1200-1400MPa [9]. The tensile properties for sample 3 are also better than those for the same material produced by extrusion using a 100 ton press and described in Chapters 4 to 6.

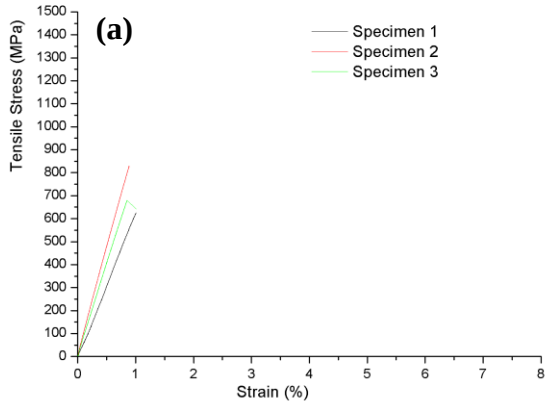
(a)
Specimen 1
Specimen 2
Specimen 3
Tensile Stress (MPa)
Strain (%)

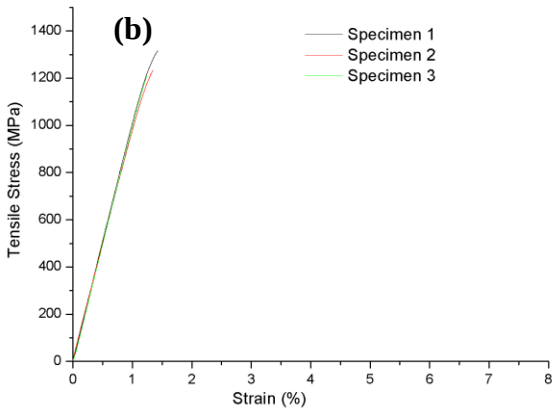
(b)
Specimen 1
Specimen 2
Specimen 3
Tensile Stress (MPa)
Strain (%)

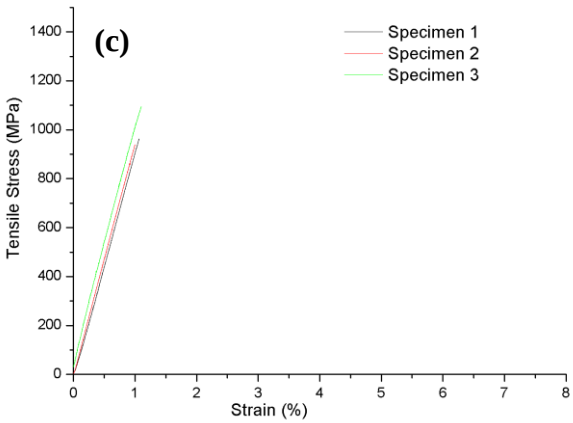
(c)
Specimen 1
Specimen 2
Specimen 3
Tensile Stress (MPa)
Strain (%)

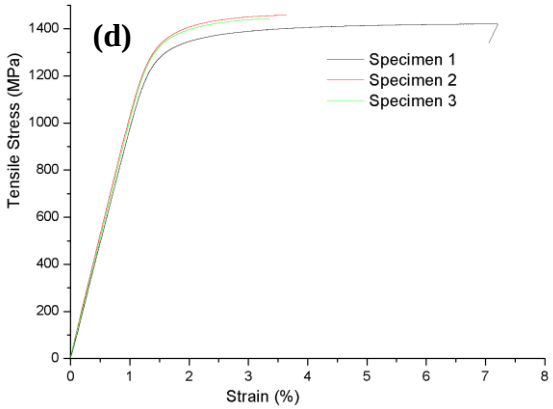

Fig.7.8 Room temperature tensile test results: (a) pre-consolidated compact, (b) sample 1 extruded at 1025ºC, (c) sample 2 extruded at 1125ºC and (d) sample 3 extruded at 1200ºC.

Table 7.4 Tensile test results in specific details

		UTS (MPa)	YS (MPa)	Elongation %
Sample HP	Specimen 1	627		
	Specimen 2	830		
	Specimen 3	680		
Sample 1	Specimen 1	1318	1227	1.4
	Specimen 2	1236	1133	1.3
	Specimen 3	1210	-	-
Sample 2	Specimen 1	902	-	-
	Specimen 2	980	-	-
	Specimen 3	1098	-	-
Sample 3	Specimen 1	1421	1278	7.2
	Specimen 2	1458	1327	3.6
	Specimen 3	1446	1325	3.3

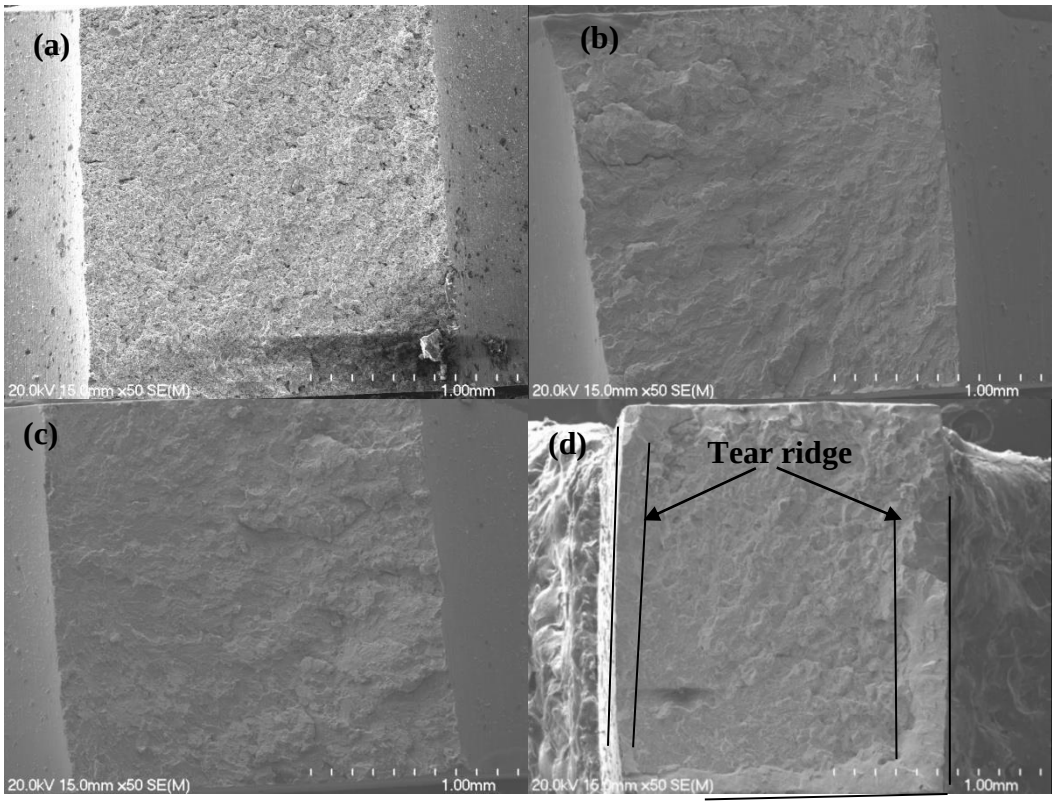

Fig.7.9 Low magnification SEM images of fracture surfaces: (a) a pre-consolidated compact, (b) sample 1 extruded at 1025ºC, (c) sample 2 extruded at 1125ºC and (d) sample 3 extruded at 1200ºC.

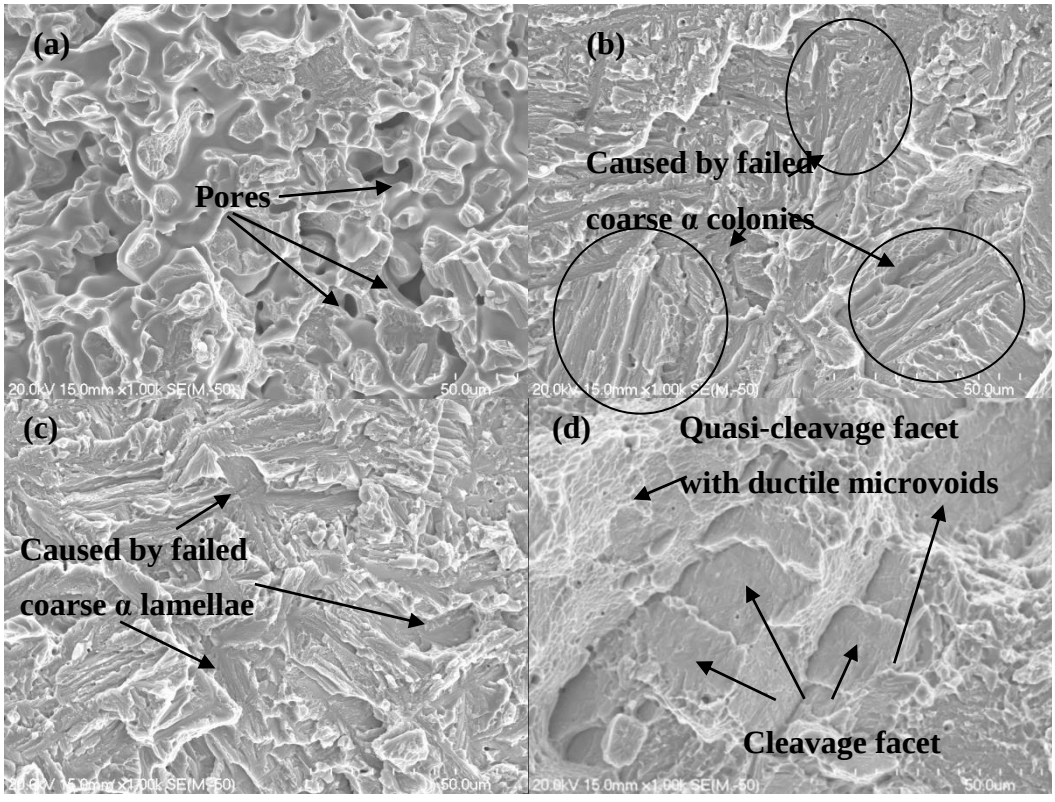

Fig.7.10 High magnification SEM images of fracture surface: (a) pre-consolidated compact, (b) sample 1 extruded at 1025ºC, (c) sample 2 extruded at 1125ºC and (d) sample 3 extruded at 1200ºC.

Fig.7.9 and Fig.7.10 are low and high magnification SEM images, of the fracture surfaces from each of the tested samples. As shown in Fig.7.9 (a) and Fig.7.10 (a) the fracture surface shows evidence of porosity. This explains the premature failure of tensile test pieces taken from this sample. There was no porosity evident in the fracture surfaces of the other three samples, which implies that full density was achieved during extrusion.

The fracture surfaces in Fig.7.9 (b) and (c) and Fig.7.10 (b) and (c) show evidence of flat cleavage fracture consistent with poor tensile strength and ductility. Many areas on the fracture surface indicate failure deriving from coarse α colonies and α lamellae as shown in Fig.7.10 (b) and (c) and Fig.7.11. It is known that the α phase has lower ductility than the β phase [11] and is the source for initiation of micro cracks. Microcracks occur in the α phase with little or no plastic deformation. The coarse α phase indicates an inhomogeneous elemental distribution which directly leads to silicide precipitation between phases or along grain boundaries (see the EDS analysis Table 7.3). Silicide or other intermetallic precipitation are likely locations for crack nucleation leading to premature failure of the materials [11]. Cleavage fracture was therefore mainly initiated by the coarse α colonies and lamellae and this contributed to premature failure during tensile testing. The fracture mechanism, illustrated in Fig.7.5 is also consistent with features observed in the fracture surfaces showing that coarse lamellar areas are crack initiators. Small particles are also visible around the ductile microvoids as shown in Fig.7.11. These particles are probably β phase or other precipitated intermetallic phases which might have initiated the growth and propagation of microvoids, which then provided a pathway for cracking and eventual failure of the material [12-14]. This observation of particles could account for the fact that although ductile microvoids were found on the fracture surface, the material cannot achieve a satisfactory tensile strength and ductility. Furthermore this may explain some yielding and a low elongation to fracture of about 1% in sample 1. There is a greater area of ductile microvoids without any visible particles associated with them in Fig.7.12 compared with Fig.7.11.

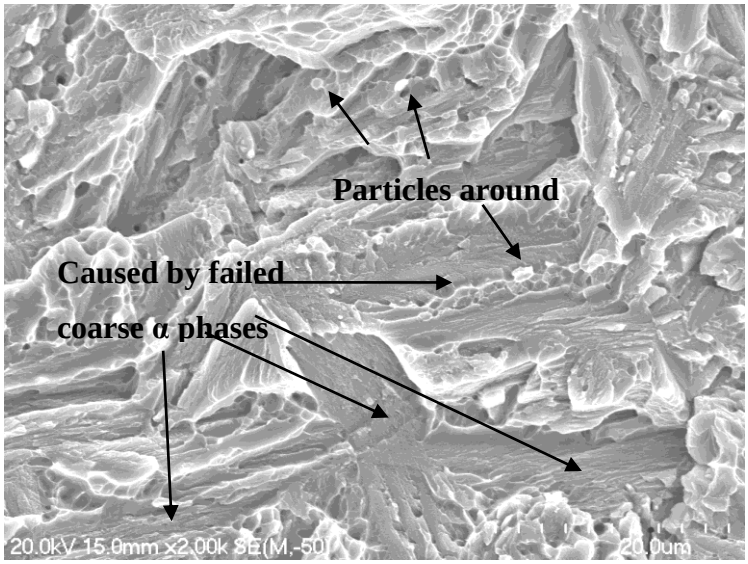

Fig.7.11 High magnification fracture surface SEM image of sample 2.

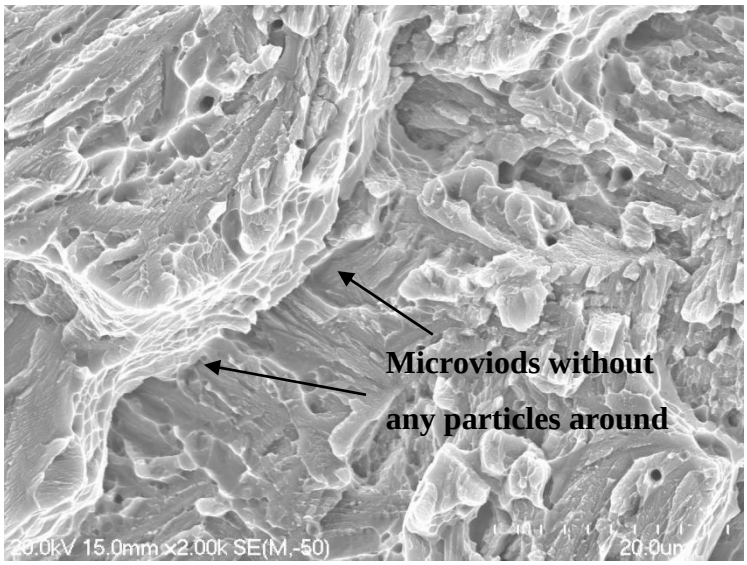

Fig.7.12 High magnification fracture surface SEM image of sample 1.

As shown in Fig.7.9 (d) and Fig.10 (d) a typical ductile fracture surface with some quasi-cleavage and cleavage facets [15] can be observed in the fracture surface from tensile specimens taken from sample 3. This sample has a high yield strength, UTS and elongation of 1278 MPa, 1421MPa and 7.2%, respectively. The fracture surface in Fig. 7.9 (d) has a ductile tear ridge and other features which are typical of those found in a high strength titanium alloy [15]. The cleavage facets are smaller than the grain size when a comparison is made with the grain size shown in Fig.7.3 (d). This means that most of the cleavage facets are associated with the β phase inside the grains. The cracks develop along cleavage facets and then into other α colonies or the grain boundaries, which have a higher strength than the

grains [16]. The fracture mechanism is explained by Fig.7.5, The proposed mechanism is the nucleation of microvoids and the emergence of microcracks which then develop into cleavage facets. These then progress into the finer lamellae areas or grain boundaries to form quasi-cleavage facets with plenty of dimples. It is suggested that the microvoids are associated with the coarser lamellae because of the relatively lower strength of coarser lamellae compared with other phases and a high probability of other precipitated phases along interphase boundaries within the coarser phases.

In conclusion, the extrusion temperature has a great effect on the degree of elemental distribution and microstructural evolution. When the extrusion temperature is increased to 1200^{o}C a fine lamellae microstructure is obtained and good strength and ductility can be achieved. The formation of a coarse lamellar structure is detrimental to tensile ductility, but if these coarse lamellae can be eliminated, the tensile properties can be significantly improved.

7.4 High temperature properties of material extruded at 1200^{o}C

It was stated in the introduction that Timetal551 has satisfactory mechanical properties at an elevated temperature of 400^{o}C, so an investigation of the elevated temperature mechanical properties of Timetal551 is meaningful. To examine the high temperature properties of Timetal551 a sample extruded at 1200^{o}C was selected for elevated temperature tensile testing. Stress-strain curves for tensile tests carried out between 300^{o}C and 500^{o}C are shown in Fig.7.13. From the data we can see that this alloy has a high tensile strength at 500^{o}C. With increasing temperature the tensile strength decreased from 907MPa to 720MPa and the elongation to fracture varied between 10% and 13%. Between 350^{o}C and 450^{o}C the mechanical properties showed little variation and these results indicate that this alloy has relatively stable mechanical properties in this temperature range.

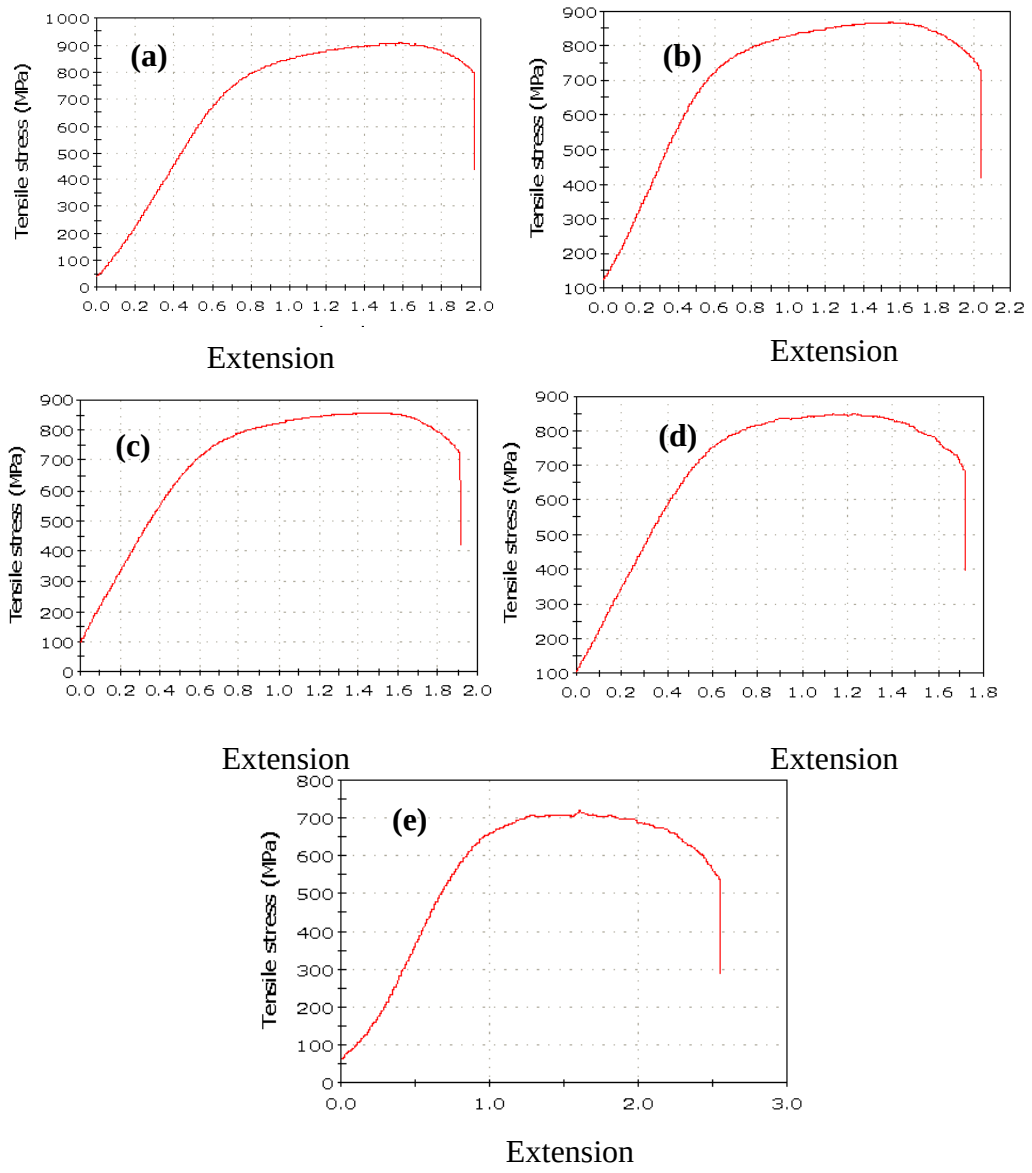

Temp. (ºC)	300	350	400	450	500
UTS (MPa)	907	870	860	850	720
YS (MPa)(zero slop)	907	870	860	850	710
Elongation %	10%	10.2%	10%	8.5%	13%

Fig.7.13 High temperature tensile curves for samples tested at (a) 300ºC, (b) 350ºC, (c) 400ºC, (d) 450ºC and (e) 500ºC, followed table shows the specific results.

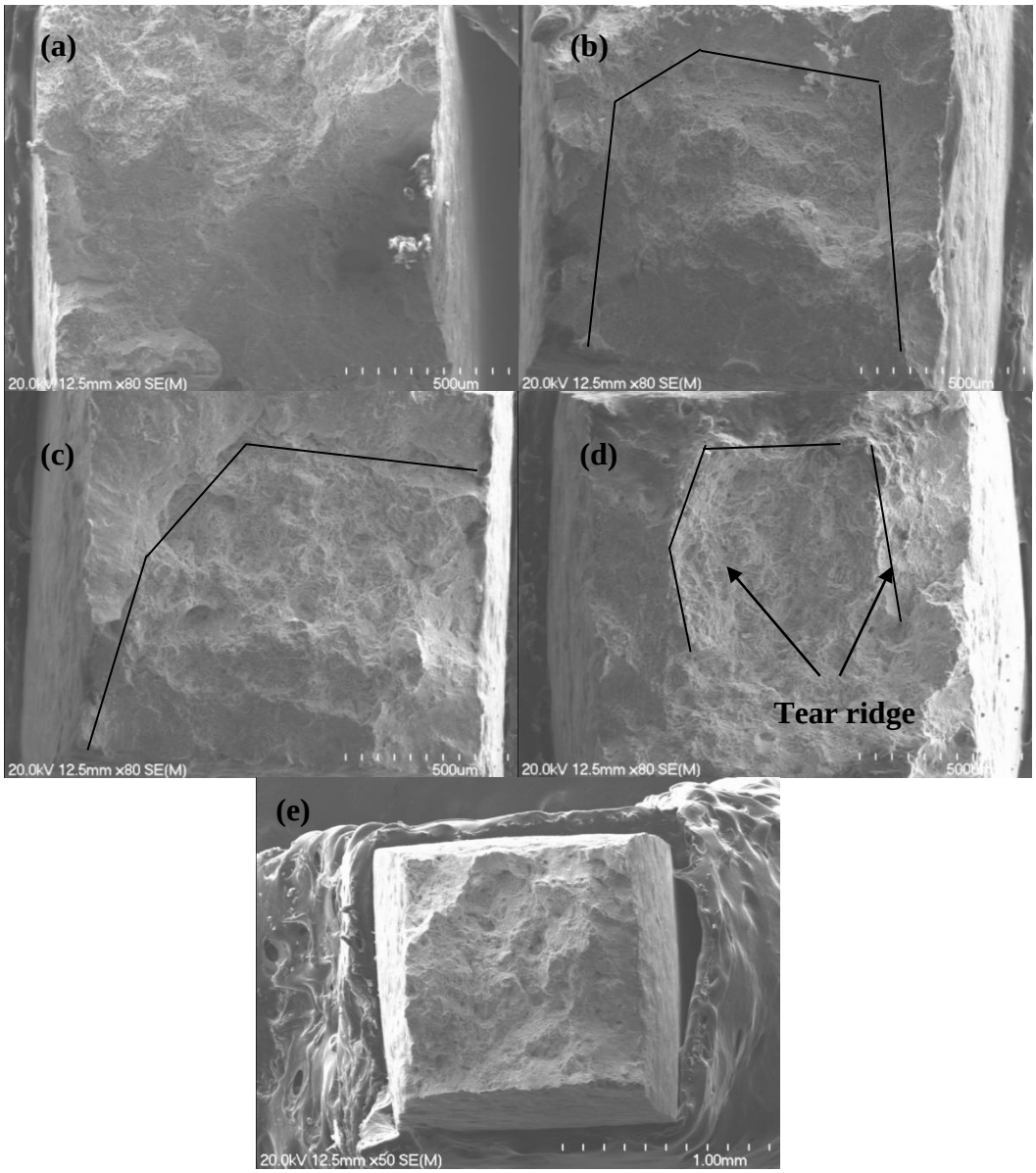

Fig.7.14 Low magnification fracture surface SEM images of the samples tested at (a) 300ºC, (b) 350 ºC, (c) 400 ºC, (d) 450 ºC and (e) 500 ºC.

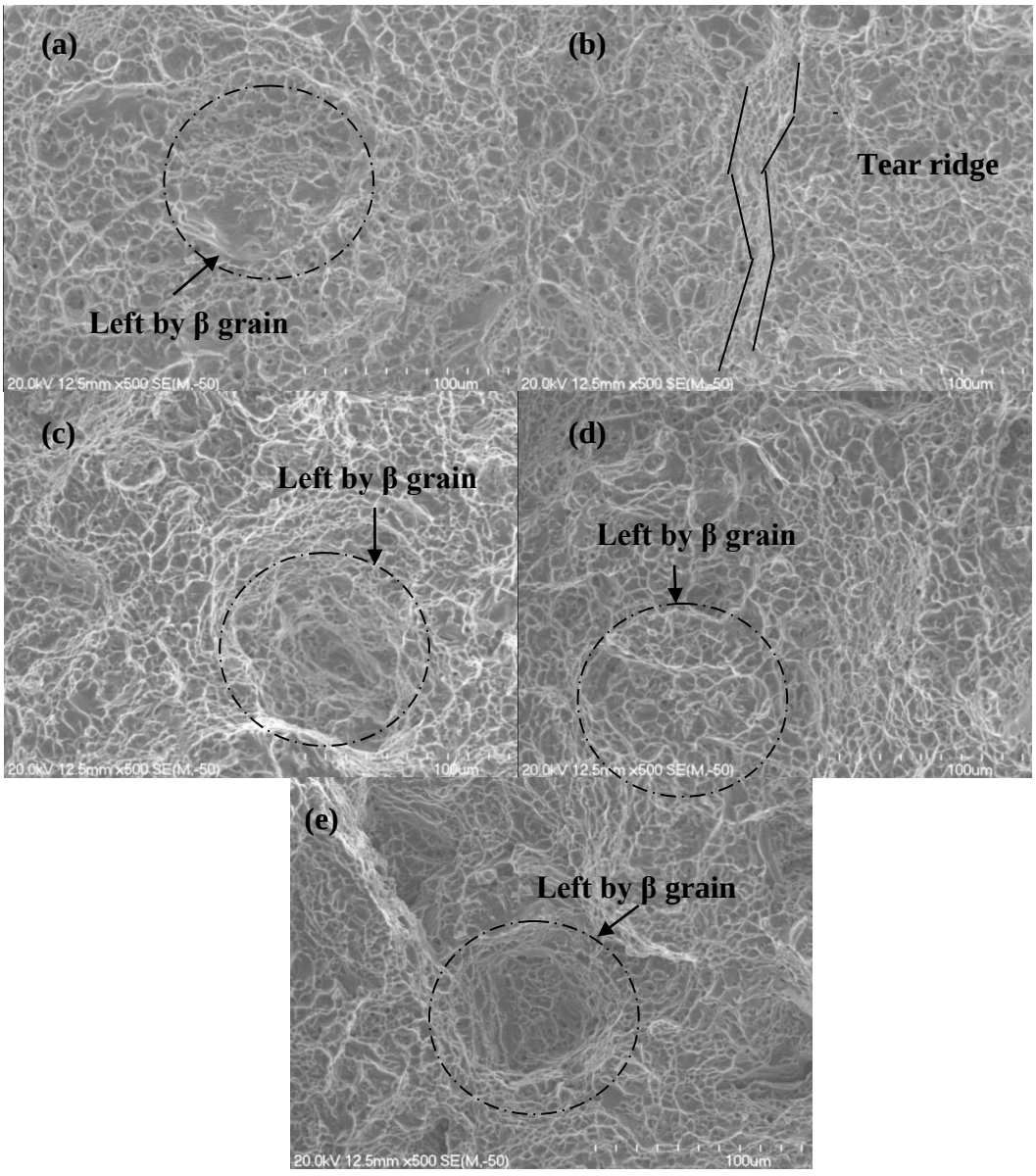

Fig.7.15 Higher magnification SEM images of the fracture surfaces from samples tested at (a) 300ºC, (b) 350 ºC, (c) 400 ºC, (d) 450 ºC and (e) 500 ºC.

Fig.7.14 and Fig.7.15 respectively show low and high magnification SEM images of fracture surfaces for each of the tested specimens. It is clear that all the images show typically ductile fracture surfaces consisting of equiaxed dimples. The images in Fig.7.14 (a) to (c) show that in the temperature range 300^{o}C - 400^{o}C the percentage reduction in area at fracture is smaller than that observed after testing at 500^{o}C. This can also can be seen in Fig.7.16 (a) to (c)), where the overall characteristic of fracture surfaces is transgranular cleavage in character. But as shown in Fig.7.15 cavities left by failed grains are evident, so a mixed transgranular and intergranular type of fracture is still the main fracture characteristic. A specimen tested at 500^{o}C fractured after necking, so the tensile

ductility, as given by an elongation to fracture of 13%, was better than that found for the other temperatures investigated. Furthermore as shown in Fig.7.14, with increasing testing temperature a tear ridge gradually moved from the edge to the middle of the fracture surface, indicating that failure occurred after necking with increasing temperature.

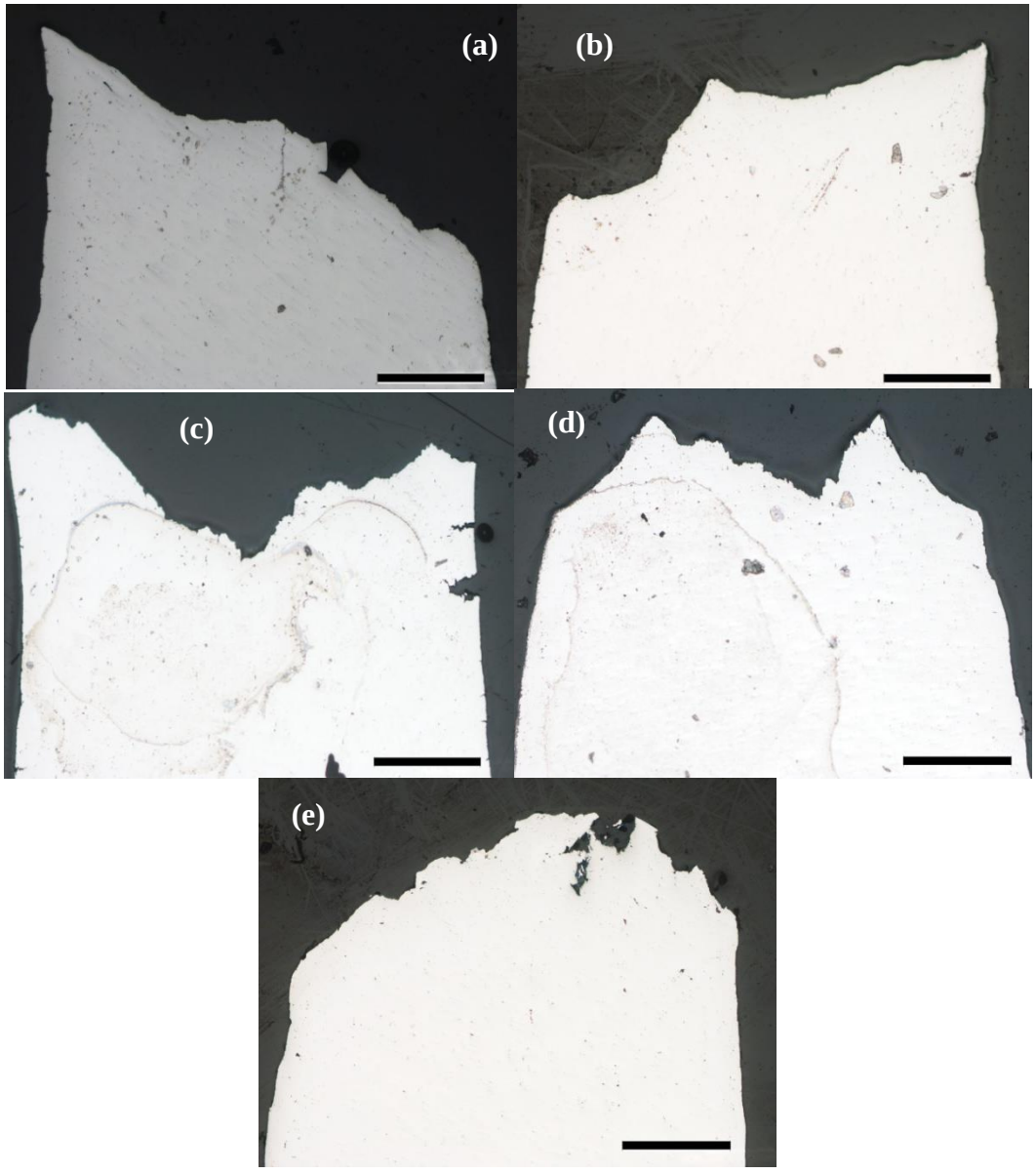

Fig.7.16 Optical micrographs of the fracture profiles of each tested specimen: (a) 300°C,(b) 350 °C, (c) 400 °C, (d) 450 °C and (e) 500 °C, the length of magnification bar is 20mm.

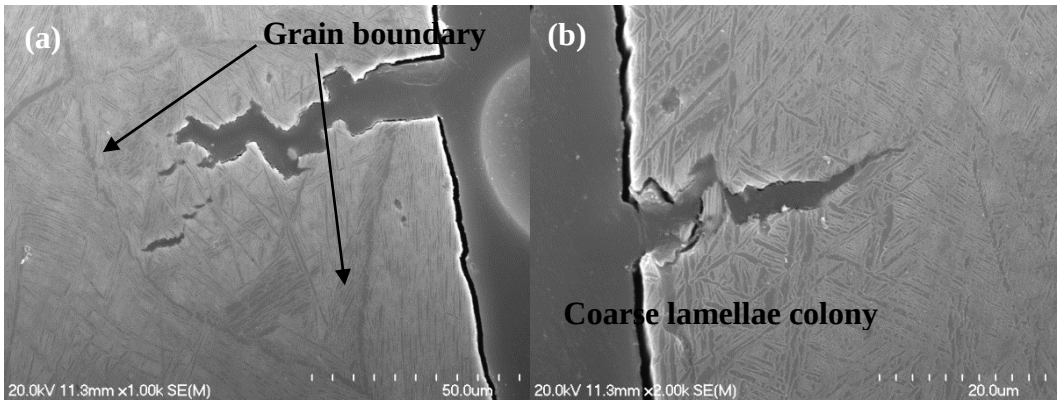

Fig.7.17 SEM images of typical fracture profiles from broken specimens.

Fig.7.17 shows SEM images giving more detail of typical fracture profiles. At high temperature cracks start inside the β grains and then develop into a transgranular fracture type as shown in Fig.7.17 (a). Initial cracking always occurs around the coarse lamellae phase, for example the lamellae phase inside the grain is relatively coarse with an irregular orientation, as shown in Fig.7.17 (a). This observation accords with the microstructure and fracture analysis at room temperature and also indicates that the fracture mechanism at high temperature, has to some extent, similarities to the fracture mechanism at room temperature. Fig.7.17 (b) also shows cracks developing at coarse lamellae areas. In other words it is hard for cracks to propagate through fine lamellae colonies. These observations indicate that the morphology of phases has a great impact on mechanical properties, and that coarsening lamellae are detrimental to tensile properties by promoting premature failure of material.

7.5 Conclusions

(a) A Ti-4%Al-4%Mo-4%Sn-0.5%Si titanium alloy was successfully prepared by powder compact extrusion from a pre-consolidated compact. This novel technique provides a feasible way to realise larger scale manufacturing.

(b) The extrusion temperature has a great effect on the elemental distribution and microstructural evolution. When the extrusion temperature is increased to 1200^{o}C a fine lamellae microstructure with good tensile properties giving a yield strength, UTS and elongation to fracture of 1278MPa, 1421MPa and 7.2%, respectively, were achieved. A microstructure with coarse lamellae is detrimental to tensile properties, but after coarse lamellae were eliminated, the tensile properties

improved significantly.

(c) Coarse lamellae colonies are sites for crack initiation and they enhance the propagation of cracks, leading to a transgranular fracture. A fine lamellae microstructure is beneficial for enhancing tensile properties.

(d) Good tensile properties were obtained at elevated temperature. Between 300^{o}C and 500^{o}C the tensile strength decreased from 907MPa to 720MPa, but the elongation to fracture increased from 10% to 13%.

References

[1] P. Esteban, L. Bolzoni, E. Ruiz-Navas, E. Gordo, Powder Metallurgy, 54 (2011) 242-252.
[2] D. Eylon, P.R. Smith, S.W. Schwenker, F.H. Froes, ASTM STP, 830 (1984) 48-65.
[3] T. Fujita, A. Ogawa, C. Ouchi, H. Tajima, Materials Science and Engineering: A, 213 (1996) 148-153.
[4] M. Hagiwara, S. Emura, Materials Science and Engineering: A, 352 (2003) 85-92.
[5] M.T. Jia, D.L. Zhang, B. Gabbitas, Key Engineering Materials, 520 (2012) 82-88.
[6] F. Yang, D.L. Zhang, H.Y. Lu, B. Gabbitas, Key Engineering Materials, 520 (2012) 70-75.
[7] F. Froes, M.A. Imam, Key Engineering Materials, 436 (2010) 1-11.
[8] F. Froes, D. Eylon, Moscow, ID: University of Idaho website, (2005).
[9] G. Welsch, R. Boyer, E. Collings, Materials properties handbook: titanium alloys, ASM international, 1993.
[10] M. Niinomi, T. Kobayashi, Materials Science and Engineering: A, 213 (1996) 16-24.
[11] T. Wang, H. Guo, Y. Wang, X. Peng, Y. Zhao, Z. Yao, Materials Science and Engineering: A, 528 (2011) 2370-2379.
[12] A. Andrade, A. Morcelli, R. Lobo, Matéria (Rio de Janeiro), 15 (2010) 364-370.
[13] M. Greenfield, H. Margolin, Metallurgical Transactions, 3 (1972) 2649-2659.
[14] Y. Krishnamohanrao, V. Kutumbarao, P.R. Rao, Acta Metallurgica, 34 (1986) 1783-1806.
[15] V.A. Joshi, Titanium alloys: an atlas of structures and fracture features, CRC Press, 2006.
[16] H. Yu, J. Chen, China Machine Press, 1999.

Chapter 8 Synthesis of TiB/Ti6Al4V composite by powder compact extrusion

8.1Introduction

An overall aim of this thesis is to investigate the synthesis of lower cost, higher strength titanium alloys for applications requiring, for example a higher hardness through enhanced yield strength, but with acceptable ductility. Previous chapters have described work carried out to achieve this using an alloy composition based on alloy Timetal551. This chapter describes an alternative approach for achieving a high yield strength and therefore high hardness through the synthesis of a TiB/Ti6Al4V composite alloy.

In-situ synthesized TiB whiskers have been identified as probably the most compatible and effective discontinuous reinforcement for Ti and Ti alloy matrices due to both their thermodynamic and mechanical stability (generating minimal residual stresses) because of good matrix bonding which generates very clean interfaces[1, 2]. This is especially the case for a Ti-6wt%Al-4wt%V alloy (Ti6Al4V) matrix reinforced by in-situ synthesized TiB whiskers and this approach has become attractive as a means of enhancing the strength of Ti6Al4V alloys. Consequently these composites have received a lot of attention [1-24]. Researchers have put a great deal of effort into improving the overall performance of titanium matrix composites (TMCs), especially for those based on a Ti6Al4V matrix and reinforced by in-situ synthesized TiB whiskers. However, a satisfactory level of mechanical properties such as high tensile strength and good ductility have still not been achieved [5]. Most research in this area tends to focus on studies of Young's modulus, hardness, microstructure and compressive properties [2, 11, 15-17, 19-22]. In Chapter 2 a review of previous work indicates two common characteristics in TiB/Ti6Al4V composites: (a) the TiB whiskers formed through in-situ reactions have a low aspect (length/diameter) ratio, and (b) when the composites are prepared using a powder metallurgy route, in combination with a blended elemental powder approach, a relatively uniform macroscopic distribution of the reinforcement in the matrix can be achieved.

However, TiB whiskers tend to form microscopic clusters in localized areas, and this microstructural feature has a significant impact on mechanical properties [5, 7-11]. A recent study by Huang et al. showed that improved tensile properties of a Ti6Al4V-5vol.% TiBw composite, with an ultimate tensile strength (UTS) of 1200MPa and elongation to fracture of 7%, is achievable by forming a novel microstructure consisting of a network of TiBw within a Ti6Al4V matrix. This structure consists of a TiBw-rich network boundary region and a TiBw-lean matrix region produced by hot extrusion [10]. However, such a network is a potential barrier to further improvement in strength, because when the volume fraction of reinforcement reaches a certain level, the network consists of many TiB clusters, which cause premature brittle failure of the material during tensile testing.

As a means of driving down the cost of PM titanium parts, powder compact extrusion or forging from blended elemental powders is now well established as a novel powder metallurgy technique. Components and structural members such as Ti6Al4V alloy rods and rocker arms for internal combustion engines and other titanium alloy products with unique mechanical properties have been successfully prepared using these low cost powder metallurgy methods [25, 26]. In this study a Ti6Al4V/TiBw composite was fabricated by powder compact extrusion from blended elemental powders. In this study the aim of using HDH Ti powder blended with Al40V powder to produce a Ti6Al4V matrix is a reduction in the cost of the starting materials and a lower oxygen content. The effects of different starting powders on the morphology of the reinforcement phases formed by the reactions, the microstructure and mechanical properties of the composites have been investigated. The influence of reinforcement morphology on the microstructure, defects and tensile properties of the as-extruded composites are also discussed.

8.2 Experimental process

The starting materials included HDH (hydride-dehydride) Ti powder (particle size -200mesh), HDH (hydride-dehydride) Ti6Al4V pre-alloyed powder (particle size -200mesh), Al40V (wt.%) master alloy powder (75mesh) and boron powder (-325mesh). Two powder mixtures were prepared to synthesize the TiBw/Ti6Al4V

composite, namely pre-alloyed HDH Ti6Al4V powder directly mixed with boron powder and HDH Ti and Al40V master alloy powder blended with boron powder, as shown in Table 8.1. Additionally in order to compare the properties and microstructures of the TiBw/Ti6Al4V composite with those of un-reinforced Ti6Al4V alloy, two as-extruded Ti6Al4V bars were also prepared from pre-alloyed Ti6Al4V powder and a powder mixture of titanium and Al40V, respectively.

Table 8.1 Composite samples prepared from different starting powders and the extrusion parameters.

Sample	Starting powders	Designed TiBw volume fraction, %	Extrusion Temperature
Sample 1	Pre-alloyed HDH Ti6Al4V and 0.5wt%B	2.6	
Sample 2	HDH Ti, Al40V and 0.5wt%B	2.6	1300ºC with a
Sample 3	HDH Ti, Al40V and 1.0wt%B	5.0	holding time of 5min
Sample 4	HDH Ti, Al40V and 1.5wt%B	7.4	

The powder blending was carried out for 24 hours in a roller mill with the container rotating at 200rpm. The blended powders were compacted at room temperature in a 40mm diameter die under a maximum pressure of 718MPa. For powder compact extrusion, all the powder compacts were heated to 1300ºC using an induction coil with a holding time of 5min and then directly extruded. The extrusion cylinder and die were heated to 500ºC, and the extrusion was carried out at an extrusion ratio of 9:1. The heating and extrusion of powder compacts were done in an argon atmosphere with an oxygen content <200ppm. Four extruded composite samples were made using different powder mixtures, as given in Table 1: another two Ti6Al4V alloy extruded bars were also produced from pre-alloyed Ti6Al4V powder and a powder mixture of HDH titanium and Al40V powder, using the same extrusion conditions.

The microstructures of longitudinal sections of extruded samples were characterized using an X-ray diffractometer (XRD) (Philips X' Pert system) and scanning electron microscopy (SEM) (HITACHI S4000). Kroll's reagent (100ml distilled water, 2ml HF and 4ml HNO_3) was used to etch the polished surfaces of the samples for SEM examination. Tensile testing was carried out using a 4204 Instron universal testing machine, using dog-bone shaped specimens with a rectangular cross-section of 2mm× 2.5mm, and a gauge length of 20mm, cut from

longitudinal sections of the extruded bar. The strain was measured using an extensometer with a gauge length of 10mm. The strain rate used during the tensile testing was $1\times10^{-4}s^{-1}$.

8.3. Results and discussion

8.3.1 Microstructural analysis

Fig.8.1 shows XRD patterns of as-extruded samples. Clearly, only one in-situ synthesised reinforcement phase is found and almost no difference exists between the composites except that the intensity of the diffraction peaks from the reinforcement phase is enhanced with an increase in the volume fraction of the reinforcing phase. The matrix is a typical two-phase alloy which consists of α and β phases. The TiB whisker reinforcement was in-situ synthesised via the reactions, (1), (2) and (3) given below. The references [14, 23, 24] show all the reactions that can take place when titanium and boron powder are mixed together. If there is excess titanium, thermodynamically unstable TiB_2 completely reacts with titanium and transforms into TiB.

$$Ti+B=TiB \qquad \text{Eq.(1)}$$

$$Ti+2B=TiB_2 \qquad \text{Eq.(2)}$$

$$Ti+TiB_2=TiB \qquad \text{Eq.(3)}$$

The fact that only one reinforcing phase, namely thermodynamically stable TiB, was found in the microstructure, as shown in Fig.8.1, is evidence that the reaction in Eq. (3) took place and was completed under the designed experimental parameters used in this study.

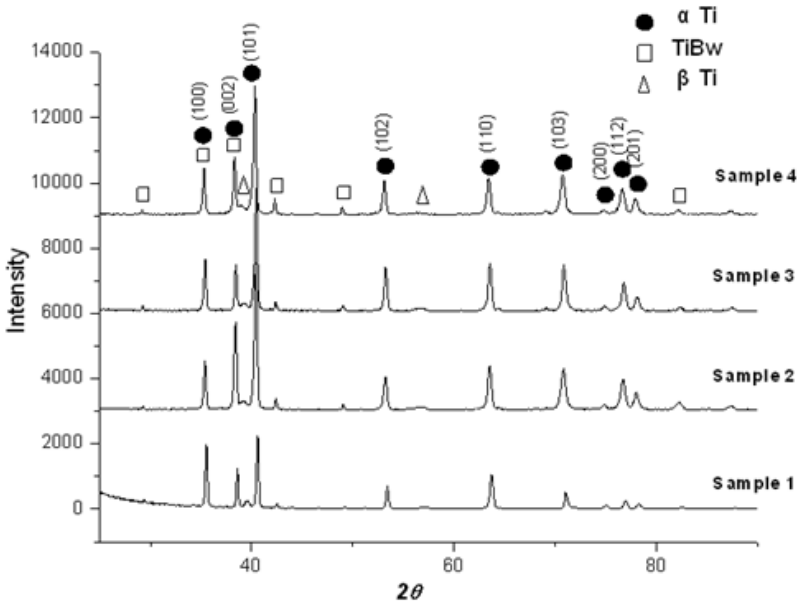

Fig.8.1 XRD patterns of the as-extruded samples, the upper three XRD patterns are from the as extruded TiBw/Ti6Al4V composites which were prepared from a blended powder mixture instead of pre-alloyed Ti6Al4V powder to synthesize the Ti6Al4V alloy matrix.

Fig.8.2 shows the microstructures of the as-extruded sample 1 (Fig.8.2 (a)), sample 2 (Fig.8.2 (b)), and the Ti6Al4V alloy without reinforcement prepared from pre-alloyed Ti6Al4V powders (Fig.8.2 (c)) and a powder mixture of HDH titanium and Al40V powders (Fig.8.2 (d)), respectively. EDS mapping shown below the SEM images of Fig.8.2 indicates a homogenous elemental distribution of the Ti6Al4V alloy which was produced from a powder mixture of HDH titanium and Al40V powders. The morphology of the TiB in sample 1 was revealed by removing the matrix from the surface by chemical etching, as shown in the inset micrograph of Fig.8.2 (a). In Fig.8.2 (a) it can be seen that the in-situ synthesized TiBw reinforcement from sample 1, which was prepared from a mixture of pre-alloyed Ti6Al4V and B powders, is much finer and has a much larger aspect ratio than the TiBw in sample 2, which was prepared from a powder mixture of HDH titanium powder, Al40V master alloy powder and boron powder. The aspect ratio of TiBw in sample 1 is also much larger than that found in samples 8.3 and 4 as shown in Fig.8.3.

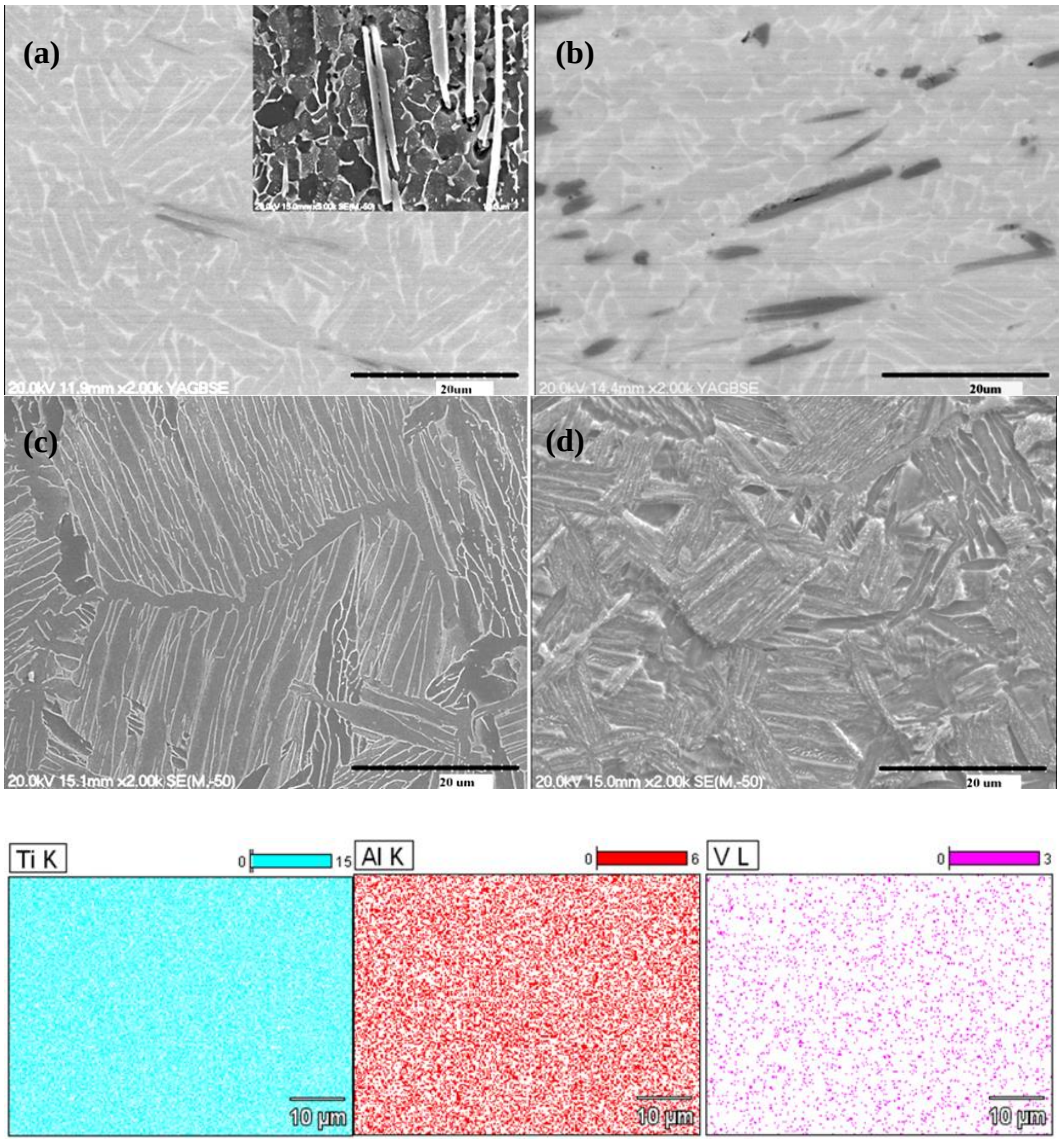

Fig.8.2 (a) and (b) SEM backscattered electron images of the longitudinal sections of sample 1 and sample 2, respectively, (c) and (d) SEM secondary electron images showing the microstructure of as-extruded Ti6Al4V alloy without reinforcement prepared from pre-alloyed Ti6Al4V powders and a powder mixture of titanium and 60Al40V powders, respectively. EDS mapping results below the images show a homogenous elemental distribution from microstructure Fig.2 (d).

The morphology of TiB whiskers is very hard to control because the growth of TiB can occur isotropically within a short time during high temperature processing [13]. When the boron powder directly contacts and reacts with titanium powder, there is a high reaction speed due to the efficient interface area between the boron and the titanium, and this leads to isotropic growth of the TiB whisker, until finally there are coarse TiB whiskers formed with a low aspect ratio. Another probable explanation for the fabrication of coarse TiB whiskers might be that the fast and efficient reaction between boron and titanium promotes crystal

growth and decreases the nucleation rate of the new reinforcing phases, so that a much higher crystal growth rate than nucleation rate produces the coarse morphology of the TiB whiskers. On the other hand, when the B powder is mixed with pre-alloyed HDH Ti6Al4V powders, it maybe that the reaction efficiency is dramatically affected by the existence of other metallic phases. An inefficient contact area causes the reaction between boron and titanium to reduce the crystal growth rate of the new phases. In other words it limits the isotropic growth of the whisker and directly produces fine TiB whiskers with a high aspect ratio. Based on the observation we can say that using a different starting powder has an impact on the final in-situ synthesized reinforcement.

From Fig.8.2 it can be seen that large lamella α colonies are present in the Ti6Al4V alloy matrix without reinforcement (Fig.8.2 (c) and (d)), whereas a fine equiaxed and short platelet α phase constitutes the microstructure of the alloy matrix. It also can be seen from Fig.8.2 (a) and (b), that a short platelet α phase is dominant in the reinforcement free area, while the reinforcement populated areas mainly consist of fine equiaxed α phases. This phenomenon is particularly evident in Fig.8.2 (a), where the matrix seems to almost exclusively contain short α platelets. This is because the reinforcement is too small to have any impact on dramatic microstructural changes in the matrix, but equiaxed α grains can still be easily found around the reinforcement after etching (as shown in the high magnification SEM image of inset micrograph in Fig.8.2 (a)). The above observation strongly supports the argument that the precipitation of reinforcement TiB has a significant effect on the matrix microstructure.

Fig.8.3 shows the backscattered electron images of as-extruded composite samples 1, 2, 3 and 4. The microstructures of the matrix are not affected by an increase in the volume fraction of reinforcement and the micrographs from (b) to (d), still mainly consist of fine equiaxed α grains. Apparently, the TiB whiskers found in sample 1 are much finer than those in the other three samples, with no pores present in sample 1. Many visible defects can be found in the other three samples. A high magnification SEM image in the inset micrograph in Fig.8.3 (b) shows that pores always emerge at or around the end of the reinforcement phase. Due to the fine TiB whiskers present in sample 1, whisker agglomerates are hard

to find, but TiB clusters are visible in the other three samples and these become more apparent with increasing reinforcement volume fraction. Other than an inhomogeneous distribution of boron in the powder mixture, the most appropriate explanation for the existence of TiB clusters in samples 2-4 is the use of a blended powder mixture instead of pre-alloyed Ti6Al4V powder to synthesize the Ti6Al4V alloy matrix. Therefore the reaction between boron and titanium not only leads to a coarse reaction product, but also provides local barriers for the homogeneous distribution of boron in the microstructure. The Al40V master alloy powder particles and the thin oxide layer on them are perhaps another obstacle to achieving a homogeneous distribution of boron.

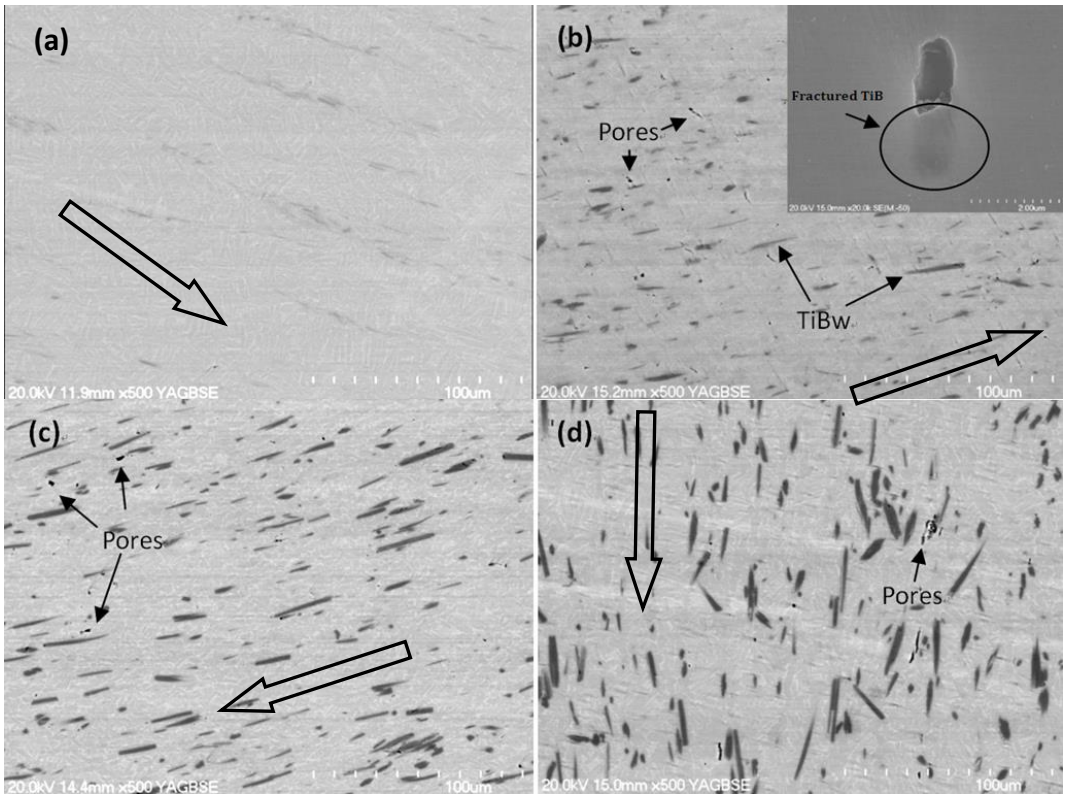

Fig.8.3 SEM backscattered electron images of the longitudinal sections of as-extruded samples (a) sample 1, (b) sample 2, (c) sample 3 and (d) sample 4. The inset in (b) is a high magnification SEM image of a typical fractured TiB whisker existing in sample 2. The hollow arrows indicate the extrusion directions of each sample.

The residual compact, after extrusion, contains microstructural and deformation information about the composite material from the un-extruded state to the extruded state. An investigation on a lengthwise cut section of the residual compact is of great significance for revealing the reinforcement phase transformation and the cause of defects during the extrusion process. Because

some porosity was found in as-extruded samples prepared from a powder mixture of titanium, Al40V and boron powders, the non-extruded part of sample 3 was prepared for SEM analysis. To monitor the development of the porosity and reinforcing phase transformation during extrusion, six points were selected for microstructural observation, as shown in Fig.8.4.

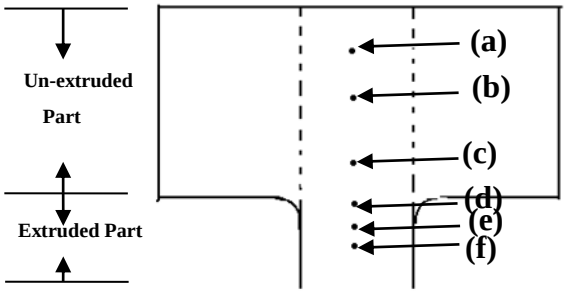

Fig.8.4 An illustration of the un-extruded sample cut by lengthways sectioning; six points were selected for microstructural analysis, shown as (a) to (f).

Fig.8.5 shows typical microstructures of the six selected points (a)-(f) shown in Fig.8.4. Some TiB_2 particles were found at point (a) but could not be seen at the other five points, which indicates that TiB_2 does not completely react with titanium at the early stage of extrusion. Because of the relative motion created by the extrusion pressure, the interfacial area between particles and matrix increases and this contributes to a further reaction between TiB_2 particles and the matrix. That no TiB_2 particles were seen at other points in the un-extruded end demonstrates that the in-situ synthesized TiB_2 particles were totally transformed into the TiB phase with the assistance of the pressure and high temperature in this un-extruded area. This also answers the question of why longer TiB whiskers emerged at point (b).

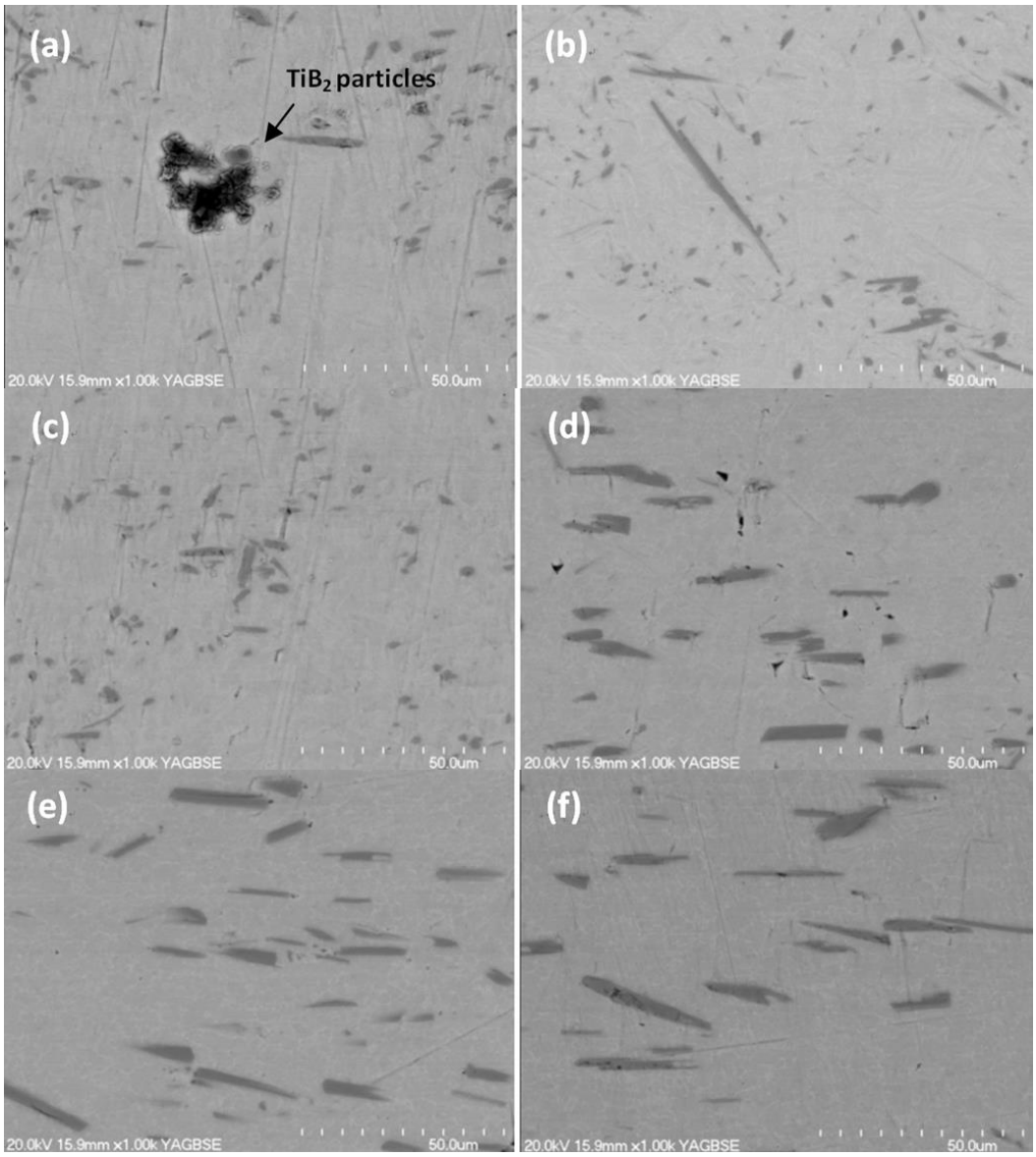

Fig.8.5 Backscattered electron images of the six points given in Fig.4.

As can be seen from the images shown in Figs.8.5(b) to (f), the image shown in (b) does not contain defects, whereas defects exist in Figs.8.5(c) to (f). The quantity and size of matrix defects reach a maximum at point (d), while decreasing and remaining stable at points (e) and (f). Some authors [10] have also reported that matrix defects exist after extrusion, because of the residual stress generated by the processing pressure, as a result of the deformation mismatch between the reinforcement and matrix. In this study, it can be seen that the amount of deformation begins at point (a) and gradually increases from point (b) through to point (f) and that points (e) and (f) are located in the highly deformed extruded

section. Because of the extrusion pressure the reinforcements undergo re-orientation as they move from points (a) to (f). Before moving through the extrusion cavity, as illustrated by point (b), the orientation of the reinforcements is random. With increasing deformation, defects appear at point (c) and then, because of the deformation mismatch between reinforcement and matrix and as the external force on the matrix increases, the quantity and size of defects reaches a maximum at point (d). Some reinforcements begin to break at points(c) and (d). This observation is consistent with that reported by other authors [5]. Because of the intense extrusion deformation at points (e) and (f), the TiB whiskers are almost completely re-aligned along the extrusion direction, and the interactions between them and the matrix decrease dramatically. In the meantime, the quantity and size of defects at points (e) and (f) are much smaller compared with those observed at (d), showing that the pores in the matrix are either closed or squeezed to smaller sizes under the extrusion pressure.

From the above observations and analysis, we can say that the extrusion deformation results in the re-orientation of TiB whiskers which is beneficial to material strengthening. During reinforcement re-orientation, the TiB whiskers break and defects emerge due to the deformation mismatch between reinforcement and matrix. So an increase in the extrusion ratio will help with defect elimination in the matrix and give an improvement in the material properties.

8.3.2 Tensile properties and fracture analysis

Room temperature tensile stress-strain curves for the as-extruded Ti6Al4V alloy and TiBw/Ti6Al4V composites are shown in Fig.8.6. As shown in Fig.8.6, the mechanical properties of as-extruded un-reinforced Ti6Al4V alloys shows a not so much difference, the alloy prepared from powder mixture of HDH Ti and Al40V shows a yield strength (YS) and tensile strength (TS) of 1216MPa and 1254MPa, respectively, with an elongation to fracture of 8.1%; while the alloy prepared from pre-alloyed HDH Ti6Al4V powder shows a YS 1130MPa and TS 1353MPa with an elongation to fracture of 10%. Their mechanical properties are reasonable according to their oxygen content after test, 0.4wt% and 0.42wt%, respectively.

With an addition of 0.5 wt% B, giving 2.6% volume fraction of reinforcement, and using only pre-alloyed Ti6Al4V powders for the matrix, the YS and TS are 1361MPa and 1436MPa respectively. This is an increase of 12% and 15% respectively in YS and TS compared with a Ti6Al4V alloy without reinforcement, and this is achieved while retaining reasonable ductility reflected by a 5.6% elongation to fracture. However, when titanium powder and Al40V master alloy powder are mixed with different amounts of boron powder to prepare a composite, there is a significant change in tensile properties with the stress at fracture falling to 1300MPa with slight ductility (sample 3) with 1wt% boron and premature fracture at a stress of 1138MPa with no ductility with 1.5wt% boron (sample 4).

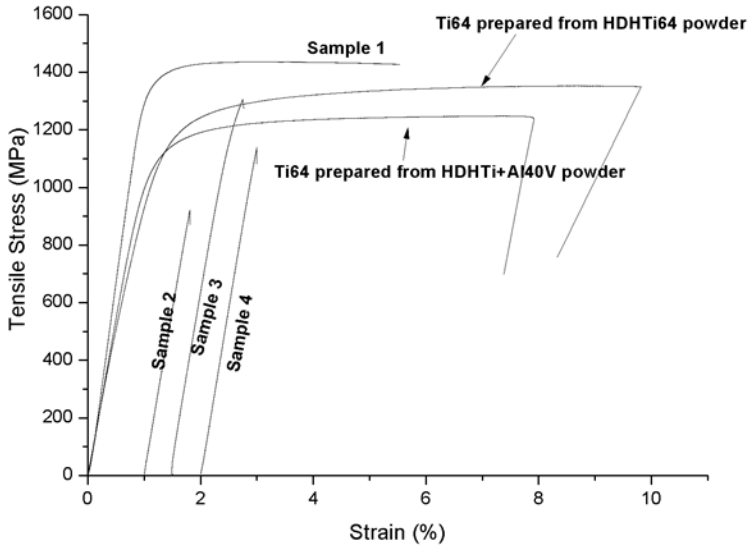

Fig.8.6 Tensile property curves of the as-extruded samples.

It is clear that the TiB whiskers in sample 1 are effective at strengthening the Ti6Al4V matrix. As shown in Figs.8.7 (a) and (b), the TiB whiskers have a large aspect ratio, and each of them fractured at several places during tensile deformation and fracture of the tensile test specimen. This indicates (i) that good interfacial bonding between the reinforcement and matrix formed during the reaction and hot extrusion, and (ii) that the whiskers were effective in carrying a higher load than the matrix, leading to the reinforcement effect. Furthermore plastic deformation of the matrix near or around the TiB whiskers also provides evidence for the strengthening effect of the reinforcement and the strong interfaces. The fracture surface shown in Fig.8.8(a), indicates a typical ductile

fracture near to the failed TiB whiskers with evidence of dimples and ductile tearing ridges. These observations are consistent with the fracture profile shown in Fig.8.7 (a) and (b), and offer another credible explanation for the good ductility of the composite.

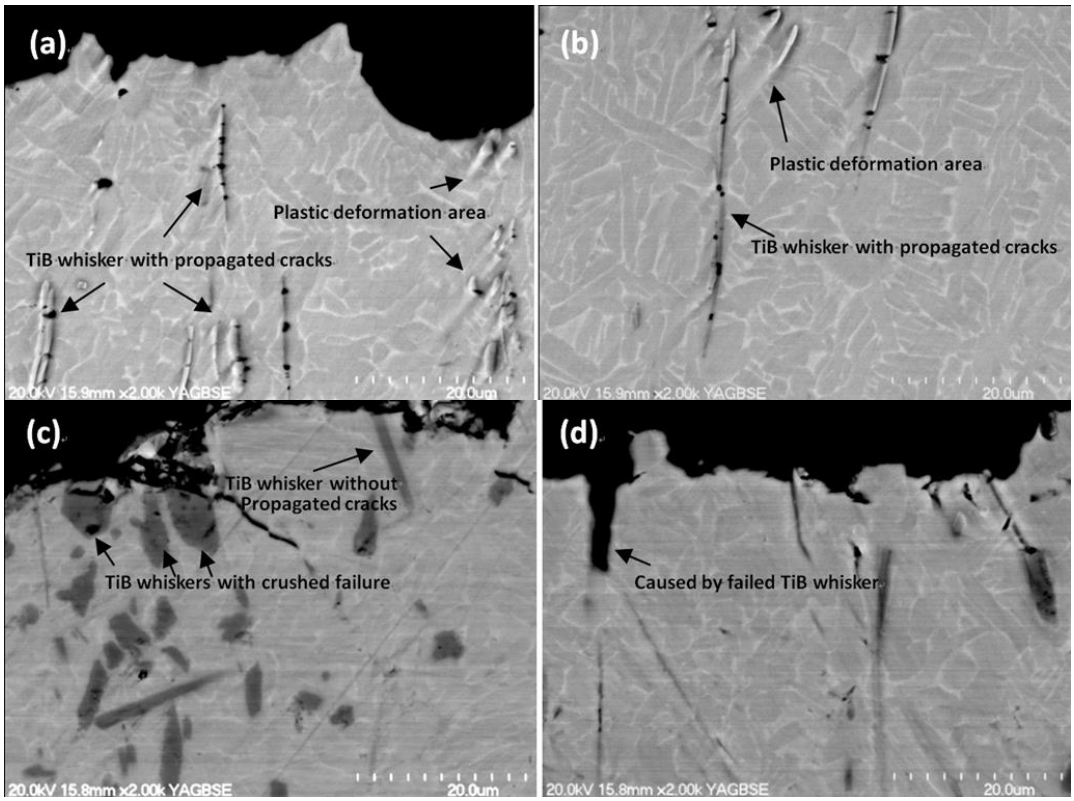

Fig.8.7 SEM backscattered electron images of the longitudinal sections of tensile test specimens cut from different samples: (a) sample 1, close to the fracture surface, (b) sample 1, slight away from the fracture surface, (c) sample 3, and (d) sample 4.

As shown in Figs.8.7(c) and (d), longitudinal sections close to the fracture surfaces of tensile test specimens, cut from samples 3 and 4, show that the TiB phase in the composite is in the form of TiB particles with a small aspect ratio, TiB whiskers with fairly large cross sectional sizes in the range of 1-2μm, and very fine TiB whiskers with high aspect ratios. The coarse TiB particles and whiskers exhibit a brittle cleavage fracture (Figs .8.7(c) and (d)). In addition there are residual parts of the TiB whiskers remaining on the fracture surface (Fig.8.8 (c) (d)) indicating that the coarse and brittle TiB particles prevented the achievement of good strengthening. A relatively flat fracture profile, shown in Fig.8.7 (d), and large pores in the fracture surface in Figs.8.8 (b)-(d) are directly caused by the failure of coarse TiB particles and whiskers. Some TiB whiskers have been pulled out before fracture, showing a poorer bonding strength between the

matrix/whisker interfaces. Furthermore, aggregates of TiB whiskers and particles and the pores around them (as explained in previous microstructural analysis section) can be important crack initiators, and contribute to the poor ductility of the composites.

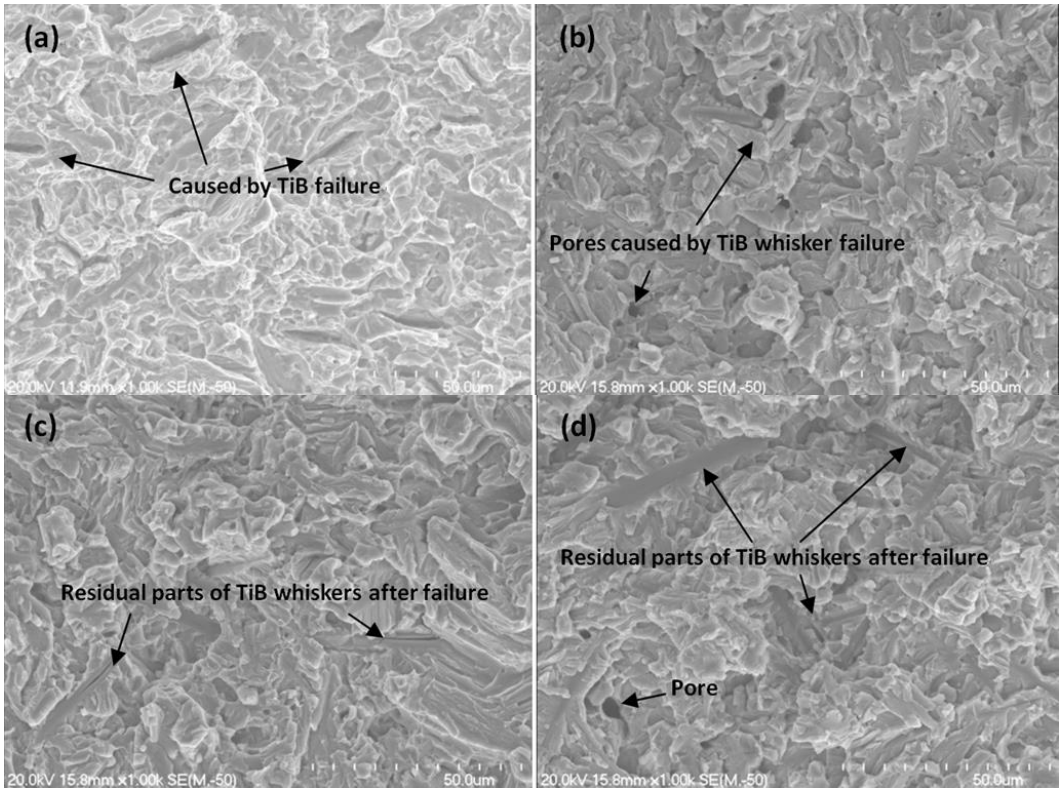

Fig.8.8 SEM secondary electron images of the fracture surfaces of the samples after tensile testing: (a) sample 1, (b) sample 2, (c) sample 3, and (d) sample 4.

Based on the previous analysis, a satisfactory strengthening effect could not be achieved when coarse TiB particles and whiskers form in the Ti6Al4V matrix, because of the residual pores in the matrix, poor reinforcement/matrix interfacial strength and the ease of fracture of the coarse TiB particles and whiskers. Without any strengthening effect from the reinforcements, the matrix fracture surface is a typical transgranular and translamellar cleavage fracture, as shown in Fig.8.8 (b), (c) and (d).

8.4. Conclusions

TiBw/Ti6Al4V composites were successfully fabricated by powder compact extrusion from a blended elemental powder mixture. Based on an investigation of their microstructures and mechanical properties, it was found that:

(1) Different kinds of starting powder have an impact on the morphologies of the in-situ synthesized TiB whiskers and particles and the pores in the composite. When pre-alloyed HDH Ti6Al4V powder and boron powder were used, fine TiB whiskers with a large aspect ratio formed in the composite without any defects. Whereas when HDH Ti, Al40V master alloy and boron powders were used, coarse TiB whiskers and particles with low aspect ratios formed, and many visible pores were found in the composite.

(2) A composite with a dispersion of fine TiB whiskers with large aspect ratio, which was prepared from a mixture of pre-alloyed HDH Ti6Al4V and boron powders, exhibited a good ductility and YS of 1361MPa and a TS of 1436MPa, showing significant improvement compared with that for a Ti6Al4V alloy without reinforcement. A Fracture strength of up to 1300MPa with almost no ductility was obtained in composites fabricated from a mixture of Ti, Al40V and boron powders.

(3) Avoiding the formation of coarse TiB whiskers and particles is the key for achieving high strength and good ductility in TiBw/Ti6Al4V composites, made using powder compact extrusion.

References

[1] Z. Ma, S. Tjong, L. Gen, In-situ Ti-TiB metal-matrix composite prepared by a reactive pressing process, Scripta materialia, 42 (2000) 367-374.
[2] Z. Ma, S. Tjong, X. Meng, Creep behavior of in situ dual-scale particles-TiB whisker and TiC particulate-reinforced titanium composites, Journal of materials research, 17 (2002) 2307-2313.
[3] W. Chen, C. Boehlert, E.A. Payzant, J.Y. Howe, The effect of processing on the 455° C tensile and fatigue behavior of boron-modified Ti–6Al–4V, International Journal of Fatigue, 32 (2010) 627-638.
[4] S. Lieberman, A. Gokhale, S. Tamirisakandala, R. Bhat, Three-dimensional microstructural characterization of discontinuously reinforced Ti64–TiB composites produced via blended elemental powder metallurgy, Materials Characterization, 60 (2009) 957-963.
[5] S. Gorsse, D. Miracle, Mechanical properties of Ti-6Al-4V/TiB composites with randomly oriented and aligned TiB reinforcements, Acta Materialia, 51 (2003) 2427-2442.
[6] S. Tjong, Y.-W. Mai, Processing-structure-property aspects of particulate-and whisker-reinforced titanium matrix composites, Composites Science and Technology, 68 (2008) 583-601.
[7] L. Huang, L. Geng, A. Li, F. Yang, H. Peng, In situ TiBw/Ti–6Al–4V composites with novel reinforcement architecture fabricated by reaction hot pressing, Scripta materialia, 60 (2009) 996-999.
[8] L. Huang, L. Geng, H. Peng, K. Balasubramaniam, G. Wang, Effects of sintering parameters on the microstructure and tensile properties of in-situ TiBw/Ti6Al4V composites with a novel network architecture, Materials & Design, 32 (2011) 3347-3353.
[9] L. Huang, L. Geng, H. Peng, J. Zhang, Room temperature tensile fracture characteristics of in situ TiBw/Ti6Al4V composites with a quasi-continuous network architecture, Scripta materialia, 64 (2011) 844-847.
[10] L. Huang, L. Geng, B. Wang, H. Xu, B. Kaveendran, Effects of extrusion and heat treatment on the microstructure and tensile properties of in-situ TiBw/Ti6Al4V composite with a network architecture, Composites Part A: Applied Science and Manufacturing, 43 (2012) 486-491.
[11] L. Huang, H. Xu, B. Wang, Y. Zhang, L. Geng, Effects of heat treatment parameters on the microstructure and mechanical properties of in-situ TiBw/Ti6Al4V composite with a network architecture, Materials & Design, 36 (2012) 694-698.
[12] R. Banerjee, P. Collins, A. Genc, H. Fraser, Direct laser deposition of in situ Ti–6Al–4V–TiB composites, Materials Science and Engineering: A, 358 (2003) 343-349.
[13] M.Y. Koo, J.S. Park, M.K. Park, K.T. Kim, S.H. Hong, Effect of aspect ratios of in situ formed TiB whiskers on the mechanical properties of TiBw/Ti–6Al–4V composites, Scripta materialia, 66 (2012) 487-490.
[14] Y. Liang, Y. Che, Notebook of thermodynamic data of inorganic, East-north University Press, Shen yang, (1996).
[15] J. Lu, J. Qin, Y. Chen, Z. Zhang, W. Lu, D. Zhang, Superplasticity of coarse-grained (TiB+ TiC)/Ti–6Al–4V composite, Journal of Alloys and Compounds,

490 (2010) 118-123.
[16] J. Lu, J. Qin, W. Lu, Y. Chen, D. Zhang, H. Hou, Effect of hydrogen on superplastic deformation of (TiB+ TiC)/Ti–6Al–4V composite, International Journal of Hydrogen Energy, 34 (2009) 8308-8314.
[17] K. Morsi, V. Patel, Processing and properties of titanium–titanium boride (TiBw) matrix composites—a review, Journal of materials science, 42 (2007) 2037-2047.
[18] T. Saito, H. Takamiya, T. Furuta, Thermomechanical properties of P/M titanium metal matrix composite, Materials Science and Engineering: A, 243 (1998) 273-278.
[19] C. Schuh, D. Dunand, Load transfer during transformation superplasticity of Ti–6Al–4V/TiB whisker-reinforced composites, Scripta materialia, 45 (2001) 631-638.
[20] C. Schuh, D. Dunand, Whisker alignment of Ti–6Al–4V/TiB composites during deformation by transformation superplasticity, International Journal of Plasticity, 17 (2001) 317-340.
[21] M.-m. Wang, W.-j. Lu, J.-n. Qin, D. Zhang, B. Ji, F. Zhu, The effect of reinforcements on superplasticity of in situ synthesized (TiB+ TiC)/Ti matrix composite, Scripta materialia, 54 (2006) 1955-1959.
[22] L. Xiao, W. Lu, J. Qin, D. Zhang, M. Wang, F. Zhu, B. Ji, High-temperature tensile properties of in situ-synthesized titanium matrix composites with strong dependence on strain rates, Journal of materials research, 23 (2008) 3066-3074.
[23] Z. Xinghong, Z. Chuncheng, Q. Wei, H. Xiaodong, V. Kvanin, Self-propagating high temperature combustion synthesis of TiC/TiB_2 ceramic–matrix composites, Composites Science and Technology, 62 (2002) 2037-2041.
[24] Z. Xinghong, X. Qiang, H. Jiecai, V. Kvanin, Self-propagating high temperature combustion synthesis of TiB/Ti composites, Materials Science and Engineering: A, 348 (2003) 41-46.
[25] M.T. Jia, D.L. Zhang, B. Gabbitas, Comparison of blended elemental (BE) and mechanical alloyed (MA) powder compact forging into Ti-6Al-4V rocker arms, Key Engineering Materials, 520 (2012) 82-88.
[26] F. Yang, D.L. Zhang, H.Y. Lu, B. Gabbitas, Preparation, Microstructure and Properties of Ti-6Al-4V Rods by Powder Compact Extrusion of Powder Mixture, Key Engineering Materials, 520 (2012) 70-75.

Chapter 9 Conclusions and recommendations

9.1 Conclusions

- An increase in the extrusion temperature significantly improves the elemental dissolution especially for Si and Mo. By using an extrusion temperature of 1350^{o}C with a holding time of 5 min prior to extrusion, elemental dissolution was much improved and a relatively homogenous microstructure was achieved. As-extruded bars with undissolved elemental particles showed low tensile strength without any ductility, while those samples without any inhomogeneities in the microstructure, caused by undissolved particles and defects, showed an ultimate tensile strength and elongation to fracture of 1423MPa and 5.1%, respectively.
- When as-milled alloying powders were blended with HDH titanium powder to prepare as-extruded samples, the uniformity in tensile strength improved, but ductility was sacrificed. A relatively higher Si content in the coarse lamellar areas and grain boundaries is the most likely reason for poor tensile properties especially poor ductility. GA titanium powders have a beneficial effect on elemental diffusion and the achievement of more uniformity in mechanical properties. When the starting powders were dominated by gas atomized (GA) titanium powders, a good combination of tensile strength and ductility was achieved which showed a UTS of 1220-1250 MPa with an elongation to fracture of 7-11%. More uniform mechanical properties were given by this alloy when GA titanium powder was introduced.
- A beta transus temperature of 1075^{o}C has been confirmed. The solutioning temperature and the concentration of beta stabilizer, especially Mo, in the beta matrix have a significant effect on martensite phase transformation. The cooling rate after solutioning plays a key role in determining the morphology of the α lamellar structure and the α colony and beta grain size. A faster cooling rate causes a decrease in the width of α the lamellae, the size of the α colonies and the beta grain size. After heat treatment HT-1, a high tensile strength of 1567MPa could be obtained but without any ductility. After heat treatment HT-2 an ultimate tensile strength of

1584MPa, a yield strength of 1505MPa and an elongation to fracture of 2.5% were obtained. After heat treatment HT-3 a tensile strength of 1315MPa, a yield strength of 1255MPa and an elongation to fracture of 1.7% were obtained.

- This alloy was successfully prepared by powder compact extrusion from a pre-consolidated compact. When the extrusion temperature was increased to 1200^{o}C a fine lamellae microstructure with good tensile properties giving a yield strength, UTS and elongation to fracture of 1278MPa, 1421MPa and 7.2%, respectively, was achieved. A microstructure with coarse lamellae is detrimental to tensile properties. Coarse lamellae colonies are sites for crack initiation and they enhance the propagation of cracks, leading to a transgranular fracture. Good tensile properties were obtained at elevated temperature, between 300^{o}C and 500^{o}C the tensile strength decreased from 907MPa to 720MPa, but the elongation to fracture increased from 10% to 13%.
- Different kinds of starting powder have an impact on the morphologies of the in-situ synthesized TiB whiskers and particles and the pores in the composite. When pre-alloyed HDH Ti6Al4V powder and boron powder were used, fine TiB whiskers with a large aspect ratio formed in the composite without any defects. Whereas when HDH Ti, Al40V master alloy and boron powders were used, coarse TiB whiskers and particles with low aspect ratios formed, and many visible pores were found in the composite.
- A composite with a dispersion of fine TiB whiskers with large aspect ratio, which was prepared from a mixture of pre-alloyed HDH Ti6Al4V and boron powders, exhibited a good ductility and YS of 1361MPa and a TS of 1436MPa, showing significant improvement compared with that for a Ti6Al4V alloy without reinforcement. A Fracture strength of up to 1300MPa with almost no ductility was obtained in composites fabricated from a mixture of Ti, Al40V and boron powders.

9.2 Recommendations

- After achieving dissolution of the elemental particles, some localized areas with an inhomogeneous elemental distribution still existed. These most likely derive from non-uniform blending during powder mixing and the diffusion interactions between different elements during high temperature processing. So the effect of blending apparatus and parameters should be investigated to get a uniform elemental dispersion especially for the element which is easy to be agglomerated such as Si.
- If Si is precipitated with titanium or other elements around the Si rich area, due to localized inhomogeneous elemental distribution, an extensive formation of silicides or other compounds could be a serious drawback. The precipitation of silicide and its effect on the fracture mechanism of titanium alloys should be monitored and investigated, and a way found to control its amount and size which is beneficial to mechanical properties.
- The extrusion parameters should be optimized when the starting powders are dominated by gas atomized (GA) titanium powders to get better mechanical properties. Furthermore the beneficial effects of GA titanium powders on the elemental diffusion should be studied.
- Following on from the elevated tensile properties studied in this thesis, the creep properties of this kind of alloy produced by powder compact extrusion should also be studied in the future.
- It is meaning to investigate the mechanism of the effect of pre-alloyed HDH Ti64 powder and HDH Ti powder on the morphology of in-situ synthesized TiB reinforcements.

Appendix I

Journal of Alloys and Compounds 606 (2014) 262–268

Contents lists available at ScienceDirect

Journal of Alloys and Compounds

journal homepage: www.elsevier.com/locate/jalcom

Synthesis of a TiBw/Ti6Al4V composite by powder compact extrusion using a blended powder mixture

Huiyang Lu [a], Deliang Zhang [b], Brian Gabbitas [a,*], Fei Yang [a], Steven Matthews [c]

[a] Waikato Center for Advanced Materials, School of Engineering, University of Waikato, Hamilton, New Zealand
[b] State Key Laboratory of Metal Matrix Composites, School of Materials Science and Engineering, Shanghai Jiao Tong University, Shanghai, China
[c] School of Engineering and Advanced Technology, Massey University, Auckland, New Zealand

ARTICLE INFO

Article history:
Received 11 February 2014
Received in revised form 18 March 2014
Accepted 22 March 2014
Available online 2 April 2014

Keywords:
Titanium matrix composites (TMCs)
Powder compact extrusion
TiB whiskers
Microstructure and mechanical property

ABSTRACT

A Ti–6 wt%Al–4 wt%V alloy (Ti6Al4V) matrix composite, reinforced by in situ synthesized TiB whiskers (TiBw) has been successfully fabricated by powder compact extrusion using a blended powder mixture. The microstructural characterization of the various extruded samples showed that the different starting powders, pre-alloyed powder plus boron powder or titanium plus Al–40V master alloy powder plus boron powder, had a significant effect on the morphology of the in situ synthesized TiB whiskers. It is also evident that the TiB whiskers affect the microstructural evolution of the Ti6Al4V matrix. The tensile test results indicated that the composite with a dispersion of fine TiB whiskers with high aspect ratios exhibited a high ultimate tensile stress (UTS) and yield stress (YS) of 1436 MPa and 1361 MPa, respectively, a reasonably good tensile ductility reflected by an elongation to fracture of 5.6% was also achieved. This is a significant improvement compared with as-extruded monolithic Ti6Al4V alloy produced in this study.

1. Introduction

In situ synthesized TiB whiskers have been identified as probably the most compatible and effective discontinuous reinforcement for Ti and Ti alloy matrices due to both their thermodynamic and mechanical stability (generating minimal residual stresses) because of good matrix bonding which generates very clean interfaces [1,2]. This is especially the case for a Ti–6 wt%Al–4 wt%V alloy (Ti6Al4V) matrix reinforced by in situ synthesized TiB whiskers which have become more attractive as a means of enhancing the strength of Ti6Al4V alloys. Consequently these composites have received a lot of attention [1–24]. Researchers have put a great deal of effort into improving the overall performance of titanium matrix composites (TMCs), especially for those based on a Ti6Al4V matrix and reinforced by in situ synthesized TiB whiskers. However, a satisfactory level of mechanical properties such as tensile strength and ductility still has not been achieved [5], and most research in this area tends to focus on studies of Young's modulus, hardness, microstructure and compressive properties [2,11,15–17,19–22]. A review of previous work indicates two common characteristics in TiB/Ti6Al4V composites: (a) the TiB whiskers formed through in situ reactions have a low aspect (length/diameter) ratio, and (b) when the composites are prepared using a powder metallurgy route, in combination with a blended elemental powder approach, a relatively uniform macroscopic distribution of the reinforcement in the matrix can be achieved. However, TiB whiskers tend to form microscopic clusters in localized areas, and this microstructural feature has a significant impact on mechanical properties [5,7–11]. A recent study by Huang et al. showed that improved tensile properties of a Ti6Al4V–5 vol.% TiBw composite, with an ultimate tensile strength (UTS) of 1200 MPa and elongation to fracture of 7%, can be achieved by forming a novel microstructure consisting of a network of TiBw within a Ti6Al4V matrix. This structure consists of a TiBw-rich network boundary region and a TiBw-lean matrix region produced by hot extrusion [10]. However, such a network is a potential barrier to further improvement in strength, because when the volume fraction of reinforcement reaches a certain level, the network consists of many TiB clusters which cause brittle premature failure of the material during tensile testing.

As a means of driving down the cost of PM titanium parts, powder compact extrusion or forging from blended elemental powders is now well established as a novel powder metallurgy technique. Components and structural members such as Ti6Al4V alloy rods and rocker arms for internal combustion engines and other titanium alloy products with unique mechanical properties have been successfully prepared using these low cost powder metallurgy methods [25,26]. In this study a Ti6Al4V/TiBw composite was

* Corresponding author.
E-mail addresses: hl209@waikato.ac.nz (H. Lu), zhangdeliang@sjtu.edu.cn (D. Zhang), briang@waikato.ac.nz (B. Gabbitas), fyang@waikato.ac.nz (F. Yang), S.Matthews@massey.ac.nz (S. Matthews).

http://dx.doi.org/10.1016/j.jallcom.2014.03.144
0925-8388/